MÖSSBAUER STUDIES OF IRON ALLOYS AND COMPOUNDS

Thesis

Submitted to the University of Roorkee
for the award of the degree
of
DOCTOR OF PHILOSOPHY
in
PHYSICS

By
BHUSHAN KUMAR JAIN
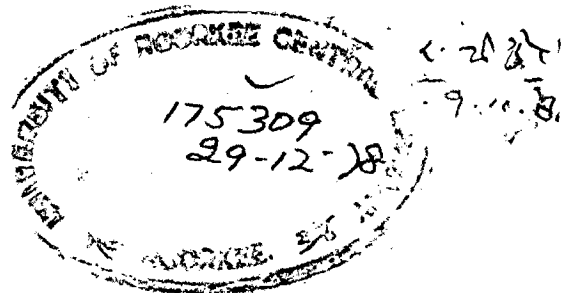
DEPARTMENT OF PHYSICS
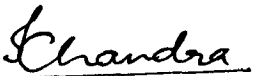UNIVERSITY OF ROORKEE
ROORKEE (INDIA)
OCTOBER, 1977

To late Sri Munshi Lal Jain
my grand father
whose memory has been
of continuous inspiration

CERTIFICATE

This is to certify that the thesis entitled ' MÖSSBAUER STUDIES OF IRON ALLOYS AND COMPOUNDS' which is being submitted by Sri Bhushan Kumar Jain in fulfilment for the award of the degree of Doctor of Philosophy in Physics of the University of Roorkee, Roorkee is a record of his own work carried out by him under my supervision and guidance. The matter embodied in this thesis has not been submitted for the award of any other degree.

Further it is certified that he has worked from January 1973 to June 1977 for preparing his thesis for the Ph.D. degree at the University.

Dated: 4th October, 1977

(K. Chandra)
Department of Physics
University of Roorkee
ROORKEE (INDIA)

ACKNOWLEDGEMENT

getting unreserved affection and stimulus from my reverend parents, brothers, sisters and other members of the family. Their regards and expectations in true Hindu way have served as light house for me and no words available in a Dictionary can express my feelings for these.

During my stay at Roorkee, I have been provided a nice and cordial company by a number of friends. Running the risk of missing many names I would like to express my gratitude to Madan, Hem, Sri Krishan, Anil, Govind, Ashok, Indra, Mahendra, Rajendra and Ramkrishna.

I will be failing in my duty if I do not acknowledge the award of fellowships by CSIR and UGC, which left me completely free from financial worries. The credit for nice presentation of my hieroglyphics goes to Sri Chaman Lal and Sri V.K. Sharma.

Bhushan Kumar Jain

(B.K.Jain)

R E'S U M E'

The phenomenon of Mössbauer effect has been used to study the hyperfine interactions in some alloys and compounds of iron. The source of recoilfree gamma radiation used was Co^{57} embedded in Pd or Cu matrices and the 14.4 keV gamma ray was used to observe the above phenomenon.

The subject matter of the thesis has been arranged in six chapters and is presented as below:

Chapter 1. The importance of Mössbauer spectroscopy (as a tool)for the study of hyperfine interactions has been appraised in comparison with other methods which can be used for these investigations. The motivation for the problems undertaken in this study has also been described.

Chapter 2. Introduction to the Mössbauer effect and the range of fields where it finds applications has been presented in brief. A compendium based on the survey of the literature including various text-books, review articles and important research papers has been given. Hyperfine interaction parameters, their source of origin and the effect of impurities on these have been discussed. Since in the last chapters we frequently deal with various phase diagrams, a brief introduction to these as well as other important factors has also been incorporated

Chapter 3. The discussion of instruments used in the investigations constitutes the contents of this chapter. Emphasis has been given to the constant acceleration Mössbauer drive fabricatted locally. The experiments were performed in transmission geometry, employing argon-methane filled proportional counter, which gave an energy resolution of $\sim 14\%$. The storing device, used for gamma radiation, was a 256 channel analyser whose velocity resolution was doubled by using a binary frequency divider (discussed by A.K. Singh in his Ph.D. thesis being submitted to the University of Roorkee). The output coupling unit for multichannel analyser was a addo-X type printer, in which data were printed per channel in one line.

A discussion of the design and fabrication of a dynamic type temperature controller has also been included in this chapter. It can control temperature upto an accuracy of ± 0.05 K and works from liquid nitrogen temperature to 900 K.

Chapter 4. This chapter is based on the studies on corroded steels (corroded in the presence of reinforced cement and concrete, rcc). The different products formed were analysed on the basis of hyperfine interaction parameters and other studies like chemical analysis,microstructural investigations were performed to supplement the obtained results.

It was concluded that the steels having more cementite corroded to Fe_3O_4 while others end up with the corrosion product $\beta FeOOH$. Different possible reasons of faster corrosion in presence of rcc have been discussed.

Chapter 5. Effects of alloying elements in plain carbon steels, used to improve the mechanical and other properties, have been discussed. It was found that for low concentration of carbon, the alloying elements mainly form solid solution with ferrite (going substitutionally) while with the increased concentration of carbon the alloying elements form carbides other than iron carbide in addition to occupying the substitutional sites.

Chapter 6. This chapter has been divided into two parts.

Part A. In this part the findings on the binary system iron-selenium, in the lower concentration range of selenium, have been reported. Effect of various thermal treatments was seen. It was found that in this range a two phase system between Fe and FeSe exists and that Se does not dissolve in Fe. The FeSe formed was assigned as $\alpha FeSe$ having tetragonal structure. At a temperature greater than $1000^\circ C$, α-FeSe separates out from the other phase Fe and crystallizes into a white silvery luster compound. Iron was found to exist in 2+ oxidation state with a major covalent

contribution. The covalent contribution has been calculated using Sanderson's method of equalisation of electronegativities and compared with those of some other typical systems. The values of isomer shift and quadrupole splitting have been discussed in the light of these facts. A d^3s type hybridization has been suggested in this compound.

Part B.

ε phase of iron antimonide having NiAs type hexagonal structure with formula Fe_3Sb_2 has been studied. This phase can not be prepared separately and hence a two phase system Fe_3Sb_2 and $FeSb_2$ was prepared. Since $FeSb_2$ is very well studied hence Fe_3Sb_2 can be studied in this way without any disturbance due to the other phase. This phase shows quadrupole splitting at room temperature and this was assigned to the distortion caused by the excess Fe atoms going to the interstitial positions. Fe_3Sb_2 is paramagnetic at room temperature and antiferromagnetism sets in at or below the liquid nitrogen temperature. It was concluded that the ordering of spin is due to the regular site iron atoms at liquid nitrogen temperature.

Appendices:

The hybridization scheme for σ bonds in α-FeSe is discussed in the group theoretical language in Appendix A (1) and it is shown that d^3s is the possible hybridization. The crystal field splitting

of d levels appropriate to the site symmetry in
α-FeSe has been carried out under the assumptions
of point charge model and the details are presented
in Appendix A (2).

LIST OF PUBLICATIONS

A. Included in the thesis.

1. A dynamic type of temperature controller: Indian Journal of Pure and Applied Physics $\underline{14}$, 858 (1977).
   (with .K. Chandra)

2. Effect of alloying elements in plain carbon steels: Phys. Stat. Sol.(a)$\underline{43}$ (1977). in press.
   (with Ajay K.Singh and K.Chandra).

3. Mössbauer Studies of Corroded steels: Japanese J. of Applied Physics $\underline{16}$ (Dec. 1977) To appear.
   (with Ajay K.Singh, K.Chandra and I.P.Saraswat).

4. An investigation of binary system FeSe: J. Phys. (F)
   (Communicated).
   (with Ajay K.Singh and K.Chandra).

5. Observation of antiferromagnetism in ε iron antimonide: Appl. Phys. Letts. (Communicated).
   (with Ajay K.Singh and K.Chandra) .

B. Not included in the thesis.

1. Effect of Pressure on the Lamb-Mössbauer fraction of surface atoms in F.C.C. Lattices:Phys. Stat. Sol. (a) 21, K69 (1974).

(with G.C. Shukla).

2. Mössbauer Effect studies of addition complexes of hydro-ferro and ferri cyanide with organic bases: J. Inorg.and Nucl. Chem. 38, 1451(1976).

(with Y.P.Singh,Wahid U.Malik a nd K.Chandra).

3. Mössbauer studies of iron ore: Proc. NP and SSP Symposium 19C, 420 (1976).

(with Ajay K.Singh and K.Chandra).

4. Mössbauer studies of natural red and yellow ochre: J. Phys. (D) accepted for publication.

(with Ajay K.Singh and K.Chandra).

5. Mössbauer studies of natural goethite and bog iron ore: Phys. Stat. Sol.(a) 44 (1977) in press.

(with Ajay K.Singh and K.Chandra).

6. Structural and compositional study of natural chromites of Indian origin: J.Phys. (D) (Communicated).

(with Ajay K.Singh,S.K.Date and K.Chandra).

CONTENTS

CHAPTER 1

INTRODUCTION

The nuclear hyperfine interactions, which are the interactions of the charge and intrinsic spin of a nucleus with its surrounding electrons, can be studied using various techniques such as nuclear magnetic resonance (NMR), perturbed angular correlation (PAC), electron paramagnetic resonance (EPR), Mössbauer effect spectroscopy or nuclear gamma resonance (NGR) etc.. Other techniques like atomic beam resonance, optical hyperfine measurements and nuclear specific heat measurements can also be used but are of lesser importance. The techniques NMR, EPR, NGR and PAC also show some advantages and disadvantages over each other. For example limitation of both NMR and EPR, particularly in metals, arises because of skin effect. As a result, the measurements are limited only to small particles. Further in NMR the transitions within ground state levels are observed and thus if the ground state has zero angular momentum, which is the case for even-even nuclei, then conventional resonance methods can not be used to study hyperfine interactions. Similarly, EPR is generally limited to atoms or ions where the electronic ground state is degenerate. PAC also suffers from some problems such as prior knowledge of unperturbed correlation pattern (which is not always possible), difficulty in separating the electric quadrupole and magnetic hyperfine interactions, etc..

Mössbauer effect spectroscopy (NGR) does not suffer
from these drawbacks, though it has its own limitations
e.g.₀ the study is only possible in low energy range, which res-
tricts its applications to a limited number of elements.
Further, it supplies direct information about the proper-
ties of the Mössbauer nuclei only and the impurity para-
meters are the indirect outcome of the technique.

The resolution in the case of NMR is better than
that in Mössbauer spectroscopy which helps in the accurate
measurement of splittings. But the sharpness of the
NMR resonance line causes problems in its detection and
even in observation in the presence of strong spin-spin
interactions between neighbouring ions because the lines
may be broadened too much. The Mössbauer effect spectro-
scopy provides resonance lines of compromising line
width. The radiations observed are monochromatic and
the line width is in general small compared to the
hyperfine interactions. An extra peculiarity of the
Mössbauer effect spectroscopy lies in the possibility
of the measurement of monopole interaction leading to
the isomer shift. All these qualities make the Mössbauer
effect spectroscopy a more effective tool to obtain the
information on hyperfine interactions.

In the present dissertation the Mössbauer effect
spectroscopy (NGR) has been used as basic tool to
study hyperfine interactions in some alloys and compounds
of iron , using Co^{57} gamma rays of energy 14.4 keV.

In Mössbauer effect | 1,2 | the recoil free emission and resonant absorption of gamma rays is observed. If the chemical environment in source and absorber is different then either the emitted gamma rays will not be absorbed resonantly or the resonance will be partial. In such a case to make the resonant absorption possible the energy levels of either the source or the absorber should be modified. Accordingly an important part of a Mössbauer spectrometer is a device which provides extra energy either to the source or the absorber to compensate the effect of hyperfine interactions and is known as Mössbauer drive. Thus a Mössbauer spectrometer consists mainly of a photon source, an absorber, a Mössbauer drive and a photon detection and counting system. The gamma ray energy from a radioactive nucleus is modulated by imparting a Doppler velocity to the source and the gamma rays of discrete energies are resonantly absorbed by the absorber nuclei. A plot of the number of transmitted photons versus change in photon energy (Doppler velocity) gives peak or peaks at the energies where resonance occurs. This plot is called Mössbauer spectrum.

To make the technique more effective and draw certain important conclusions it is desirable to perform studies at higher and lower temperatures along with room temperature studies. Application of external high pressure and magnetic field supplies additional information and

thereby leads to better understanding. We have also per-
formed some temperature dependent studies. While per-
forming temperature dependent studies it is necessary
to control the temperature very accurately. A new dyna-
mic type temperature controller has been designed and
fabricated in the laboratory and is discussed here. It
can control the temperature from liquid nitrogen tempe-
rature to 900K with an accuracy of $\pm$ 0.05K over any
length of time.

The motivation of the present investigations has
been of applied nature. The application of Mössbauer
effect spectroscopy in studying the corrosion problems
was introduced long back in 1965 by Suzdalev et. al.[3].
But all the investigations performed till now have been
concerned either with oxidation of iron in pure air or
with the formation of rust layers in the presence of H_2O,
HCl and chromate solutions etc.. However, so far no
attempt has been made to study the corrosion in the
presence of reinforced cement and concrete (rcc),
although this problem is of great interest to metallur-
gists and civil engineers. Guided by this urge, we
used the Mössbauer spectroscopy along with chemical
analysis and microstructural studies, to understand the
behaviour of corrosion and corrosion products formed in
structural steels in rcc.

The other problem studied here demonstrates the
application of Mössbauer spectroscopy to plain carbon

steels. The alloying elements like silicon, manganese are added to plain carbon steels to improve their mechanical and chemical properties. These increased properties are obtained due to the change in phases formed and the way in which various phases are arranged. Mössbauer spectroscopy yields information on both these aspects. So, the technique has been used to observe the changes in phases formed in the presence of these alloying elements and also to understand how the impurities exist; interstitially or substitutionally?

Keeping in view the importance of the role played by Se (i) in heat absorbing glasses, (ii) as decolourizer as well as colourizer in iron containing glasses,(iii) on the inclusions present in carbon steels, and the academic interest in the study of binary alloys of iron and chalcogens, we carried out investigations on Fe-Se intermetallic compound (αFeSe) having PbO type tetragonal form. A method for the preparation of α-FeSe has been suggested and the crystal field splitting of 3d levels and hybridization schemes have been discussed. In order to correlate the nature of bonding with isomer shift and quadrupole splitting, Sanderson's method of equalisation of electronegativities has been used to find ionicity and then employed to compare this system with others. Also included are the findings of the Mössbauer study on Fe_3Sb_2 system which has NiAs type structure and shows antiferromagnetic transition near 77K.

CHAPTER 2

PRELIMINARY THEORETICAL BACKGROUND

2.1 INTRODUCTION TO MÖSSBAUER EFFECT

In 1958, R.L. Mössbauer |1,2| discovered and expl-
ained the phenomenon of nuclear gamma resonance, popularly
known as Mössbauer effect. According to the phenomenon
the nuclei of atoms embeded in solid crystalline lattice
can, under certain conditions, emit or absorb gamma rays
without the loss of energy due to recoil. Further, the
observed gamma rays do not suffer from thermal broade-
ning and show the Heisenberg natural line width. Since
in this case the nuclei are bound in the solid, the recoil
momentum (from which the emitting or absorbing nuclei
suffer due to emission or absorption of the gamma rays)
is taken up by the solid as a whole through center of mass
motion and thus the recoil energy can be neglected due to
the large mass of the solid. However for efficient reso-
nance absorption one still has to compensate for the
natural line width.

This discovery made available the purest radia-
tion and stimulated interest in hitherto desirable but
unattempted fields like the phonon spectrum of a solid,
Gravitational red shift and hyperfine interactions etc.,
so much so that Mössbauer became a co-sharer of Noble
Prize for Physics in 1961 |4|. At present the technique
has got its application in most of the disciplines of
natural science viz. solid state physics, chemistry

metallurgy, mineralogy, technology and even in biophysics etc..

The utility and applicability of the phenomenon can further be judged from the literature which has come up in a period of less than two decades in this field |5-8|. Various review articles and books have been written which describe the basic aspects and applications of this spectroscopy in detail | 9-26|.

2.2 GENERAL PARAMETERS OF A MÖSSBAUER SPECTRUM

A plot of transmitted or scattered gamma ray intensity versus the Doppler velocity provided either to the source or absorber is a Mössbauer spectrum. It may be a singlet, a doublet, a six line pattern and even more complicated depending on the type of interactions present. For the correct analysis of the Mössbauer spectrum following factors should be considered (a) the line position (or line shift), (b) the line width, (c) line intensity and (d) the line shape.

(a) LINE POSITION

Line position or line shift tells about the position of various energy levels and is of great importance. One can calculate important parameters like isomer shift, quadrupole splitting, Zeeman splitting, temperature shift, pressure shift, or Gravitational red shift with the help of line positions. Hence it should be determined very

carefully.

(b) LINE WIDTH

For an ideal case, the line width is related to its life time through the Heisenberg uncertainty relation.

$$\Gamma = \frac{\hbar}{\tau} = \frac{0.693h}{t_{1/2}} \qquad \ldots (2.1)$$

Thus, the observed line width should be double the natural line width Γ due to the resonance overlap of emission and absorption lines. Normally observed line width is broader than the theoretical one. This extra broadening may be due to two types of factors one due to experimental effects and other due to solid state effects.

Experimental effects include extra vibrations, finite source and absorber thickness and usually also the finite resolution. These should be minimized before conducting the experiment. Visscher |27| discussed the absorber thickness effect on line width which can be expressed as

$$\Gamma_{exp} = \Gamma_a + \Gamma_s + 0.27 \, \Gamma \, X \qquad \ldots (2.2)$$

$\Gamma_a + \Gamma_s$ is the width of Γ_{exp} extrapolated to $X = 0$, and $X = n \, f_a \sigma_o$ where: n is the number of atoms of the Mössbauer isotope per cm^2, f_a is the recoil free fraction for the absorber and σ_o is the maximum cross

section at resonance. Margulies and Ehrmann[28] discussed theoretically the effect of thickness on line width for various absorbers. Wertheim [29] investigated the effect of solid angle on line broadening and suggested that to have minimum effect of this parameter the source detector distance should be four times the detector diameter.

Solid state effects give microscopic information about the solid. Various mechanisms which lead to line broadening are processes with relaxation times nearly equal to the life time of the excited state, imperfections, anharmonic lattice behaviour and impurities and defects associated with Mössbauer source and absorber. Wignall[30] considered some of these effects in detail while Wickman and Wertheim [31] and Blume [32] kept these factors in mind during the discussion of relaxation mechanisms.

In some cases the line width can be even narrower than the natural line width. This can be obtained by increasing the effective life time. This was achieved by Albert and Neuwirth [33] and Lynch and coworkers [34] through selective decay coincidence technique while Gonser and Wiedersich [35] used the thermal spike by the foregoing decay for this purpose.

(c) LINE INTENSITY

Different spectral lines may have different depths and area. Because of the distortion in line shape and

broadening in the line width it is the area and not the depth of the absorption line which should be considered. But if the line is Lorentzian and unbroadened, line depth can be considered as the representative of the total absorption being proportional to the area. Various line intensities arise due to following reasons: different transition probabilities for different hyperfine components; anulgar dependence of the transmitted radiation |36|; relaxation effects | 32 | and the anisotropic f factor |37|.

(d) LINE SHAPE

Theoretically the gamma ray spectral energy distribution or the frequency spectrum or the so called line shape could be measured and it should be a (Breit Wigner) Lorentzian line shape given by

$$\frac{1}{(\omega - \omega_0)^2 + \frac{\gamma^2}{4}} \sim \frac{1}{(E-E_0)^2 + \frac{\Gamma^2}{4}} \quad \ldots (2.3)$$

where $E = \hbar\omega$ and $\Gamma = \hbar\gamma$.

In general the observed line shapes are not Lorentzian but intermediate between Lorentzian and Gaussian. Generally line shape is affected by lack of complete homogeneity in the samples, finite thickness of source and absorber, hyperfine interactions, back ground of non resonant gamma rays and also by the instrumental limitations. The study of line shape yields information about the lattice

properties of source and absorber. The exact determination

of line shape has been discussed in literature | 38|. If the

shape of the spectrum in the left and right side of the

peak is different it gives idea about the presence of

another peak superimposed on the first peak.

2.3 MÖSSBAUER FRACTION, f

When an emitting nucleus is bound in a crystalline

lattice then there can be substantial probability for the

emission of a photon without any recoil energy loss. This

probability is called the Mössbauer fraction f. It has a

value zero for free atom and increases with the increase

of lattice rigidity, becoming unity for a completely rigid

lattice. Under harmonic approximation, it can be written as .

$$f = \exp (- \langle x^2 \rangle \, k^2) \qquad \qquad \dots (2.4)$$

where k ($2\pi/\lambda$) is the wave vector of the photon having

wave length λ , $\langle x^2 \rangle$ is the mean square displacement of

the emitting nucleus in the direction of gamma ray prop-

agation. It is often desirable to use Debye approximation

to understand the phenomenon and to express Eq. (2.4) in

terms of more familiar quantities. In a general lattice

f < 1 and in Debye approximation it is given by |21|

$$f = e^{-2W}$$

where

$$2W = \frac{E_R}{K\theta_D} \left[3/2 + \frac{\pi^2 T^2}{\theta_D^2} \right] . \qquad \ldots (2.5)$$

This Eq. is valid for $\theta_D > T$. This is the familiar form for the Debye-Waller factor 2W. The characteristic values of f are 0.91 for 14.4 keV gamma rays of Fe^{57} and 0.06 for the 129 keV gamma rays of Ir^{191}, both for the natural metallic host lattice. In a Mössbauer experiment——the Debye - Waller factors of the source and absorber jointly determine the magnitude of observable effect.

2.4 CHOICE OF A MÖSSBAUER ISOTOPE

The choice of a Mössbauer isotope depends upon the sample to be studied. But in general an isotope is said to be good for Mössbauer studies if it has the following features: (i) high Lamb-Mössbauer fraction (low energy Mössbauer transition),(ii) long life time,(iii) few energy precursor gamma rays (to make the electronic circuitry easy),(iv) narrow line width,(v) low internal conversion coefficient.

Till now roughly 80 isotopes of 40 elements have been tried. But the most studied are few e.g. Co^{57}, Sn^{119}, Sb^{121}. Co^{57} which shows all the above characteristics has been used by us in all our present studies. This isotope is commercially available diffused in various lattice e.g. Cr, Pt, Cu, Pd, Rh, stainless steel etc.. The decay scheme

of Co^{57} is given in Fig. 2.1 while some important parameters
are tabulated in Table 2.1.

2.5 HYPERFINE INTERACTIONS

The main emphasis of the Mössbauer effect studies
has been on the interactions between electrons and nucleus,
known as hyperfine interactions. This is possible because
the hyperfine interactions are often of the order of 10^{-7} eV,
which is two orders of magnitude larger than the natural
line width Γ of a Fe^{57} 14.4 keV gamma photon. These
hyperfine interactions comprise of two types of interaction
having origin in the static and dynamic (current) charge
distribution of the atomic electrons and nucleus. These
are the electrostatic and magnetic interactions. Either
one or both may be present at a time. The measurement
of these hyperfine interactions provides the basis | 39 |
for the determination of the electronic charge and spin
distribution, magnetization and nuclear electric and
magnetic moments, ionicities (or valences), electron
configuration in metals and alloys, crystal field parame-
ters and splitting of crystal field states, ordering
mechanism in alloys, magnetic and crystallographic trans-
itions and magnetic ordering processes, magnetic impuri-
ties and spin structure etc..

The total Hamiltonian giving the interaction of
a nucleus with the extra nuclear electrons can be written as

Co^{57} $(T_{1/2} - 270\,days)$

K - electron capture

99.84 % $(\sim 0.6\,MeV)$

$26\,Fe^{57}$

5/2

$\cdot 136.4\,KeV$ $(T = 1.25 \times 10^{-8}\,sec)$

136.4 KeV

122.0 KeV

9 %

91 %

3/2 ⸳ $\cdot 14.4\,KeV$ $(T = 1.45 \times 10^{-7}\,sec)$

Mössbauer
Transition

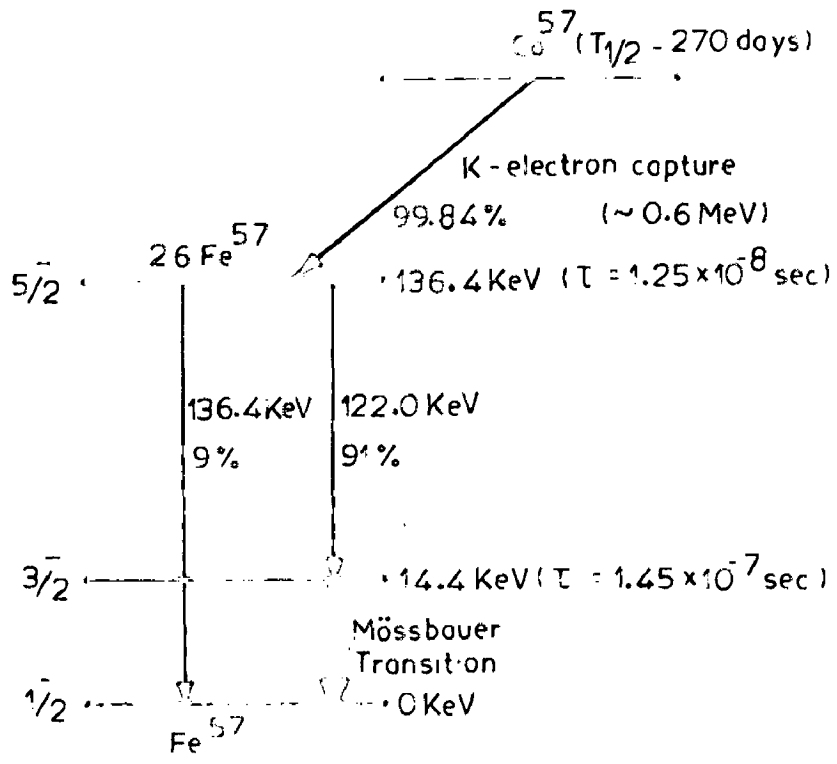1/2 $\cdot \cdot 0\,KeV$

Fe^{57}

FIG. 2.1 _ DECAY SCHEME OF Co^{57} TO Fe^{57} SHOWING

THE 14.4 KeV MÖSSBAUER TRANSITION .

TABLE 2.1: IMPORTANT PHYSICAL PARAMETERS OF 14.4 keV
GAMMA-RAY MÖSSBAUER TRANSITION

(1) Measured Properties

Energy of γ-ray, E_γ	= 14.4125 ± 0.0006 keV
Half life of the excited state, $\tau_{1/2}$	= 97.81 ± 0.14 ns
Total internal conversion coefficient, α_T	= 8.18 ± 0.16
Natural isotopic abundance, IA	= 2.19 %
Spin and polarity of ground state, I_g	= 1/2⁻
Spin and polarity of excited state, I_e	= 3/2⁻
Magnetic moment of the ground state, μ_g	= + 0.09042 nm
Magnetic moment of the excited state, μ_e	= − 0.15491 nm
Quadrupole moment of the ground state, Q_g	= 0.0 barn
Quadrupole moment of the excited state, Q_e	= + 0.187 ± 0.005 barn

(ii) Derived Parameters

Maximum resonance cross section, σ_o	= 2.566x10⁻¹⁸ cm²
Atomic scattering cross section, $\sigma_{at.}$	= 5.5x10⁻²¹ cm²
Natural line width, Γ	= 4.651x 10⁻⁹ eV ≈ [0.0969 mm/sec.)
Observable width, w_o	= 0.1940 mm/sec.
Recoil Energy, E_R	= 1.957x10⁻³ eV
Debye temperature, θ_D	= 420K
Recoilless fraction, f with θ_D=420K	= f(90K)=0.92 f(300K)=0.79

Note: Most of the values have been taken from the Mössbauer
Effect Data Index 1972 Ed. by J.G. Stevens and V.E.Stevens
Plenum Press, New York,1973.

$$H = H_S + H_Q + H_M \qquad\qquad \ldots (2.6)$$

where H_S is the Hamiltonian giving the electric monopole interactions between nucleus and the electrons, H_Q represents the interaction of the nuclear electric quadrupole moment with the electric field gradient around the nucleus and H_M involves the interaction of the nuclear dipole moment with the effective magnetic field produced due to the electrons. The other higher terms are negligibly small.

The theory of these hyperfine interactions has been discussed in various books | 19-26, 39-40 | on Mössbauer effect spectroscopy and therefore only a brief summary of these will be outlined here.

(a) <u>MONOPOLE INTERACTION</u> (Chemical or isomer shift)

The isomer shift arises from the electrostatic interaction between the charge distribution of the nucleus and those electrons which have a finite probability of being found in the region of the nucleus. This interaction causes a small energy shift of the nuclear levels Fig.2.2a. Only s electrons take part directly in this interaction because these have finite probability of being found in the region of nucleus. The other electrons p and d etc. contribute indirectly. The isomer shift | Fig.2.2b| which denotes the shift of energy levels of the nucleus in the source relative to that of absorber can be written as
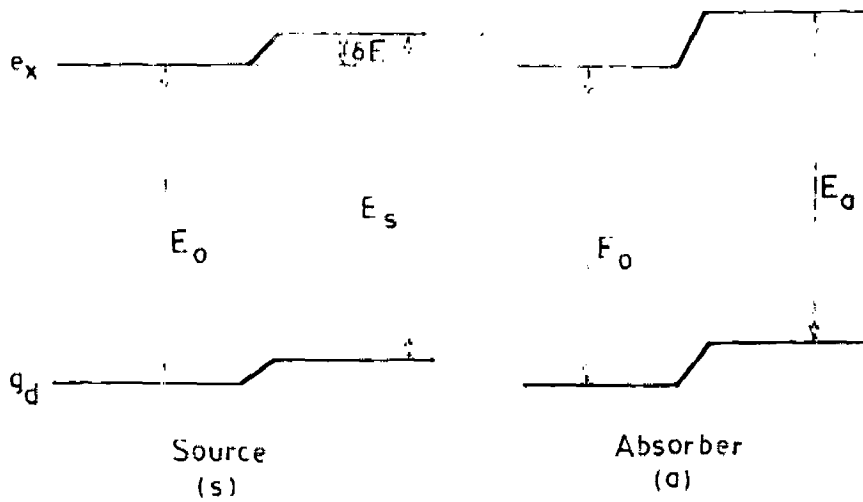
$$\delta = IS = E_a - E_s = \frac{4\pi}{5} Z e^2 R^2 \frac{\delta R}{R} [\, | \psi_a(0)|^2 - | \psi_s(0)|^2 \,]$$

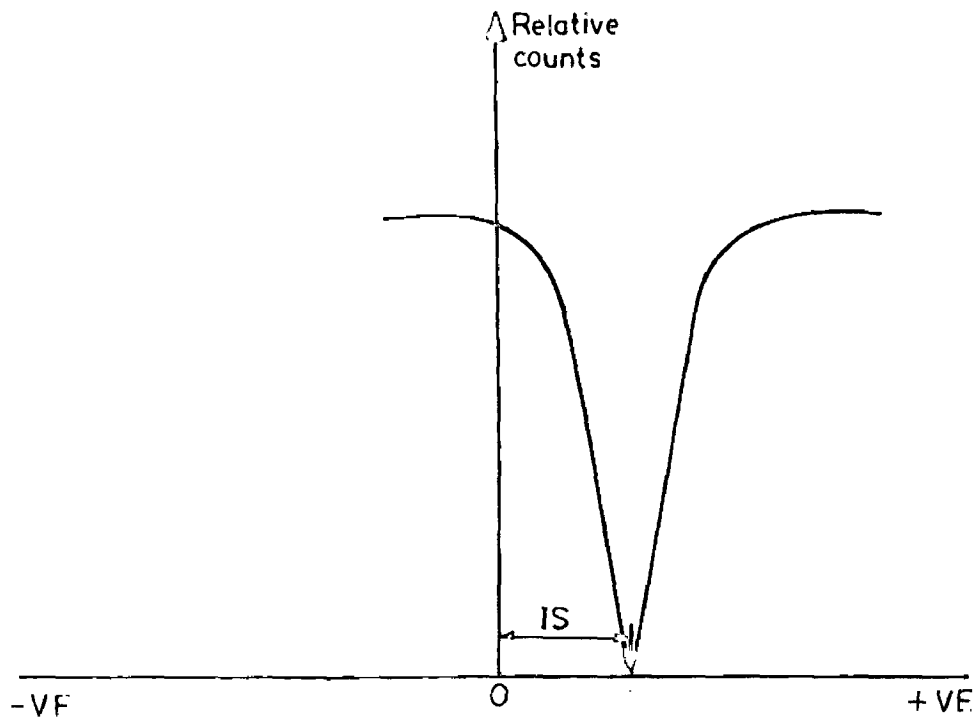FIG. 2.2 (a) - SHIFT OF NUCLEAR ENERGY LEVELS OF Fe^{57} DUE TO MONOPOLE INTERACTION.

FIG. 2.2 (b) - MÖSSBAUER TRANSMISSION SPECTRUM OF Fe^{57} SHOWING IS. ONLY.

$$\delta = E_a - E_s = \frac{2\pi}{5} Z e^2 \left\{ |\psi_a(0)|^2 - |\psi_s(0)|^2 \right\} (R^2_{ex} - R^2_{gd})$$

$$= \frac{4\pi}{5} Z e^2 R^2 \frac{\delta R}{R} \quad |\psi_a(0)|^2 - |\psi_s(0)|^2 \quad \ldots (2.7)$$

where $\delta R = R_{ex} - R_{gd}$ and $R_{ex} + R_{gd} \cong 2R$.

R_{ex} and R_{gd} represents the nuclear radii in the excited and ground states, respectively, $|\psi_a(0)|^2$ and $|\psi_s(0)|^2$ denote the s electron densities at the nucleus in the absorber and source respectively.

The expression (2.7) is a non-relativistic expression and relativistic effects were calculated by Shirley |41|. Further, the observed shift is the sum of isomer shift and second order Doppler shift | 42 |. The observation of isomer shift was first of all reported by Kistner and Sunyar | 43 |.

Eq.(2.7) consists of two factors; the first contains only nuclear parameters, in particular the difference between the radii of the excited and ground states; the second factor contains the electronic charge density at the nucleus which is basically an atomic or chemical parameter. The sign of isomer shift depends on the sign of δR, which is negative for Fe^{57} and positive for Sn^{119}.

The characteristic values of I.S. have been found

for different valence states of iron. The general observation shows that the I.S. value is more for ionic Fe^{2+} than for Fe^{3+}. This observation was understood by considering the effect of p and d electrons which arises indirectly due to shielding of the 3s electrons which pass their little time away from the nucleus. Thus one can identify the oxidation. state of iron with the help of I.S.

This identification of valence state on the basis of I.S. is difficult in spin paired (covalent) compounds since their values of I.S. overlap | 12 |. In covalent complexes the relative importance of s,p and d wave functions in .bonding as well as the extent of d-electron delocalization to the ligands should be taken into account. Hartree-Fock calculations give the d electrons contribution while the s electron contribution to $|\psi(0)|^2$ can be obtained using Fermi-Segre-Goudsmit formula |44|. The s electron contribution comes out to be large and opposite to the d-electron contribution while p-electrons contribution is very small.

Experimentally the following trend has been observed for the values of I.S.:

$$Fe^{2+}_{spin\ free} > Fe^{3+}_{spin\ free} > Fe^{2+}_{spin\ paired} > Fe^{3+}_{spin\ paired}$$
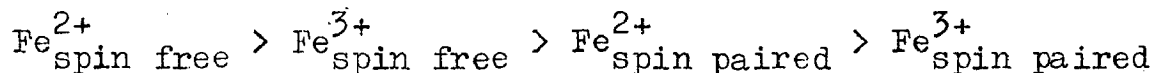
The I.S. values can be used to obtain information about the electron configuration in metals and alloys |45| and also to study the ordering mechanisms |46-47| in alloys.

The dependence of I.S. on volume expansion and pressure has been extensively studied by various workers |19, 48 |.

(b) ELECTRIC QUADRUPOLE INTERACTION

This arises from the interaction between the electric quadrupole moment Q of the nucleus and the electric field gradient (EFG) at the nucleus. Any nucleus having spin quantum number greater than 1/2 will have a non spherical shape and hence non uniform charge distribution giving rise to the electric quadrupole moment. The sign of quadrupole moment Q depends on the nuclear shape and the type of deformation. If the nucleus is oblate or flattened along the spin axis its quadrupole moment is negative while for a prolate nucleus it is positive. If the extra nuclear electric field is non cubic then this gives rise to a net EFG, which leads to the splitting of nuclear energy levels. The Hamiltonian for this interaction can be written as

$$H_Q = \frac{eQV_{zz}}{4I(2I-1)} \left[3I_z^2 - I(I+1) + \eta(I_x^2 - I_y^2) \right] \dots (2.8)$$

here I is the nuclear spin, I_x, I_y, I_z are the nuclear spin component operators, V_{zz} is the largest component of the EFG at the nucleus along the principal axis z and η is the asymmetry parameter of the EFG tensor and can be defined as below

$$\eta = \frac{V_{xx} - V_{yy}}{V_{zz}}$$

where V_{xx} and V_{yy} are the components of the EFG tensor in directions x and y and are usually chosen so that $|V_{zz}| \geqslant |V_{xx}| \geqslant |V_{yy}|$ making $0 \leqslant \eta \leqslant 1$. In the foregoing discussion V_{zz} has been expressed as $V_{zz} = -$ eq.

This interaction splits the nuclear energy levels of the excited state of Fe^{57} ($I_e = 3/2$) into two sublevels as shown in Fig. 2.3a. The energy levels for zero magnetic field are given by

$$E_Q = \frac{e^2qQ}{4I(2I-1)} \left[3m_I^2 - I(I+1) \right] (1 + \frac{\eta^2}{3})^{1/2} \quad \dots (2.9)$$

The ground state ($I_g = 1/2$) remains degenerate. Both the possible transitions between excited state ($I_e = \pm 3/2$ and $\pm 1/2$) and ground state ($I_g = 1/2$) are allowed and thus the use of single line Mössbauer source gives a characteristic two line pattern Fig. 2.3 (a,b). The separation between these two lines gives the value of quadrupole splitting. When $\eta = 0$, for Fe^{57} the quadrupole splitting comes out to be $\frac{e^2qQ}{2}$. For the I = 3/2 case (e.g., Fe^{57} and Sn^{119}), the quadrupole splitting can be expressed as

$$Q.S. = \frac{1}{2} e^2 qQ (1 + \frac{\eta^2}{3})^{1/2} \quad \dots (2.10)$$

The Eq.(2.10) suggests that measurement of quadrupole splitting (in a Mössbauer experiment) can give informations about the magnitude of q and η and sign of q.

The EFG has its origin in two factors; firstly the
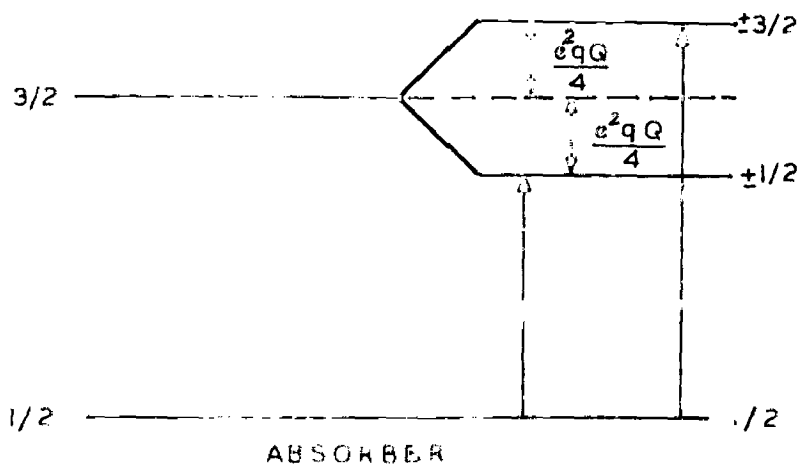
$$Q.S = \frac{e^2qQ}{2}$$

FIG.2.3 (a) _ SPLITTING OF NUCLEAR ENERGY LEVELS

OF Fe^{57} DUE TO ELECTRIC QUADRUPOLE

INTERACTION.

FIG.2.3 (b) _ MÖSSBAUER TRANSMISSION SPECTRUM

OF Fe^{57} SHOWING Q.S. ONLY.

charge on distinct ions ($q_{lattice}$) and secondly the elect-
rons in incompletely filled shells of the parent atom itself
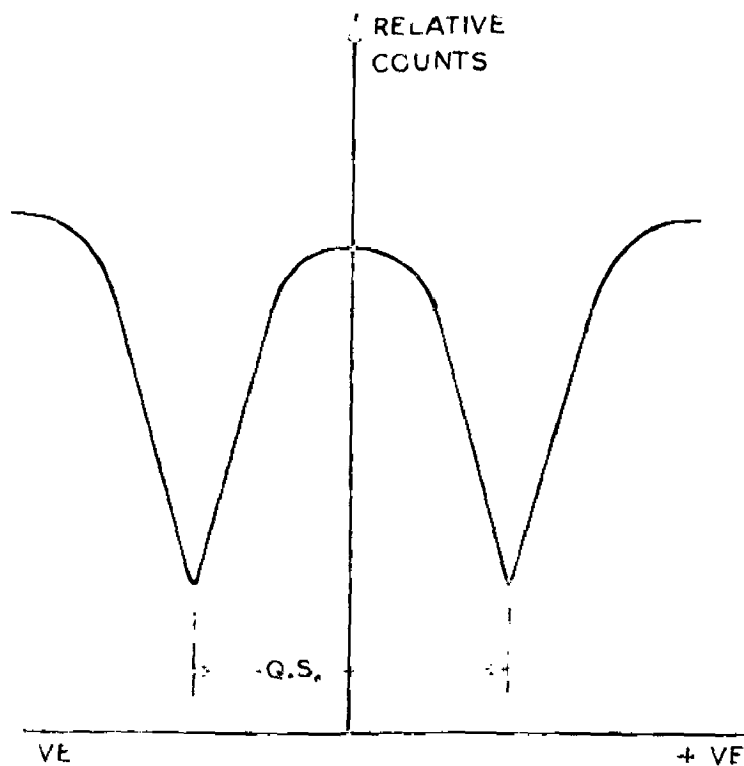($q_{valence}$). Thus q can be expressed as

$$q = (1 - \gamma_\infty) q_{lattice} + (1 - R) q_{valence} \cdots (2.11)$$

The term $q_{valence}$ may come either from p or d electrons.
The γ_∞ and R are the Sternheimer antishielding factors
and arise due to the polarization of inner, non valence
filled shells. These polarization terms enhance both
$q_{valence}$ and $q_{lattice}$.

The quadrupole splitting in a Mössbauer spectrum was
first observed by Kistner and Sunyar [43]. For iron coor-
dination compounds one expects maximum quadrupole splitting
in the high spin $3d^6$ configuration (Fe^{2+}) of iron with the
low spin $3d^5$ (Fe^{III}) next. The high spin $3d^5$ (Fe^{3+})
and low spin $3d^6$ (Fe^{II}) produce very small quadrupole
splitting. Thus the quadrupole splitting values are the
characteristic of ferrous and ferric compounds with further
differentiation of low and high spins [6,20, 49]. The
compounds of $3d^5$ low spin $|Fe^{III}|$ and $3d^6$ high spin $|Fe^{2+}|$
show a large temperature dependence due to the change in
occupation probability of uncompensated d electron (d^6
configuration)and positive hole (for d^5). It is suggested
that a preponderence of unpaired electron spins in d level

can influence the EFG through spin - spin coupling. A correlation between the magnetic susceptibility and electric quadrupole splitting has been found by Duncan | 12 | and Nicholson | 50 |. The presence of Jahn - Teller distortion also contributes to the EFG.

In a quadrupole split spectrum the intensity ratio of the peaks gives information about the anisotropy of the f fraction. The relative transition probabilities and angular intensity dependence of the two quadrupole lines for $I = 3/2$ to $I = 1/2$ transitions are tabulated below

Transition	Relative Transition probability	Angular Dependence
$\pm 3/2 \to \pm 1/2$	1	$3/2 (1 + \cos^2\theta)f(\theta)$
$\pm 1/2 \to \pm 1/2$	1	$(1 + 3/2 \sin^2\theta) f(\theta)$

where θ is the angle between the gamma ray direction and the highest symmetry axis. For isotropic recoilless fraction f,

$$\frac{I_3 (\pm 3/2 \to \pm 1/2)}{I_1 (\pm 1/2 \to \pm 1/2)} = \frac{3 (1 + \cos^2\theta)}{(2 + 3 \sin^2\theta)} \quad \dots \quad (2.12)$$

For a polycrystalline sample, $\cos^2\theta = 1/3$ and $\sin^2\theta = 2/3$, so that the ratio $\dfrac{I_3}{I_1} = 1$. For a single crystal the ratio

depends on θ. But when f is anisotropic, the ratio becomes unequal even for polycrystalline sample | 51 |.

Mössbauer spectroscopy can be used to determine the sign of q in both single crystals and polycrystals. In single crystals the angular dependence studies give information about the sign. For θ = 0°, if the most .intense line lies on positive velocities, then the sign of q is positive for Fe^{57}. For a polycrystal the spectrum is recorded at liquid helium temperature with a large applied magnetic field. The two line spectrum splits into a two line and three line pattern ; the two line pattern being due to $\pm 1/2 \rightarrow +3/2$ and $-1/2 \rightarrow -3/2$ transitions. For Fe^{57}, if this two line pattern lies on positive velocity then the sign of q is positive, otherwise negative. For $\eta = 1$ a triplet -triplet spectrum is obtained and the sign of q becomes indeterminate.

(c) MAGNETIC DIPOLE INTERACTION

This interaction takes place between the effective magnetic field at the nucleus and its nuclear magnetic moment $\vec{\mu}$. The Hamiltonian operator for this interaction is given by

$$H_m = -\vec{\mu} . \vec{H} = - g\mu_N \vec{I} . \vec{H} \qquad \ldots (2.13)$$

where μ_N is the nuclear magneton , $\vec{I}$ the nuclear spin and g the nuclear g factor ($g = \mu / I\mu_N$). If the magnetic field

is acting along z-axis, then

$$H_m = - g \mu_N H \hat{I}_z \qquad \qquad \ldots (2.14)$$

The resulting Hamiltonian matrix is diagonal with (2I+1)
eigen values, given by

$$E_m = - g \mu_N H m_I \qquad \qquad \ldots (2.15)$$

m_I is the magnetic quantum number representing the z component
of I and can have values $m_I = I$, I-1, ..., -I. Thus the
magnetic field splits the nuclear levels of spin I into
2I+1 equispaced nondegenerate substates. Thus in case of
Fe^{57} the excited state having spin I = 3/2 will split into
four nondegenerate substates and ground state I = 1/2 into
two substates. Since for magnetic dipole transitions only
transition with $\Delta m_I = 0$, ± 1 are allowed, six transitions
between the ground and the excited state are possible. The
value of the separation between ground state sublevels is
$\beta = g_0 \mu_N H$ and this separation for excited state sublevels
is $\alpha = g_e \mu_N H$ where g_0 and g_e are the g factors for ground
and excited states respectively. The ratio of g_0/g_e has been
found | 52 | to be -1.715. Now, if we use a single line
source this leads to Mössbauer spectrum consisting of six
absorption lines as illustrated in Fig. 2.4 and the separa-
tion between the outermost two lines , $3\alpha + \beta$, or 4.715α, is
found to be |52| 10.657 mm/s which corresponds to an effec-
tive magnetic field H of 330 kG. The relative intensities
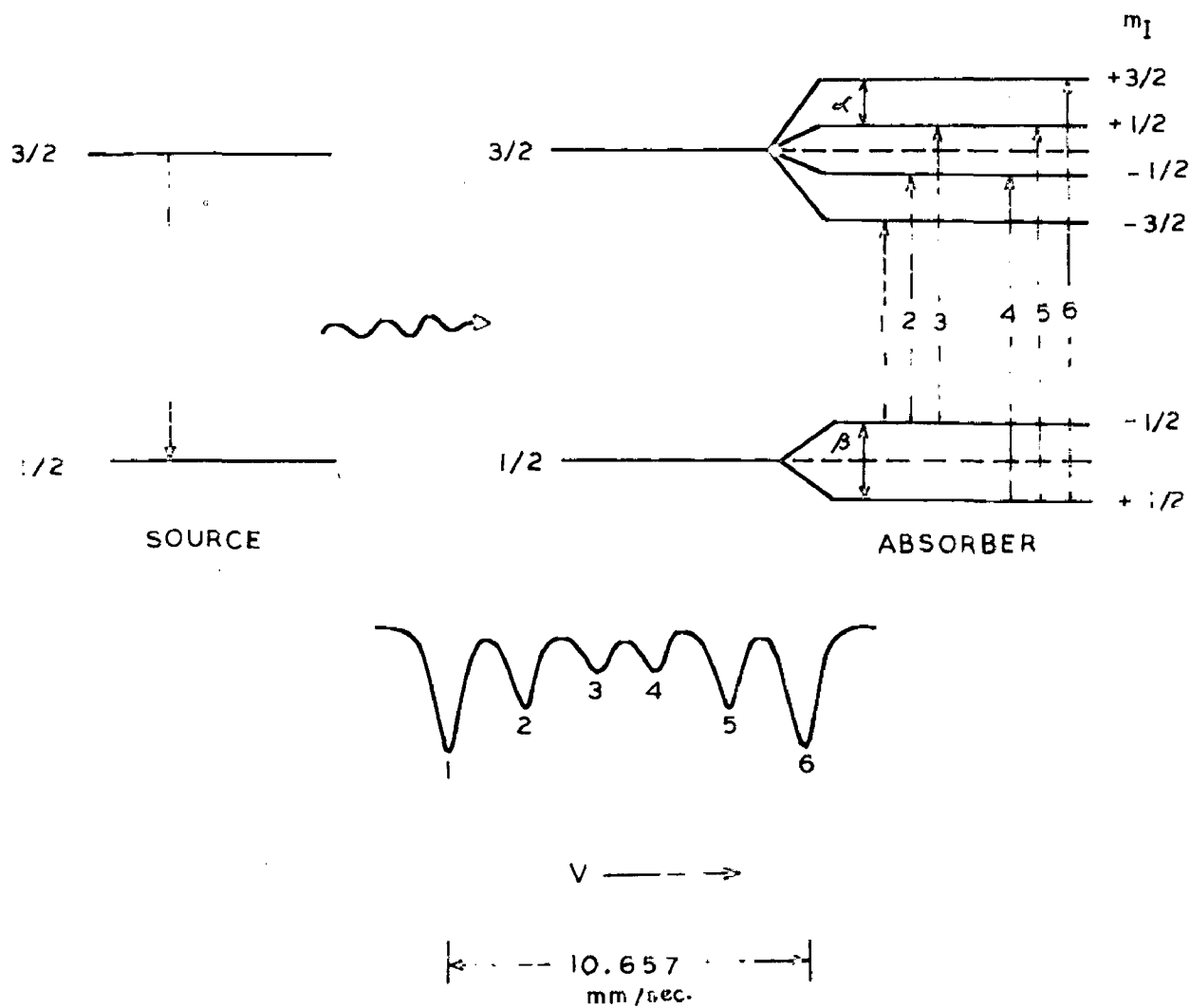of these transitions are given by | 53, 54|.

FIG.2.4 REPRESENTATION OF ENERGY LEVELS AND THEORETICAL SPECTRUM
OF Fe^{57} (ABSORBER) WITH MAGNETIC INTERACTION. THE SOURCE IS A
SINGLE LINE SOURCE.

$$| < I_g \, m_g \, LM \, | \, I_e m_e > |^2 \, F_L^M \, (\theta) \qquad \qquad \dots (\, 2.16)$$

where the first factor is the square of the Clebsch Gordan coefficients describing the vector coupling of I_g and I_e through the radiation field LM, and θ is the angle between the direction $\overrightarrow{H}$ and the incident gamma rays. The radiation pattern for dipole radiation $F_L^M \, (\theta)$ is :

$$\left. \begin{array}{l} F_1^0 \, (\theta) \; = 3/2 \, \sin^2\theta \\[3ex] F_1^{\pm 1} \, (\theta) = 3/4 \, (\, 1 + \cos^2\theta) \end{array} \right] \qquad \dots (\, 2.17 \,)$$

For Fe^{57}, where $I_g = 1/2$ and $I_e = 3/2$, $L = 1$, and the relative probabilities of the transitions involved are given in table 2.2

TABLE 2.2   The relative energies and intensities for various allowed transitions in Fe^{57}.

Sl. No.	Transition	Δm	Relative energy	Relative intensity	Total
1	$-1/2 \to -3/2$	-1	$-1/2(\beta+3\alpha)$	$9/4(1+\cos^2\theta)$	3
2	$-1/2 \to -1/2$	0	$-1/2(\beta+\alpha)$	$3 \sin^2\theta$	2
3	$-1/2 \to +1/2$	$+1$	$-1/2(\beta-\alpha)$	$3/4(1+\cos^2\theta)$	1
4	$+1/2 \to -1/2$	-1	$1/2(\beta-\alpha)$	$3/4(1+\cos^2\theta)$	1
5	$+1/2 \to +1/2$	0	$1/2(\beta+\alpha)$	$3 \sin^2\theta$	2
6	$+1/2 \to +3/2$	$+1$	$1/2(\beta+3\alpha)$	$9/4(1+\cos^2\theta)$	3

For a powder sample θ is random and by averaging

the above intensities over θ, the following intensity pattern is obtained 3:2:1:1:2:3. For θ = 90°, the ratios are 3:4:1:1:4:3 with linear polarization ||, ⊥, ||, ||, ⊥, || For axial fields (i.e. θ = 0°), the radiation is circularly polarized with Δm = 0 transition missing and remaining four lines have intensities 3:1:1:3 with polarization left, right , left, right.

The effective magnetic field H acting at Fe^{57} nucleus has several contributions and can be represented as |55|

$$H_{eff} = H_0 - \frac{4\pi}{3} M - DM + H_S + H_L + H_D \qquad \dots (2.18)$$

where H_0 is the externally applied field, which is essentially zero in our experiments. The second and third terms are the Lorentz and demagnetizing fields and are of the order of 1 kOe.

The term H_S arises from the spin density at the nucleus, and is called the Fermi contact interaction term |56,57| and contributes maximum to the observed field. It may be written as

$$H_S = - \frac{16\pi}{3} \mu_b \left\langle \sum_i (s_i^\uparrow - s_i^\downarrow) \delta (r_i) \right\rangle \qquad \dots (2.19)$$

where $s_i^\uparrow$ and $s_i^\downarrow$ are the s-electron spin densities with spin -up and spin-down respectively and δ (r) is the Dirac

delta function. Differences in spin-up and spin-down charge densities appear even in filled s-shells (1s, 2s, 3s in Fe^{57}) if the atom contains a partially filled magnetic shell, e.g., the 3d shell in our case, as well as from the conduction electrons (4s). The exchange interaction between the spin-up polarized d-shell and the spin-up s electrons is attractive while that between the d shell and a spin-down s electrons is repulsive. As a result the radial parts of the two s electrons wave functions will be different, one being pulled towards the nucleus, the other pulled outward. Hence the spin densities at the nucleus no longer cancel and a Fermi contact interaction field is observed.

The orbital magnetic moment gives rise to a field H_L

$$H_L = -2\mu_b < \frac{1}{r^3} > < \vec{L} > \cdot \qquad \ldots (2.20)$$

Here r is the radius of the 3d-orbital. In iron metal this is roughly of the order of 70 kOe. And is zero in the case of a trivalent iron in a weak crystal field environment, since L = 0.

The spin $\vec{S}$ of the parent atom and the surrounding ions give rise to a dipole magnetic field H_D at the nucleus:

$$H_D = - 2\mu_b < 3\vec{r} (\vec{S}.\vec{r}) r^{-5} - \vec{S}r^{-3}> \qquad \ldots (2.21)$$

In a cubic material in the absence of spin-orbit coupling this term vanishes.

The condition for the observation of magnetic or Zeeman splitting | 58 | in Mössbauer spectrum is that nuclear Larmor precession time must be smaller than the spin relaxation time. In this case the nucleus feels a net time averaged magnetic field. In case of most of the paramagnetic salts this nuclear Larmor precession time is larger than the spin relaxation time and hence no magnetic splitting is observed.

(d) COMBINED ELECTRIC AND MAGNETIC INTERACTION

If the nucleus experiences both electric quadrupole interaction and magnetic hyperfine interaction, the splitting of the states is not equally spaced and the spectrum is not symmetrical. The Hamiltonians H_e and H_g for the hyperfine interaction in both the excited and ground states of the nucleus, respectively, can be written as

$$H_e = H_{em} + H_{eQ}$$
$$H_g = H_{gm} + H_{gQ}$$

$$\dots (2.22)$$

where subscripts m and Q refer to the magnetic and quadrupole components of the interaction. If θ is the angle between the direction of the hyperfine field H and the principal axis of the axially symmetric EFG tensor, then the eigen values of the Hamiltonian for excited state can be written in the first order approximation as

$$E_{m_I} = -\mu_I H \left[\frac{3 \ m_I}{2} - (-1)^{|m_I| + 1/2} \lambda \ \frac{3 \cos^2\theta - 1}{2} \right] \quad ...(2.23)$$

provided $\mu_I H > e^2 qQ$.

where
$$\lambda = \frac{e^2 qQ \ /2I \ (2I-1)}{\mu \ H \ /I} \qquad ... \ (2.24 \ )$$

is the ratio of quadrupole energy to the magnetic energy. The energy level diagram for $\theta = 0^O$ and $\theta = 90^O$ is given in Fig.2.5. One can determine the value and sign of the quadrupole inte-raction and hyperfine field. The spectra observed are asymmetrical except for the case $\cos \theta = 1/\sqrt{3}$ where the spectrum will be symmetrical.

2.6 MAGNETIC HYPERFINE FIELDS IN IRON BASED ALLOYS

A composition of two or more metals is known as an alloy. It may be a compound, a solid solution, a heteroge-neous mixture, or any combination of the metals. The solid solution may be of two types: interstitial and substitutional. Here we shall discuss only the substitution alloys. These are again of two types: first in which one alloying compo-nent may substitute the other continuously. The average unit cell thus changes its dimensions progressively from those of one to other component. In the second type the substi-tution of one by other may take place only to a limited extent.

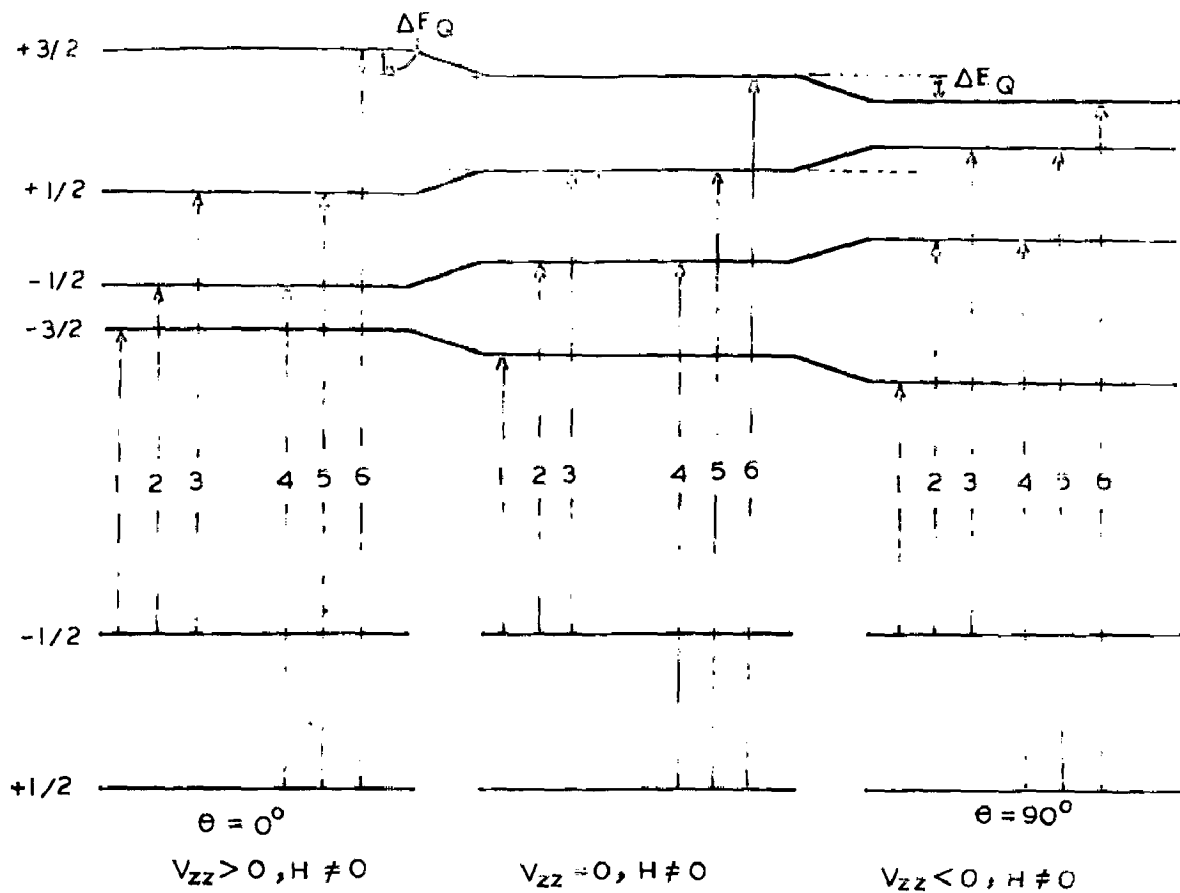In an iron based or dilute iron alloy iron is the

FIG.2.5- NUCLEAR ENERGY LEVEL DIAGRAM SHOWING THE SIMULTANEOUS

PRESENCE OF NUCLEAR QUADRUPOLE INTERACTION AND MAGNETIC

DIPOLE INTERACTION.

main constituent while the other alloying element works as an impurity. The concentration of the impurity atoms is so small that the impurity-impurity interaction may be treated as negligibly small. Further in this type of alloy the distribution of impurity may be considered random over the iron matrix.

The main aim of the study of dilute iron alloys using Mössbauer spectroscopy has been to understand the origin of ferromagnetism in iron. In general one observes the local charge and spin density distributions around impurity atoms in iron based alloys. One can also measure the magnetic field on the impurity atoms developed due to overlap etc.. If the concentration of impurity is little high (~ 6 at.%) then the phenomena like order-disorder, charge transfer in metals etc. can also be studied.

The first study in the field of dilute iron alloys using Mössbauer spectroscopy was performed by Stearns |59|. Stearns observed that Mössbauer spectra of iron alloys, having substitutional impurities, showed satellites in atleast the outer lines of the main iron spectrum and attributed their presence to the iron atoms having one or more impurities atoms in their neighbourhood. Other investigations on FeAl |60| and Fe-Rh |61| alloys could not reveal these satellites due to instrumental limitations. Later Wertheim et.al. |62| performed measurements of similar nature. Since then lot of work has been carried out by many workers. A

review of the work has recently been published by Vander
Woude and Sawatzky |63|. The main thrust of this type of study
has been to interpret the mechanism of ferromagnetism in iron.
To understand this problem Stearns |64| compared average
hyperfine magnetic fields with the bulk magnetizations in
Fe-Al and Fe-Si alloys and Schurer et. al. |65-68| performed
temperature dependent Mössbauer studies in iron alloys having
4 at.% impurities (Al, Si, Cr, Mn, Co, Ni). Both these
groups concluded that 90 percent of the 3d electrons are
localized and the remaining 10 percent are itinerent. But they
also concluded that 90 percent of the exchange interaction is
provided by the 10 percent itinerent electrons.

In the present work we were interested in investi-
gating the effect of alloying elements on the observed
magnetic field rather than the origin of ferromagnetism and
therefore a discussion of the former will be briefed here.
In addition, the procedure for the analysis of Mössbauer
spectra of alloys will also be discussed.

An impurity affects the magnetic hyperfine field
H at the neighbouring nuclei in the following ways;
(i) Spin Polarization: Due to the exchange interaction
between parallel 4s and 3d electrons at a particular iron
site, the 4s conduction electron polarization takes place.
This 4s spin polarization contributes to the magnetic field
at the iron nucleus of that site along with to the field at
neighbouring sites. Thus, if a central iron atom is substi-

tuted by some non-magnetic or magnetic impurity atom, then the polarization of the 4s spin density will be different causing a different field at the neighbouring sites.

(ii) Magnetic Moments: If an impurity having different magnetic moment than iron surrounds iron, it will cause a change in the 3d moment of iron and hence will affect the field H at the iron nucleus.

(iii) The exchange coupling Strength: The effective exchange coupling strength between the moments localized at the central iron atom and the impurity will be different than the exchange interaction between iron - iron atoms and hence will cause a change in magnetic field.

Thus various contributions discussed above decide the total change in the hyperfine field at iron nucleus due to one impurity atom in the neighbourhood. As an example, the impurities such ——as Al and Si (having no magnetic moment) behave like a hole in the iron lattice and the field changes come mainly from the first factor i.e. 4s spin polarization and in the case of impurities having some magnetic moment the field is affected by both the mechanisms; 4s spin polarization and magnetic moments. On the basis of previous studies |63| it has been concluded that ΔH_i was largely independent of the impurity, being approximately the same for a large number of different types of impurities. And it is $\sim$ 25 kOe for the first nearest neighbour impurity which is quite large as compared to the Mössbauer line width

($\sim$ 7 kOe). Thus it shows that one can obtain detailed information about the spin density around the impurity atom with the help of Mössbauer spectroscopy. Further, the change in isomer shift gives information about the charge density but this change is quite small and to draw important conclusions from isomer shift changes one has to do very accurate computer analysis of the spectrum.

Mössbauer Spectral Analysis:

Due to the presence of local effects one can expect the Mössbauer spectrum to be the sum of a large number of spectra due to iron atoms with different number of impurity atoms in the various neighbouring shells. The distribution of impurity depends on the type of alloy; ordered or disordered. The analysis of the disordered alloy spectra is simple because of the random distribution of impurities while in the case of ordered alloys the type of ordering has to be taken into account. As discussed above, in a dilute iron alloy the distibution of impurity is supposed to be random and therefore discussion of the spectral analysis of a random alloy only is presented here.

If an alloy is completely random and the measurable effect of the impurity is limited to the first n shells then the relative intensities of various spectra will be given by

$$P(l_1, l_2 \ldots l_n) = \frac{M_1! M_2! \ldots M_n! \; c^{l_1 + l_2 + \ldots l_n} (1-c)^{M_1 + M_2 + \ldots M_n - (l_1 + l_2 \ldots l_n)}}{(M_1 - l_1)! \, (M_2 - l_2)! \, \ldots (M_n - l_n)! \, l_1! l_2! \ldots l_n!}$$

$$\ldots (2.25)$$

where M_i is the total number of atoms in the ith shell, l_i is the number of impurity atoms in the ith shell, and C is the total impurity concentration. Using this formula for probability of various sites one can carry out the computer fit of the results and can separate out the various spectra due to iron atoms having different number of impurity neighbours. Iron has a b.c.c. lattice and therefore the number of nearest neighbours in first six shells are 8,6,12,24, 8 and 6. Stearns |59,69| first analysed her spectra of dilute iron alloys taking impurity only in the first nearest neighbour shell. Thus the spectrum was the composite of two hyperfine spectra: one due to impurity less system and the other with one impurity in the first nearest neighbour. Wertheim et.al. |62| analysed their spectrum taking into account the nearest as well as the next nearest neighbours effect and were able to get good fit. Various models have been used by various authors to get the good fit. Stearns |64| analysed the spectra taking the effect of first six shells into consideration and succeeded in obtaining a very good fit.

The identification of the satellite peaks in terms of various possible configurations is not an easy task. The problem becomes less complicated in the case of random alloys where one can identify the spectrum on the basis of calculated intensities of the patterns using Eq.(2.25). In this case the trouble arises in the identification of patterns due to 2nd and sixth shells because of same number of total

atoms in the shells. To, resolve this problem it is generally assumed that the disturbance caused by the impurity decreases rapidly with distance.

Cranshaw | 70,71 | used a different technique for satellite identification. He suggested that the quadrupole interactions and dipolar fields are present in alloys and depend upon ($3 \cos^2\theta-1$) where θ is the angle between the hyperfine magnetic fields and the principal axis of the electric field gradient. Thus these interactions will be different for different configurations and on the basis of these one can assign the spectrum of various configurations correctly. Using the discussed technique he observed that the largest contribution to ΔH_i comes from 1st and 5th neighbouring shells. This is in contradiction to the methods used in general where ΔH_i is a rapidly decreasing function of distance of the impurity from the iron nucleus. On the basis of previous studies | 63 | it has been found that the effect of impurities in a particular shell on the magnetic field is additive i.e. $\Delta H = 1_i \Delta H_i$ where 1_i is the number of impurity atoms in the ith shell and ΔH_i is the change in hyperfine field due to one impurity atom in the ith shell. This addition is applicable to inter shell also |64|. It has, however, been remarked by Stearns and Wilson |72| that the additivities of ΔH within inter shell and intra shell do not hold good at high impurity concentrations. The extremely good agreement between the experimental points obtained and the synthetic curve calculated by computer is shown in Fig. 2.6.
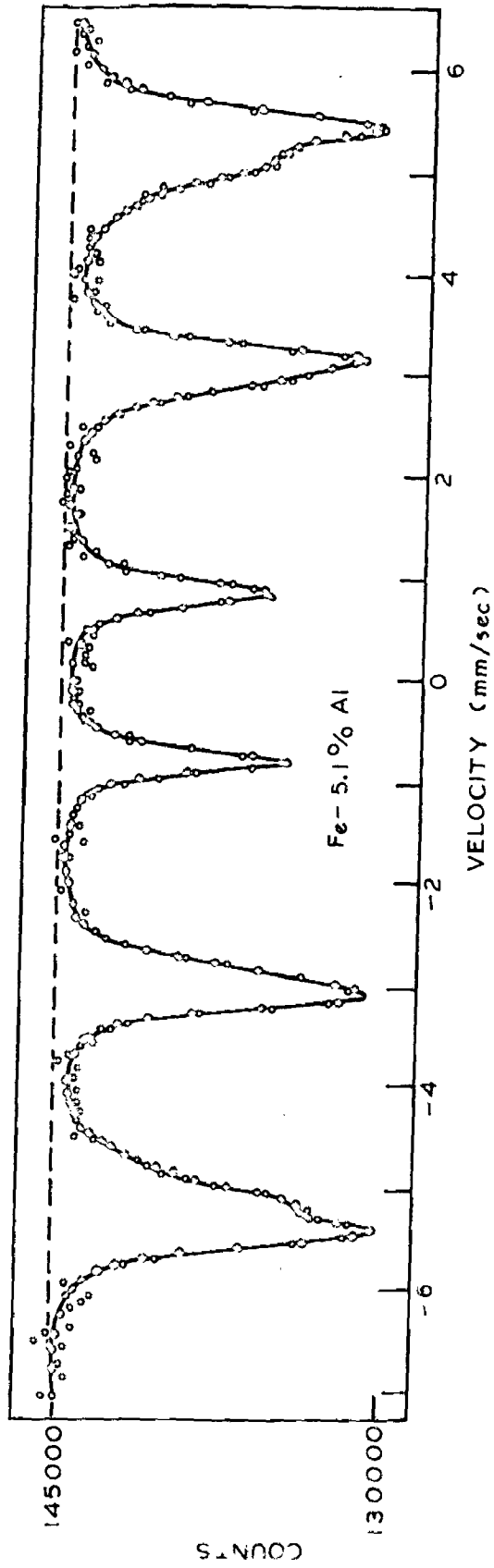
Fe − 5.1 % Al

VELOCITY (mm/sec)

COUNTS

145000

130000

FIG.2.6. COMPARISON OF THE SPECTRUM OF THE Fe−5.1at.% Al ALLOY (white circles) WITH THE
COMPUTER CALCULATED SPECTRUM (black circles).

2.7 PHASE DIAGRAMS

In the discussion of chapters 5 and 6 we shall freque-
ntly talk about the phase diagrams. It is ,therefore, pertinent
to give a brief information about the phase diagrams and vari-
ous terms which generally appear in their discussion.

When a system changes from one form to another it is
said to undergo a phase transition e.g. when a metal melts it
is said to undergo a phase change: the solid phase is tranfor-
med into the liquid phase; other phase changes occur at boiling
point (liquid changes into gas), sublimation point (solid
changes into gas) and the temperature of allotropic transfor-
mations, where one kind of solid phase is changed into another
kind of solid phase, etc.. The solid phases are always crys-
talline and differences among solid phases are the differences
in composition, crystal structure, or crystal dimensions.

Under ordinary conditions, with the pressure constant,
the phase changes in pure metals occur isothermally i.e. at a
fixed temperature. This is not in general true in case of
alloys. In alloys, the phase changes occur over a range of
temperature. Melting, for example, may begin at one tempe-
rature and not be completed until some higher temperature is
reached, the alloy meanwhile existing in a musty state compo-
sed of both the liquid and the solid phases.

A phase diagram also known as constitutional diagram
or equilibrium diagram gives information about the possible

phases formed between the constituents at different temperatures and compositions. The alloy composition is represented by horizontal scale and the temperature on the vertical scale. In a phase diagram a curve giving temperatures at which the melting is complete at different compositions is known as liquidus curve. This curve also denotes the beginning of freezing during cooling. Similarly, the solidus curve indicates the temperature at which the melting begins upon heating or at which freezing is completed upon cooling. Above the liquidus curve every alloy is in molten state and this region of the diagram is — accordingly labelled ''L'' for liquid phase or liquid solution. Below the solidus all alloys are solid, and this region is labelled ''α'' (solid solution). Fig.2.7 shows a typical phase diagram of metals Cu and Ni between a temperature range 500 to 1500°C|73|.

In general the alloy composition is expressed in ''weight percentage'', but for certain types of scientific work the '' atomic percentage'' scale is generally preferred. The two percentages can be interchanged through the following formulae:

$$\text{At.}\% \ X = \frac{(\text{wt.}\% \ X)/(\text{at. wt. } X)}{(\text{wt.}\% \ X)/(\text{at. wt. } X) + (\text{wt.}\% \ Y)/(\text{at. wt. } Y)} \ x \ 100$$

$$...(2.26)$$

and for wt.$\%$;

$$\text{wt.}\% \ X = \frac{(\text{at.}\% \ X) \ (\text{at. wt. } X)}{(\text{at.}\% \ X) \ (\text{at. wt. } X) + (\text{at.}\% \ Y) \ (\text{at.wt. } Y)} \ x \ 100$$
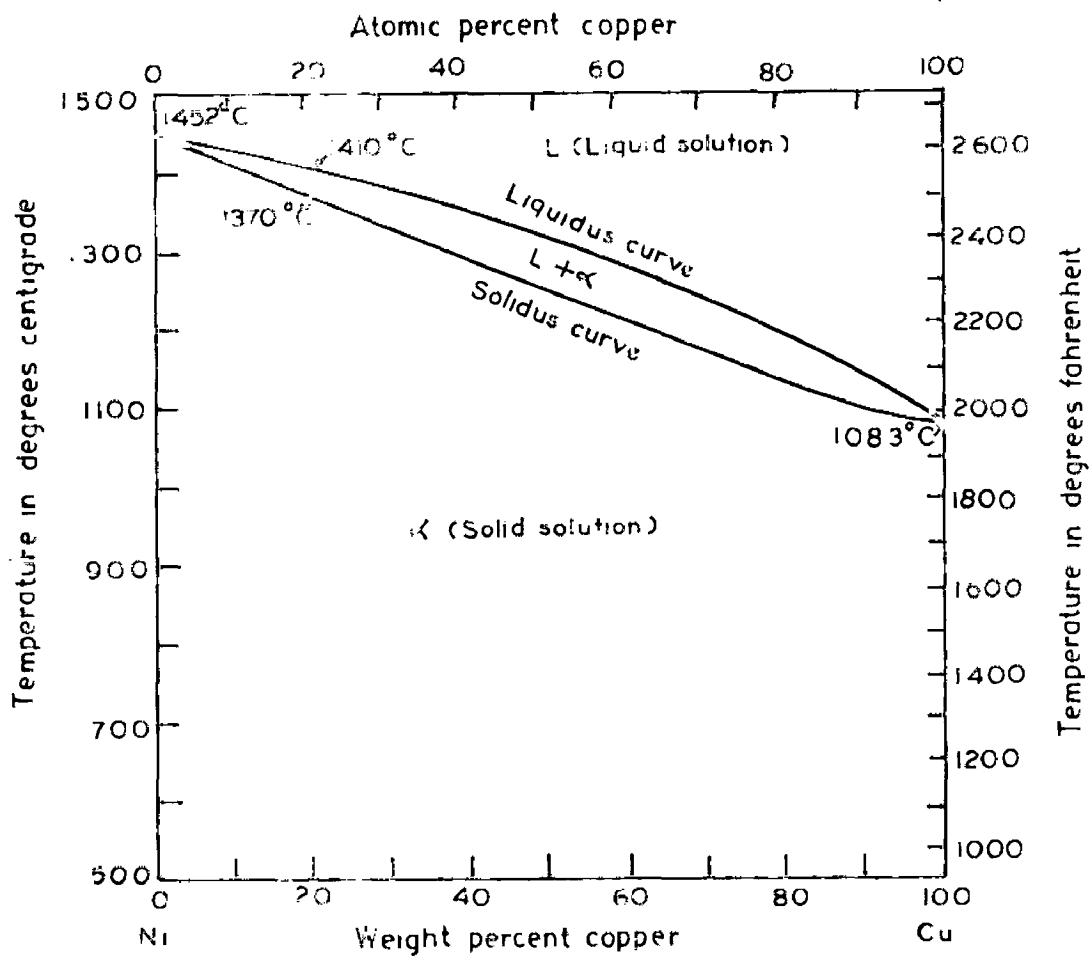
$$... (2.27)$$

FIG. 2.7 - THE NICKEL - COPPER PHASE DIAGRAM :

where X and Y represent the two metals in the alloy.

All properly constructed phase diagrams record the phase relationship only as they occur under conditions of equilibrium. This is necessary because the phase changes as observed in practice tend to occur at different temperatures, depending upon the rate of heat treatment. The equilibrium states that are represented upon phase diagrams are known as heterogeneous equilibria, because they refer to the coexistence of different states of matter. If two or more phases coexist then each phase must be in its lowest energy state. An exception to this rule that only true equilibrium states are recorded on the phase diagram is found in the occasional representation of so called metastable equilibria. In ordinary carbon steels, for example, there is found a solid phase, a carbide of iron (Fe_3C), that decomposes into graphite and iron under conditions that are favourable to the attainment of true equilibrium. The rate of decomposition of Fe_3C is very slow, however, under the most favourable conditions and is usually imperceptible under ordinary conditions. Because of its reluctance to decompose, this phase is said to be metastable, and it is represented on the usual (metastable) iron carbon phase diagram.

Depending upon the number of constituents, the phase diagram may be called as of unary, binary, ternary.....etc. type. Many phase diagrams are plotted between pressure and temperature. Here we shall discuss only about binary systems, which may be of many types as follows:

Binary isomorphous system is one in which two metals are mutually soluble in all proportions and in all states viz. liquid, solid and gas. The concept of liquid solution and gaseous solution is easy to understand. In solid solutions the solute metal simply enters and becomes a part of the crystalline solvent, without altering its basic structure. There are two types of solid solutions: (i) substitutional solid solutions, in which the solute atom occupies, in the solvent crystal, a position belonging to one of the atoms of the solvent metal, and (ii) interstitial solid solutions, in which the solute atom enters one of the vacant spaces between atoms in the lattice of the solvent crystal without displacing a solvent atom. Isomorphous solid solutions are always of substitutional type and both the metals involved must have the same type of crystal structure.

Other binary systems which do not come under this category of binary isomorphous systems may be classified as below:

(i) <u>Binary Eutectic Systems</u>: In these systems when one component is added to another component metal it causes a lowering of the melting point, so that the liquidus curve passes through a temperature minimum known as eutectic point. The composition at this point is known as eutectic alloy. The liquid is miscible in all proportions, but the miscibility in the solid state is limited. If we define as α and β the two solid phases which are the limited solid solutions of elements a and b then in this system if the composition at the eutectic point is heated then α and β phases react to form liquid. Upon cooling through

the eutectic temperature, the liquid decomposes into α and β.

$$L \underset{\text{heating}}{\overset{\text{cooling}}{\rightleftharpoons}} \alpha + \beta$$
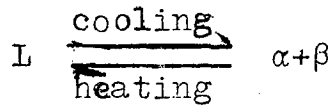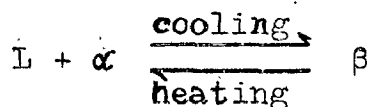
(ii) <u>Binary Eutectoid Systems</u>: These systems involve three solid phases. If two solid phases α and β are decomposed to a third solid phase γ then the system is said to be binary eutectoid system. The temperature at which the decomposition occurs is known as eutectoid temperature.

$$\gamma \underset{\text{heating}}{\overset{\text{cooling}}{\rightleftharpoons}} \alpha + \beta$$
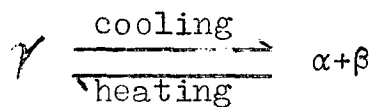
(iii) <u>Binary Peritectic System</u>: The peritectic reaction consists upon heating, of the decomposition of one solid phase into a liquid and a new solid phase

$$L + \alpha \underset{\text{heating}}{\overset{\text{cooling}}{\rightleftharpoons}} \beta$$

The systems which follow this reaction are known as binary peritectic systems.

(iv) <u>Binary Peritectoid Systems</u>: In this the solid phase β on heating decomposes into two new solid phases α and γ.
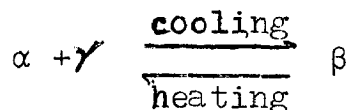
$$\alpha + \gamma \underset{\text{heating}}{\overset{\text{cooling}}{\rightleftharpoons}} \beta$$

(v) <u>Binary Monotectic Systems</u>: Another important three phase reaction of the eutectic class is the monotectic, in which one liquid phase decomposes with decreasing temperature into a solid phase and a new liquid phase.

$$L_I \xrightarrow[\text{heating}]{\text{cooling}} \alpha + L_{II}$$

The discussion of the phase diagram of any individual system will be given wherever needed in the following chapters. Various terms which are of use in the discussion of chapters 5 and 6 are briefed below:

Uper Critical Temperature: It is the temperature at which the steel structure is fully austenised.

Lower Critical Temperature: It is the temperature at which transformation from austenite to pearlite starts.

Annealing: It is a general term referred to any heating and cooling operation that is usually applied to induce softening. The specimen undergoing this treatment is first heated and then slowly cooled. More specifically, however, annealing may be divided into two operations, namely full annealing and process annealing. In full annealing, the steel is heated usually to about 100F (40°C) above the upper critical temperature and held there for the desired length of time followed by a very slow rate of cooling. The purpose of full annealing is to soften the steel and improve ductility; to relieve internal stresses present due to the previous treatment, and to refine the grain. In process annealing, the steel is heated to a temperature below or close to the lower critical temperature, followed by any desired rate of cooling. Its main purposes are to soften the steel partially and to obtain release of internal stresses. In this process grain refining is not complete as in full annealing.

Quenching: It is a process of fast cooling from an elevated temperature. Quenching is generally done to preserve the structure (or phases) obtained at the temperature from which the specimen is quenched. If one is interested in producing disordered structure, the quenching of the specimen from a temperature at which the structure is completely disordered is necessary.

Tempering: A fully hardened steel contains internal stresses and is extremely hard and brittle, in this condition even mild shock or load would cause failure and hence the steel must be toughened prior to use. Tempering is the general name given to that group of heat treatment processes which removes internal stresses from martensitic structure, and while retaining most of their hardness, replace **brittleness** with toughness. All tempering processes involve reheating the martensitic steel to some temperature well below the lower critical temperature, soaking to remove internal stresses and to allow all structural changes to go to equilibrium, followed by slow cooling to room temperature.

Aging: In a metal or alloy, a change in properties that generally occurs slowly at atmospheric temperature and more rapidly at higher temperatures is known as aging. It increases hardness and strength and ordinarily decreases ductility. Age hardening usually follows rapid cooling or cold working.

CHAPTER 3

INSTRUMENTATION AND EXPERIMENTAL TECHNIQUES

3.1 INTRODUCTION

As discussed in chapter 2, in Mössbauer effect experiment the recoil free emission of gamma photons in a source followed by the resonant absorption of a fraction of these photons in an absorber is studied. Thus, if the source and absorber have the same chemical environment then the resonant absorption will occur. Fortunately, the source and absorber have rarely the same chemical environment and thus either the resonant absorption will be partial or even disappear. The problem of the partial or complete destruction of resonant absorption was first overcome by Prof. R.L. Mössbauer |1| in his original experiment by providing a relative Doppler velocity between the source and absorber. His idea found almost universal acceptance and is supposed to be the only method for the reobservation of resonant absorption in case of different chemical environments of the source and absorber. Thus, if the source is moved relative to absorber with a Doppler velocity v then the extra energy provided to the source will be

$$\Delta E = \pm \frac{v}{c} E_\gamma \qquad \qquad \dots (3.1)$$

where c is the velocity of light and E_γ is the gamma ray energy. This extra energy will make possible the reobservation of resonant absorption. The velocity v is said to be positive and negative when the motion of the source is towards and away from the absorber, respectively.

The amplitude, of Doppler velocities required, depends on the natural line width Γ, gamma ray energy and the shift and splitting of various nuclear energy levels due to the hyperfine interactions. For Fe^{57}, these velocities range from a fraction of mm/sec. to about 10 mm/sec., the latter gives an energy modification of $\Delta E = 4.8\times10^{-7}$ eV. Thus with a velocity drive which can provide velocities within $\pm$ 10 mm/sec. hyperfine interactions causing the shift and splitting of the order of 4.8×10^{-7} eV of 14.4 keV energy levels can be investigated. Mössbauer effect thus provides a precise method of measuring very small energy differences.

One, therefore, requires a highly stable and accurate velocity drive for Mössbauer experimentation. The main emphasis in this chapter will be laid on the discussion of drive systems. A brief review of existing drive systems along with the detailed discussion of drive unit fabricated by us will be presented.

3.2 MÖSSBAUER SPECTROMETERS

The following are the main ingredients of the Mössbauer spectrometer.

(A) Mössbauer source and absorber (or scatterer)

(B) Mössbauer drive to provide controlled and well defined relative velocities.

(C) Detection and counting system

In addition to these basic components one needs some other auxiliary systems e.g. furnace and cryostat (for

temperature dependent studies), external magnetic field, high pressure devices, temperature controller etc. to get more useful informations with the help of . Mössbauer spectroscopy.

(A-i) MÖSSBAUER SOURCE

Mössbauer source is a radioactive isotope diffused into a metallic lattice (host matrix) and gives recoil free gamma radiation. There is no hard and fast procedure to prepare good sources. Benezer-Koller, in his review article |74|, pointed out that the preparation of a good source requires the combined talents of a chemist, metallurgist, nuclear physicist and also a fair amount of good luck.

Generally used procedures of putting the isotope into the lattice are; ordinary synthesis of the compound having parent nuclei |75|, doping into the material under investigation |76|, and the diffusion of isotope into a suitable lattice so as to give a single unsplit line. Some of the important qualities which a Mössbauer source should show are high Lamb-Mössbauer fraction, narrow line width, long life time, less interference of Mössbauer radiation with other radiations present, low internal conversion coefficient. Also the source material should be chemically inert, so that the chemical composition does not change by oxidation or hydration.

For the studies on iron and its alloys and compounds, the Co^{57} source is evaporated or electroplated onto a suitable host matrix and annealed in vacuo at high temperatures. Various

host lattices e.g. Cr, Cu, Pd, Pt, Rh and stainless steel have been tried but Cr, Cu, Pd and stainless steel are the most common. Stainless steel and chromium give relatively broader line widths while Cu matrix is chemically less stable. Palladium matrix seems to be the most suitable. This gives good Lorentzian lines and the line width obtained corresponds to the theoretical minimum value. These are relatively inert chemically and have little interference of other radiations when prepared properly.

Throughout the work reported here Co^{57} Mössbauer sources in Cu and Pd lattices with initial activities of 3.5 mCi and 5 mCi respectively were used. The sources were supplied by Bhabha Atomic Research Centre, Bombay, India.

(A-ii) ABSORBERS (OR SCATTERERS)

Mössbauer effect experiments can be performed both in transmission as well as scattering geometry. But the use of transmission geometry is frequent. The reason lies in the ease with which experiments can be performed in this geometry. In transmission geometry the only complication arises in the preparation of suitable absorber which should have finite thickness and should be homogeneous. As discussed in chapter 2 the line width depends on thickness and to reduce the thickness effect on line width very thin absorbers should be used. To obtain uniformity some inert material is used. The absorber mounting is also important and it must be Mössbauer isotope free as otherwise, even in traces, it may, some times, complicate the whole Mössbauer spectrum |77|.

However, one can get important informations on some systems like surfaces, thin films etc. only by performing Mössbauer experiments in scattering geometry. But the use of high activity source, careful attention to the geometry of detector and shielding problems are the few important factors which restrict the frequent use of scattering geometry. Here the measurements have been done in transmission geometry only and copper (pure metal) rings or perspex holders were used as the absorber mountings.

(B) THE DRIVE SYSTEM

Since the discovery of Mössbauer effect a great number of methods have been developed to provide the necessary Doppler velocity between the source and the absorber. All the developed devices can be basically divided into two classes - constant velocity drives and constant acceleration drives.

(a) CONSTANT VELOCITY DRIVES

The constant velocity drive moves either the source or the absorber with a controlled constant velocity for a preset time during which the gamma counts are recorded. This type of drives may be either purely mechanical or electrome-chanical. The purely mechanical type drives mainly employ various devices that transform rotational motion (given by the synchronuous or d.c. motors) to constant velocity motion. These include rotating inclined discs |78|, cams |79|, lead screws |80|, lathe |81|, rotating cylinder |82|. linkage, cable or chain |83| and crank |84|. The electromechanical

drives usually require a loudspeaker for mechanical motion, a transducer as a velocity sensor and a negative feed back circuitry to reduce extraneous motion due to building vibrations, microphonics etc.. In some exceptional cases hydraulic |85|, pendulum drives |86| and those making use of Piezo electric effect | 84,87| have also been used.

The purely mechanical type constant velocity drives appear to have the following advantages. These require very little costly electronics and can be built easily, the best type can provide very high absolute accuracy, it is easier to cool and heat the source (since the drives are normally very sturdy).

There are certain disadvantages of these mechanical drives which restrict their use. The elimination of extraneous vibrations is more difficult than in electromechanical drives, mechanical wear and tear generally causes trouble, it is usually only possible to use these drives in the constant velocity mode. This requires the building up of spectrum point by point and thus fluctuations in voltage and drift in counting system become important.
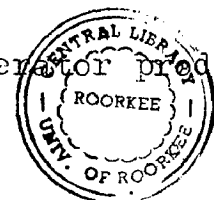
The electromechanical constant velocity drive takes care of most of the difficulties and disadvantages of purely mechanical type drives. But the problem of long term unstability remains here as well and thus limits their use in most of the experiments.

(b) CONSTANT ACCELERATION DRIVES

In this class of drives a signal generator produces

a desired increase in voltage with time. This voltage is transformed into velocity in the transducer providing constant acceleration. For stability a feedback arrangement is incorporated in these systems and this in turn is generated from another velocity sensing transducer. The feedback arrangement is particularly called for reducing extraneous motion due to building vibrations, microphonics etc.. In such a set up, employing a multichannel analyser,a single run gives the entire Mössbauer spectrum. Depending on the number n of the channels in the analyser each period T of the velocity change is divided into n intervals so that ith channel of the analyser records the number of counts received in the short period of the time from $t_a = \frac{(i-1)T}{n}$ to $t_b = \frac{iT}{n}$ of each period, which thus corresponds to some small range of velocities between v (t_a) and v (t_b). This class of drives is most widely used because of being unaffected (shape of the spectrum) by the small changes in the gross counting rate of the gamma ray pulses due to the line voltage fluctuations, detector and amplifier drifts etc., This type of drive has been fabricated and used by us and will now be discussed in detail.

The drive may chiefly be divided into two parts (i) transducer (ii) Driving and controlling circuitry.

(i) TRANSDUCER

Transducer is a device which receives signal (electrical, mechanical or acoustical) from one or more media or transmission systems and supplies related signal (not necessarily of the

same type as the input) to one or more other media or transmission system. Thus an electromechanical transducer is a device which converts electrical energy into the mechanical energy. The transducer used in Mössbauer studies for providing precisely controlled relative Doppler velocities can be divided in two broad categories. First category makes use of two loudspeakers type systems either coupled face to face or back to back |88,89|. In this, one loudspeaker is used to produce the motion and the other to sense it. Such type of devices can be used only where velocities of the order of few centimeters are required. The second class of transducers discussed in Ref. |90| consists of a loudspeaker coupled to a commercial velocity transducer. This commercial velocity transducer is used to sense the motion produced by the loudspeaker. The other transducers reported in the literature are only the modifications of these two types to obtain the desired working performance. The transducer used by us belongs to the first category which utilizes two loudspeakers.

MECHANICAL DESIGN OF TRANSDUCER

The diagram of the electromechanical transducer is shown in Fig. 3.1a. It essentially consists of two commercial type (Phillips - Norelco 9710 AM of 10″ size) loudspeakers mounted back to back with brass nuts and bolts. To avoid the interference of the magnetic field of one magnet on the other an aluminium spacer between the two magnets has been used. The magnetic assembly provides the field over a length of 10 mm
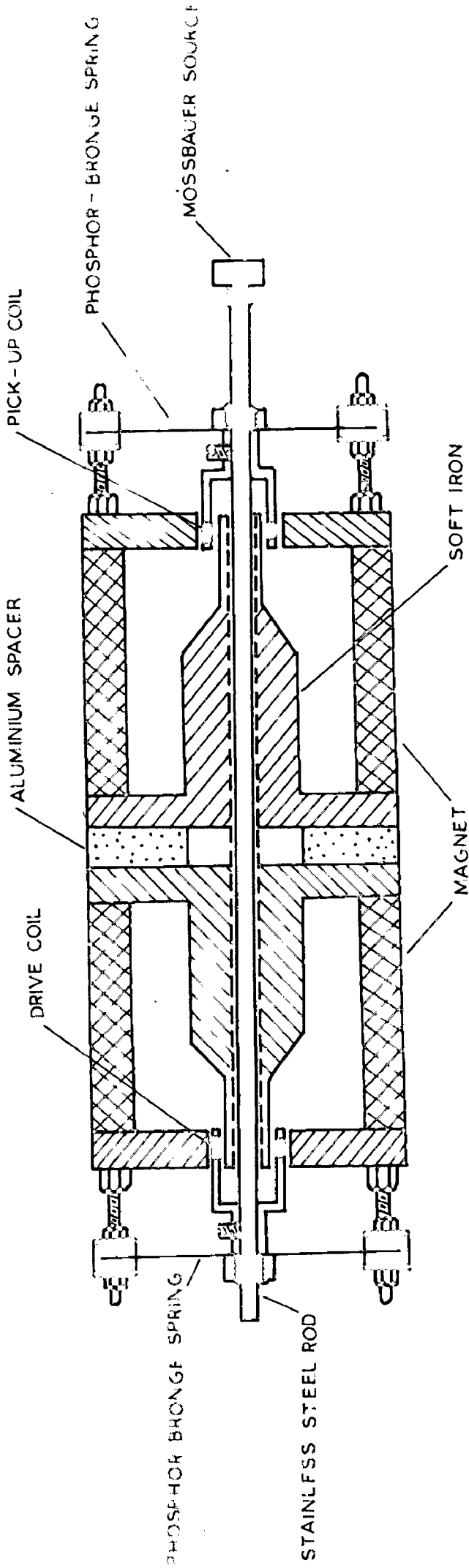
PHOSPHOR - BRONZE SPRING

MÖSSBAUER SOURCE

PICK - UP COIL

PHOSPHOR - BRONZE SPRING

STAINLESS STEEL ROD

ALUMINIUM SPACER

DRIVE COIL

SOFT IRON

MAGNET

FIG. 3.1(a). - MECHANICAL DIAGRAM OF THE TRANSDUCER.

but the coils of length 5 mm only were used. This was done to ensure that the coils always remain in a uniform magnetic field. The coils were wound on a 5 mm leatheride paper instead of any metallic former for eliminating the eddy currents. Following are the details of the coils:

DRIVE COIL

No. of turns   = 64 in two layers

gauge of wire   = 32 gauge enamelled copper wire

Impedance   = 83 ohm

PICK-UP COIL

No. of turns   = 800 in 4 layers

gauge of wire   = 46 gauge enamelled copper wire

Impedance   = 900 ohm

These two coils were coupled through a stainless steel rod. Two phosphor bronze springs of shape shown in Fig. 3.1b were used for mounting the coils at proper positions. This shape provides minimum radial displacement. The stainless steel rod and the springs material and shape were chosen in order to have the secondary resonance frequency as high as possible. This is an important consideration to have a good velocity drive set up as discussed by many workers. The fundamental resonance frequency of our transducer is 23 Hz while the secondary resonance comes at 6. kHz.

CHARACTERISTICS OF TRANSDUCER

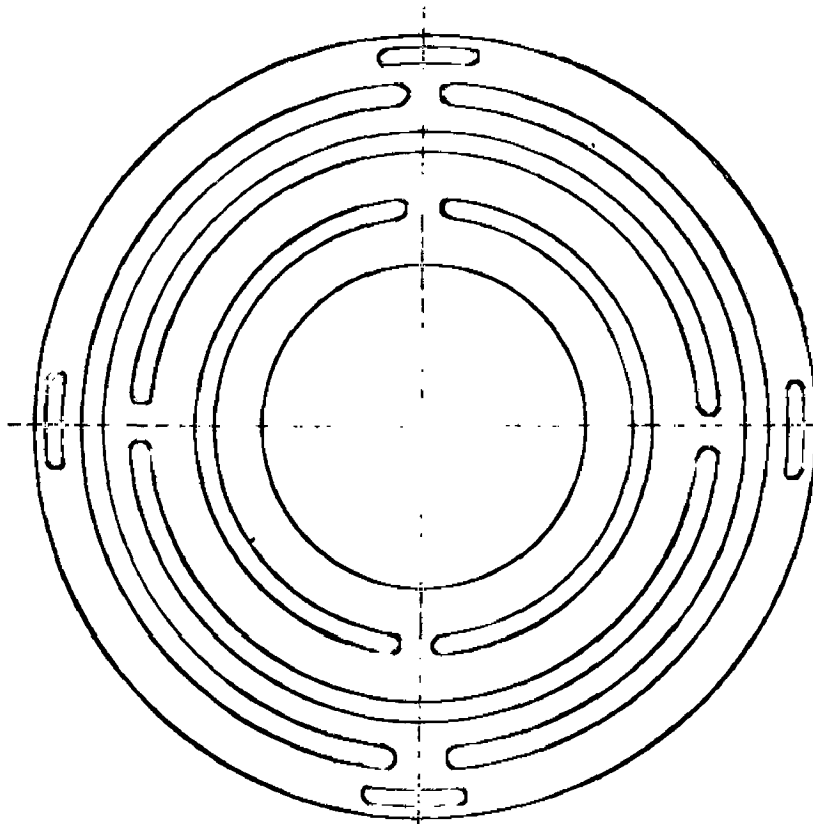We have plotted the Nyquist diagram near the fundamental

FIG.3.1(b) _ PHOSPHOR BRONGE SPRING .

frequency in Fig. 3.2 which represents the output voltage

as a function of input current of the transducer. This diagram

suggests that the maximum of the open loop transfer curve lies

at the fundamental resonance frequency (23 Hz) of the drive.

At this frequency the gain obtained will be maximum, but

slightly above or below this frequency the open loop gain as

well as the phase angle change sharply. Thus if we work at

this fundamental frequency (23 Hz) then the pick-up signal

amplitude and phase will change very much due to any instability

in the transducer mechanical construction of the operating

frequency. In order to avoid this problem we have preferred

to work at a lower frequency (10 Hz). A slight change in

frequency here will not cause any measurable change in the

phase or the gain of the pick-up signal. The gain however

will be small at this frequency and this has been taken into

consideration while designing the pick up and the feedback

electronics system. The pick-up coil gives a signal of $\sim$ 0.2 V

peak to peak at a velocity of 16 mm/sec. and frequency 10 Hz.

across an impedance of 900 Ω. The gain of the feedback ampli-

fier is high enough to obtain a good and stable mechanical

motion of the system.

(ii) DRIVING AND CONTROLLING CIRCUITRY

This is required to produce the desired motion in the

armature of the transducer. Since here the Mössbauer spectra

have been recorded in a constant acceleration mode, the velo-

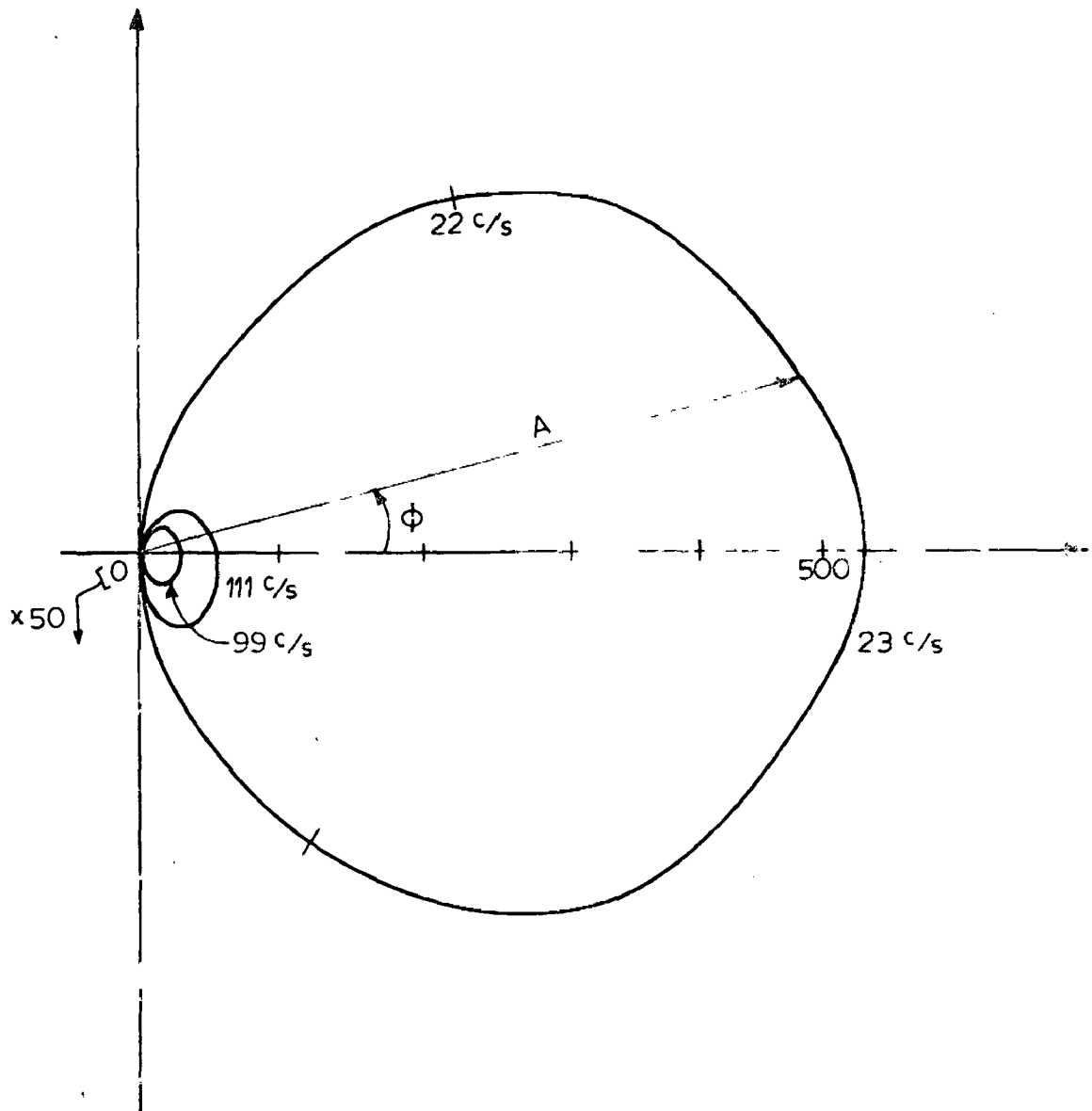city increases or decreases linearly with time between a chosen

F.G.3.2. NYQUIST DIAGRAM OF TRANSDUCER RFPRFSFNT'NG OUTPUT
VOLTAGE VS. INPUT CURRENT.

positive and negative velocity range. We therefore need a parabolic electrical signal to produce constant acceleration in the rod on which the source is mounted. Thus, in this section we will discuss the production of parabolic motion of the armature.

When a parabolic wave is given to the drive coil it induces the electrical signal in pick-up coil which will be a triangular wave. But due to the poor transfer ratio from electrical to mechanical motion and vibrations produced in springs, rod etc. the induced signal on the pick-up coil will not be exactly triangular. To compensate for this extra motion a negative feedback system was introduced. In this circuit the actual motion (as reflected in the pick-up signal) is compared with the reference signal (good triangular wave form). The difference between the two (Error signal) after ·proper amplification, integration and phase adjustment is feeded back to the drive coil. Thus, this negative feedback compensates the extra motion. The output of this feedback unit works as the input for the power amplifier. This power amplifier cir-cuit is introduced to increase the current necessary to drive the armature of the transducer. Thus, the discussion of driving and controlling unit includes the generation of a parabolic wave form, negative feedback system, power amplifier and, of course, the power supply system. Since we have int-roduced one integration unit in the feedback system so the following discussion include generation of a reference tri-angular wave form, feedback circuit, power amplifier and

power supply.

REFERENCE GENERATOR

The above discussion demands the generation of a good triangular voltage wave form called as reference wave form. Since the data are stored in a multichannel scaler (MCS) mode, the time sweep of the MCS and the velocity sweep of the transducer should be in phase. This requires either an external synchronization unit or demands the use of square wave produced by using the last bit of the binary address scaler, which defines the first and second half of the MCA memory, for the generation of reference signal necessary to produce the transducer velocity sweep. We have chosen the latter alternative and have used the square wave taken from the output of last bit of the multichannel analyser memory. This square wave must be symmetrical to a high degree in order to ensure equal slopes on the rising and falling part of the triangular wave. To make it a good square, an extra circuit known as squarer circuit was used. To make the squarer circuit free of hysteresis effects, and further to ensure temperature stability, the output of the high gain, fast rising amplifier has been clipped by zener diodes. The other operational amplifier integrates the square wave with the built in RC components. The output of the integration unit is the triangular voltage wave form. Since, the integration has been achieved through a RC network hence a d.c. balancing has been provided in the circuit for the d.c. offset. The distortion in the reference wave form, generated

as discussed above, was found to be very small and in every case less than that from one of the standard wave generator. The complete circuit diagram comprising squarer and integrator is shown in Fig.3.3. To obtain different magnitudes of the reference wave form a ten turn helipot of value 5 k has been used at the output.

FEEDBACK CIRCUIT

Basically the feedback circuit used consists of a d.c. amplifier, an integrator with internal gain control, and a high frequency filter circuit. The error which is the difference of reference signal and the signal generated across the pick-up coil is given to a d.c. amplifier with a gain of 50. A d.c. balancing circuit has been provided with the d.c. amplifier to keep the d.c. level at zero. This amplified error is fed to the integrator through a coupling condenser (unpolarized) to avoid the effect of previous circuit on the other circuits. A RC network has been used for integration. Since the signal is of low magnitude, the use of only capacitance as a integrating device will saturate the signal due to its too high open loop gain. An internal gain control has been provided with the integrator. The integrated signal which is parabola in shape is given to the drive coil through a high frequency filter circuit. A further gain control has been provided at the output point. The total gain achieved through the feedback circuit is of the order of 3750. To see the amplified error on the oscilloscope an extra d.c. ampli-
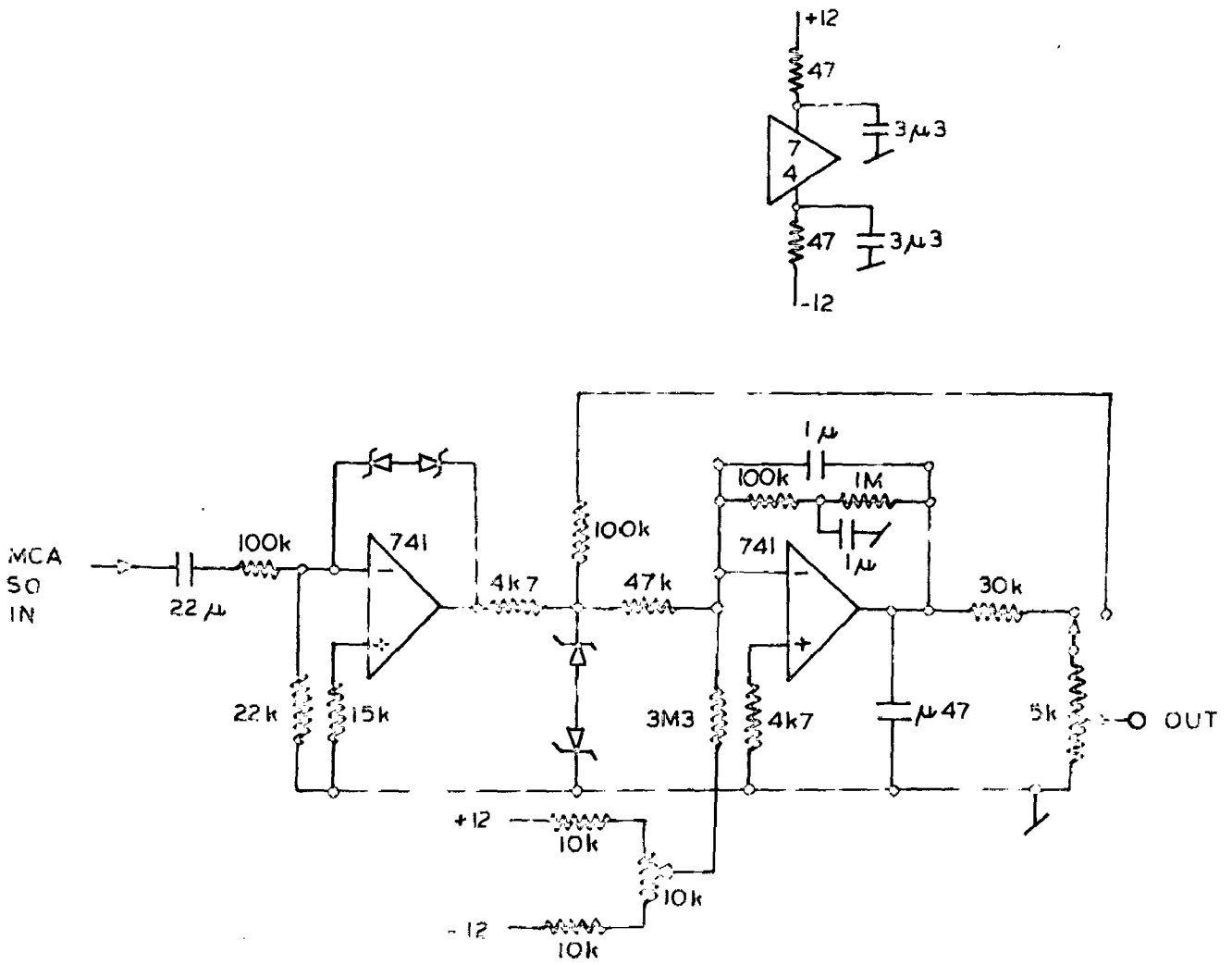
FIG.3.3 REFFRENCE WAVE GENERATOR.

fier (with a gain of 3) has been used to further amplify the error. The band width of the total feedback circuit has been adjusted such that it is always below the acoustic frequency of the transducer. The complete feedback circuit is shown in Fig. 3.4.

POWER AMPLIFIER CIRCUIT

The amplified parabolic signal is not sufficient to drive the massive transducer armature due to its low current value. Hence current amplification is necessary and has been achieved by the power amplifier circuit shown in Fig. 3.5. The parabolic wave form is given at the input through an unpolarized condenser. A d.c. balancing circuit has been provided to adjust the d.c. level. This amplified parabola is given to the current amplifier circuit. To keep the band width below the acoustic resonance frequency one condenser in parallel with a resistance has been used in the feedback circuit of the power amplifier. The power amplifier delivers 20 W power across a resistance of 8Ω.

POWER SUPPLIES CIRCUIT

The powers supplied to the above drive circuits have been generated separately using a dual trace power supply system shown in Fig. 3.6. This is a conventional low voltage supply and therefore operating details are not discussed here.

DRIVE RESPONSE

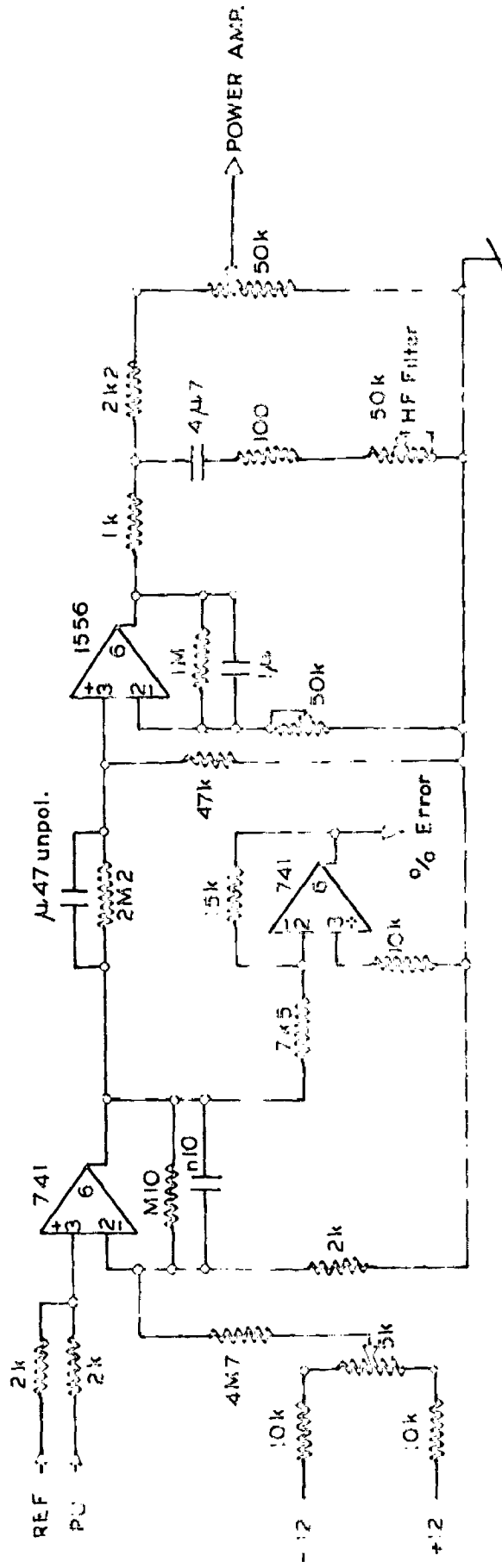The drive response showing the error to reference ratio
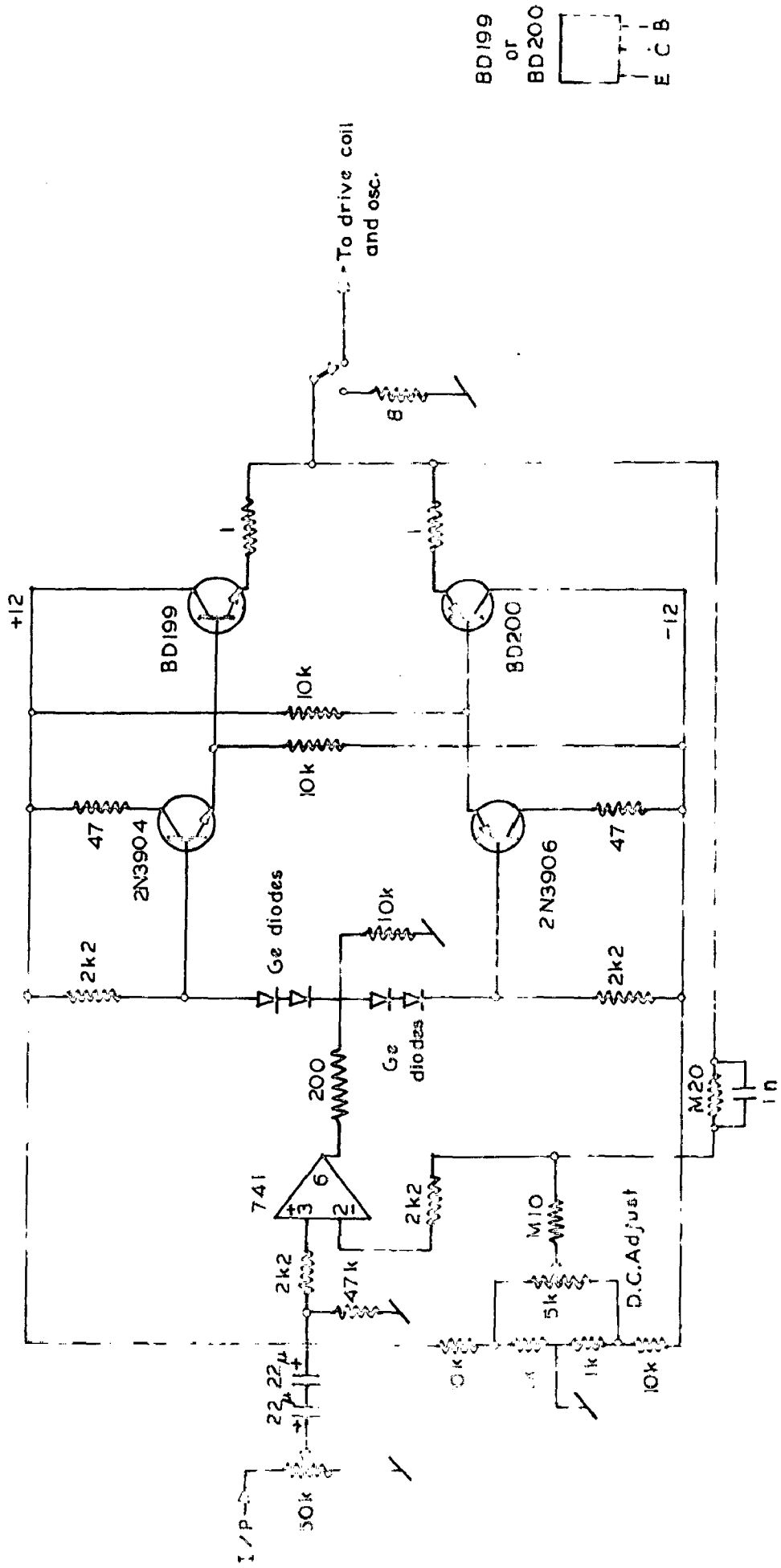
FIG. 3.4 - FEED BACK CIRCUIT.

FIG. 3.5 - POWER AMPLIFIER.
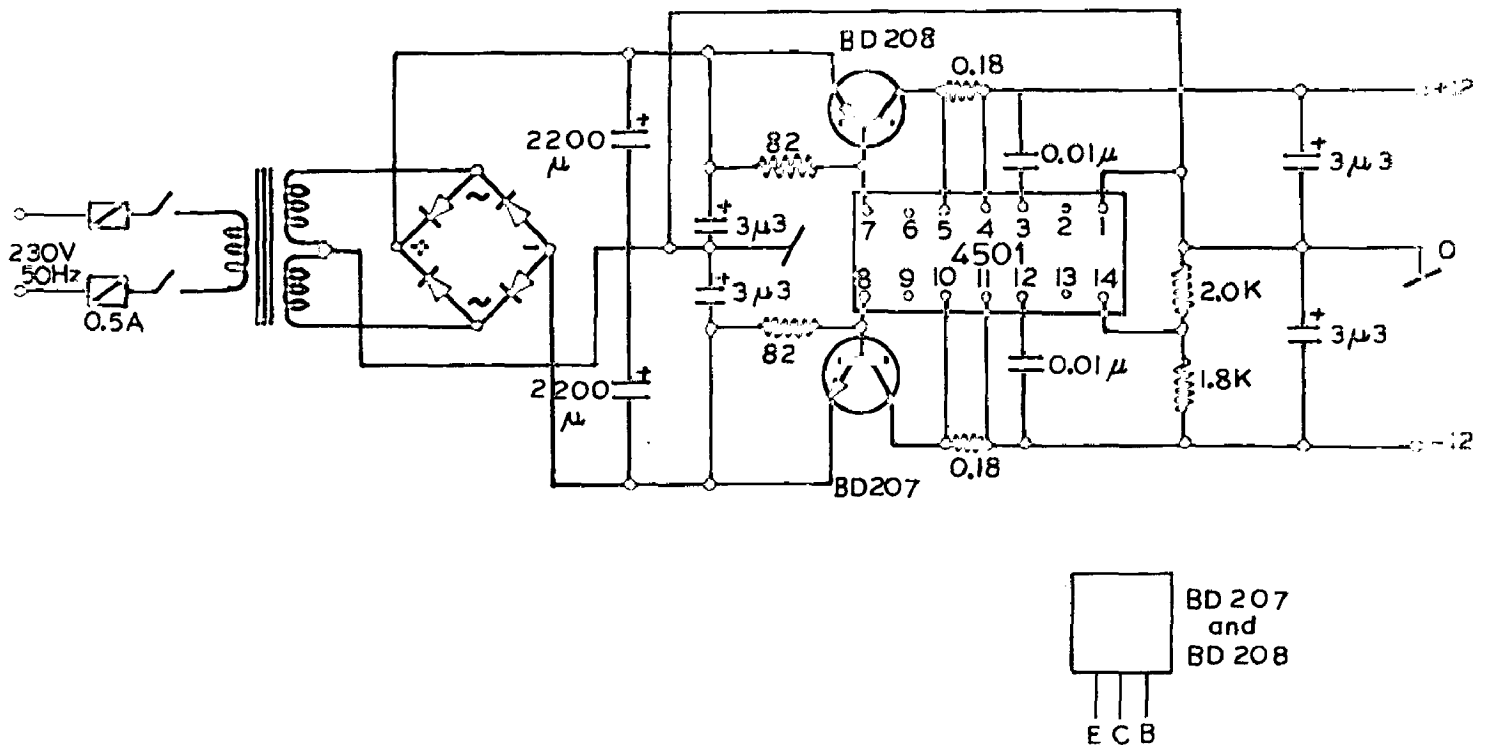
FIG.3.6. DUAL TRACE POWER SUPPLY CIRCUIT.

is shown in Fig. 3.7. The percentage error comes out to be
0.2 percent at the most used velocity.

(C) DETECTION AND COUNTING SYSTEM

It is desirable to detect the Mössbauer gamma rays as
efficiently as possible, while discriminating against the
remainder of the γ-rays, and other radiations such as X-rays.
Since Mössbauer effect has been observed only for gamma rays
whose energies lie between few keV to 150 keV one needs the
low energy detection techniques. In general three types of
detectors which have been in use in this range are: .

  (i) Proportional counters

 (ii) NaI (Tl) scintillation counter, and

(iii) Li drifted Ge counter (semiconductor radiation detector).
A comparison of the resolution of these counters is given in
Fig. 3.8

Proportional counters are limited in use to the energy
range below 40 keV, since their efficiency drops rapidly
with increasing energy. But for gamma rays having energy below
20 keV these give the best resolution |91| of the order of 10
percent with sufficient efficiency |92|. Proportional counters
are normally filled with Xe, Kr, or Ar with methane or nitrogen
as a quenching gas. The detection efficiency of a sealed pro-
portional counter filled with 90% krypton and 10% argon is
quite high (60%) as its absorption edge is slightly less
than 14.4 keV. The life of a sealed proportional counter is

Reference

Error

x 150
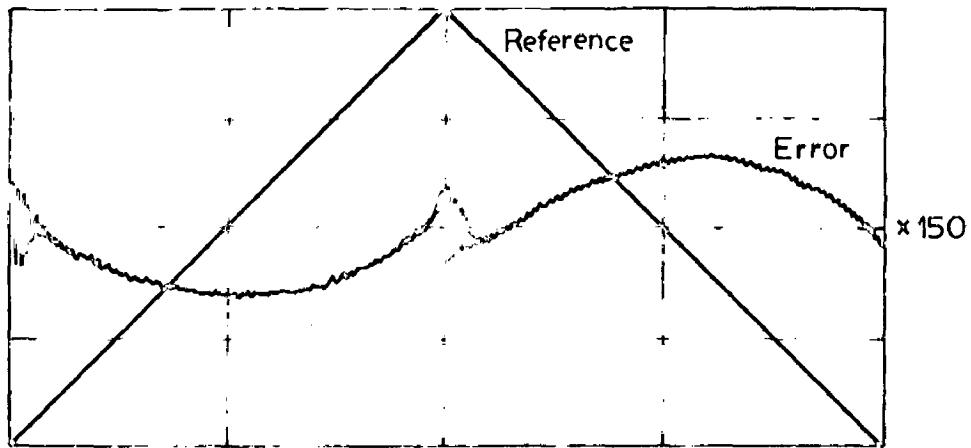
NOTE — The error shown is 150 times of the actual error .

FIG. 3.7 _ DRIVE RESPONSE IS SHOWN . THE ERROR IS
0.2 % OF THE REFERENCE .
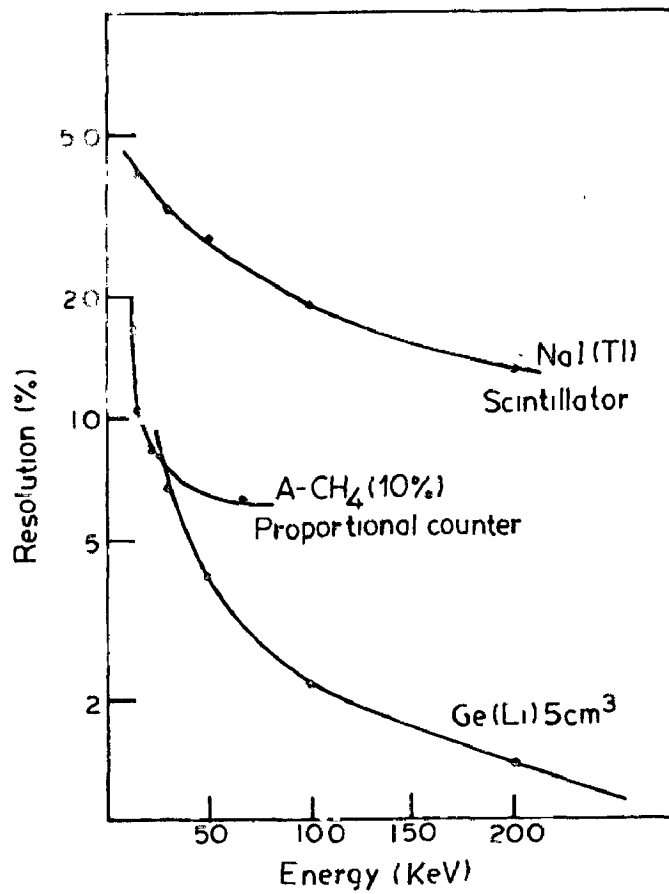
FIG.3.8. TYPICAL RESOLUTION OF COMMONLY

USED γ-RAY DETECTORS.

short and hence flow counters are preferred.

The scintillation-crystal type detector is frequently used for γ-rays with energies in the range 50-100 keV. Ordinarily about 1 mm thick NaI (Tl) crystals are used. As the energy of the radiation increases, proportionately thick crystals are required. These have very high detection efficiency but resolution decreases with decreasing energy of the gamma photons.

If pulse height resolution is a problem then solid state lithium drifted silicon or germanium detectors may be used. A resolution of 1 keV at 50 keV gamma ray energy can be easily obtained with these detectors. But these detectors are very costly (ten times costly than scintillation or proportional counters) and they must be kept at liquid nitrogen temperature.

In view of the merits and demerits of the various detectors, we decided to use sealed proportional counters (filled with 90% Ar and 10% methane) supplied by Bhabha Atomic Research Center, Bombay, India. The operating voltage was of the order of 1900 volts and the energy resolution obtained was 14%.

The block diagram of the complete Mössbauer spectrometer used during the reported measurements period is shown in Fig. 3.9. The gamma radiation of Co^{57} Mössbauer source after absorption in an absorber was detected using an argon-methane filled proportional counter. The necessary high voltage
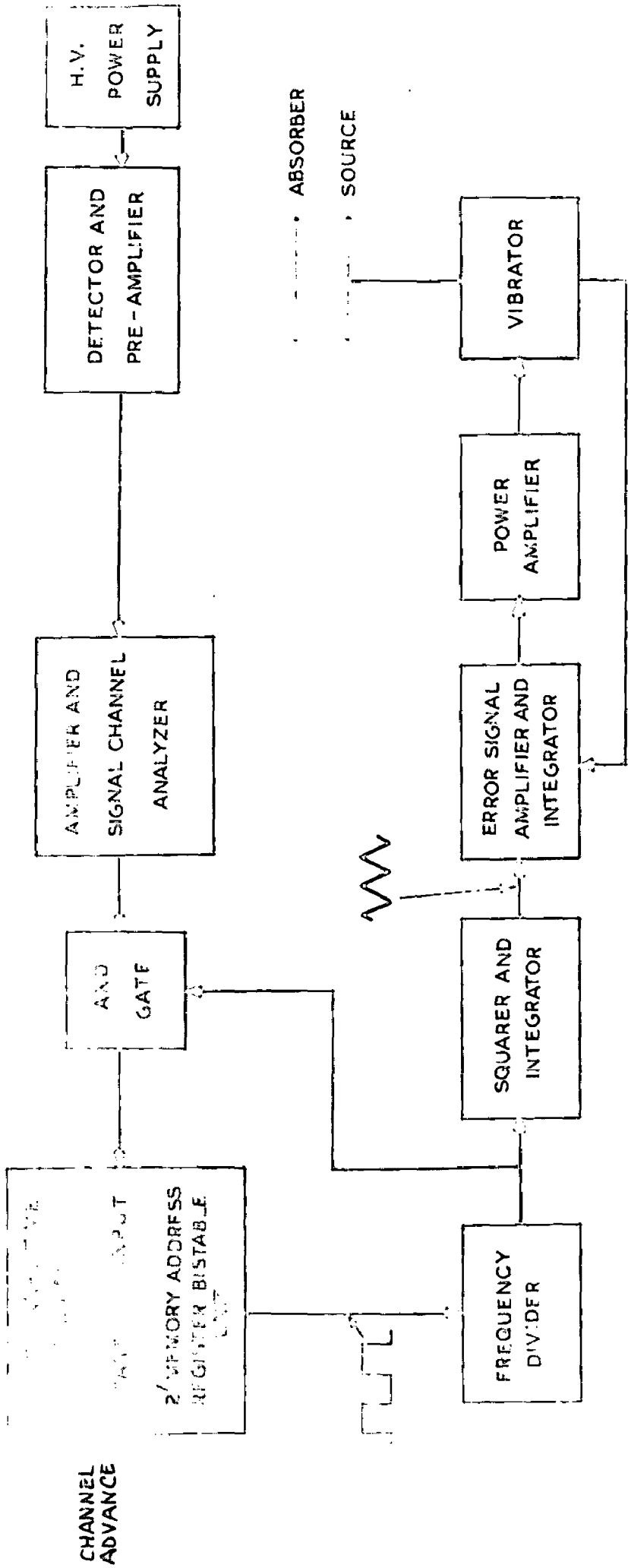
FIG. 3.9. BLOCK DIAGRAM OF MÖSSBAUER SPECTROMETER.

($\sim$ 1900 volts) for the proportional counter was provided from stablized power supply supplied by ECIL India. The proportional counter was coupled to a linear amplifier and single channel pulse height analyser (both supplied by ECIL India) through a charge sensitive pre-amplifier Fig. 3.10 and the emitter follower which is necessary for impedance matching. The discriminator setting of the pulse height analyser was adjusted so that the photo peak corresponding to the 14.4 keV is selected. The output of this analyser was given to the multichannel analyser (MCA), working in the multiscaling mode of operation, through the drive circuitry. The MCA is advanced with an externally generated advancing signal (a quartz crystal has been used for stability) as shown in Fig. 3.11. Thus MCA can be operated at any desired frequency of 5 or 10 Hz approximately which has been generally used during the measurements period. The synchronization between the time sweep of the multichannel analyser and the velocity sweep has been achieved by using the output from the last bit of the binary address scaler, which defines the first and second half of the MCA, for producing square wave used for drive. Thus the time sweep of MCA will be synchronized with the velocity sweep of the transducer. A 256 channel analyser (model No. NS - 601) supplied by Northern Scientific/INC. Wisconsin, U.S.A. was used for data storage. The maximum storing capacity of the MCA is 10^5 counts/channel. In the normal way at 10 Hz or 5 Hz MCA gives the total spectrum in first 128 channels and the mirror image of the first spectrum in the second half of the memory. This reduces the resolution

FIG.3.1C - CHARGE SENSITIVE PREAMPLIFIER.
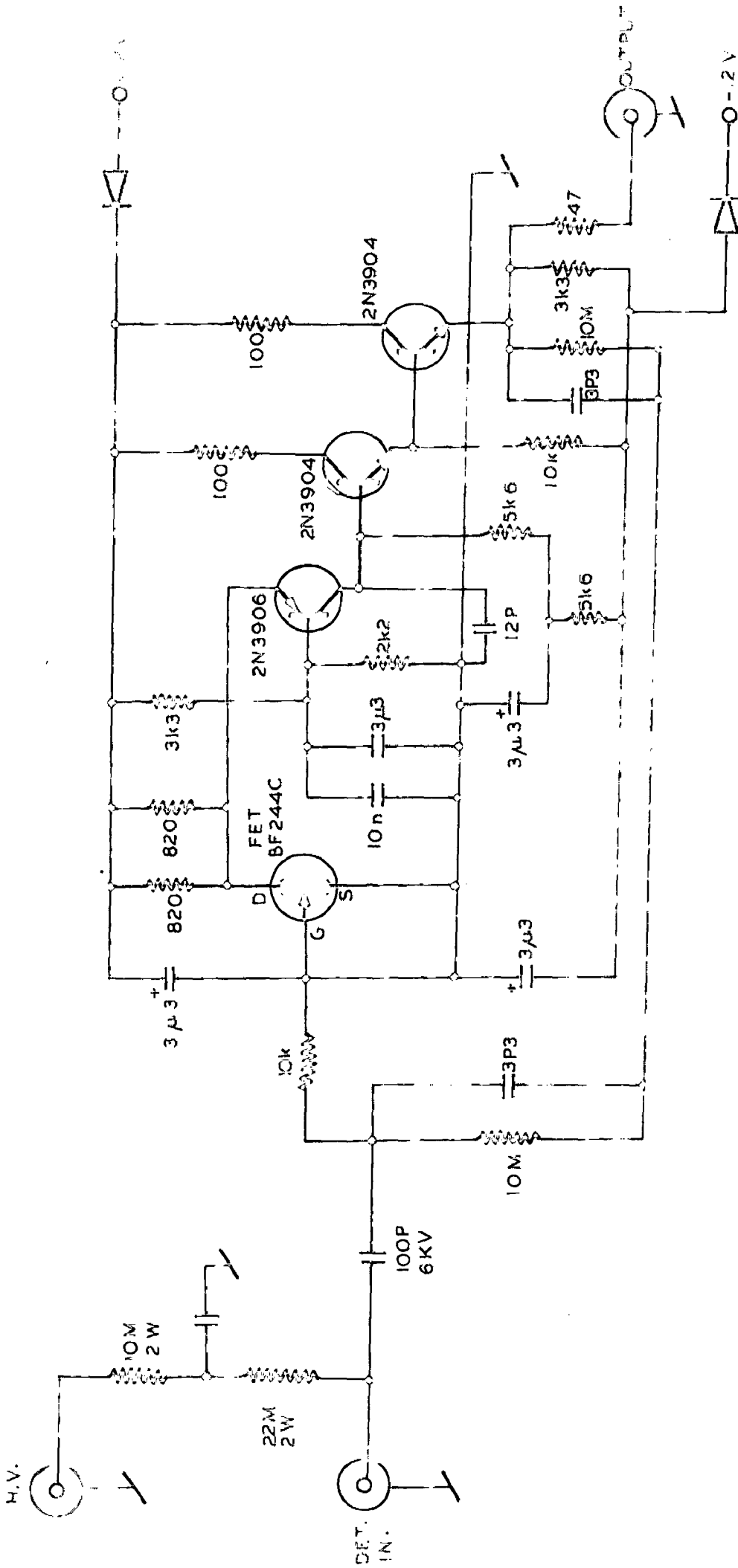
NOTE. - The BF244C input fet is selected to have $I_D(0) \geq 17mA$. If unselected units is used for replacement, remove one 820Ω resistor.
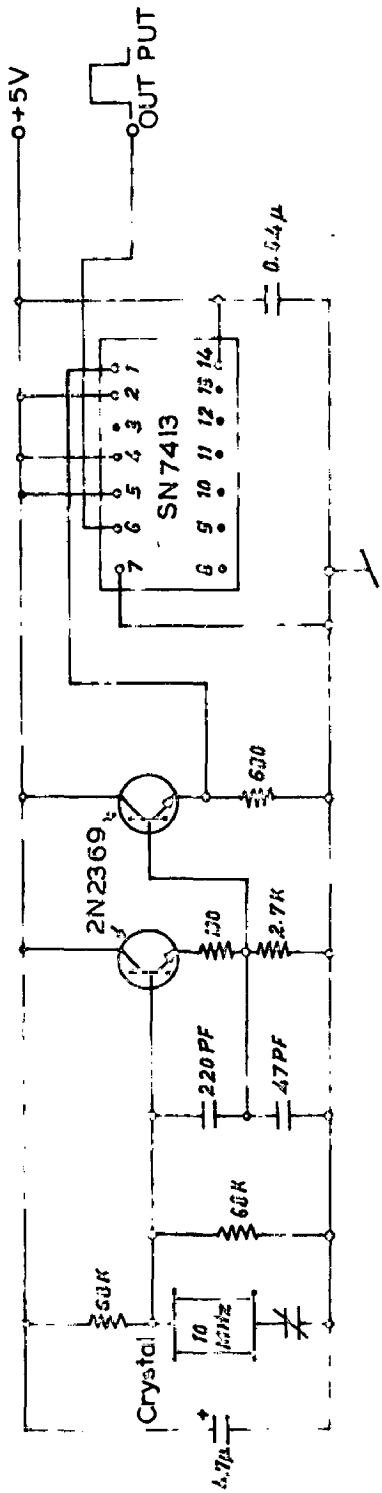
10MHz CRYSTAL CONTROLLED OSCILLATOR
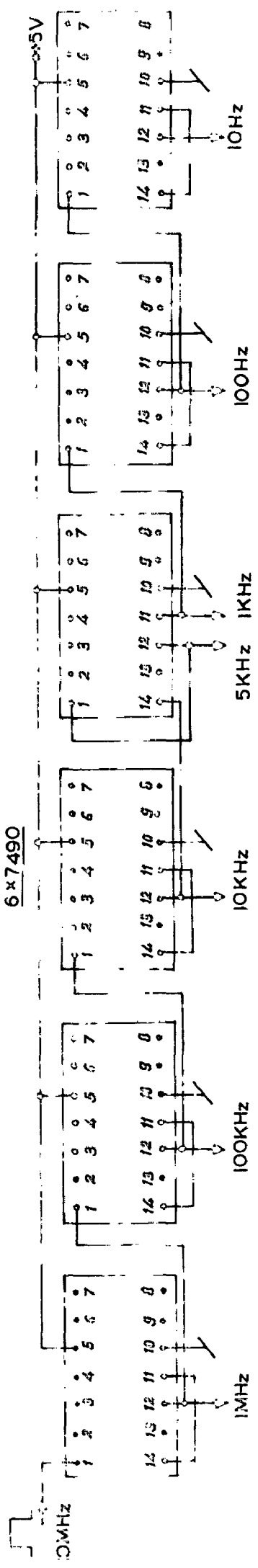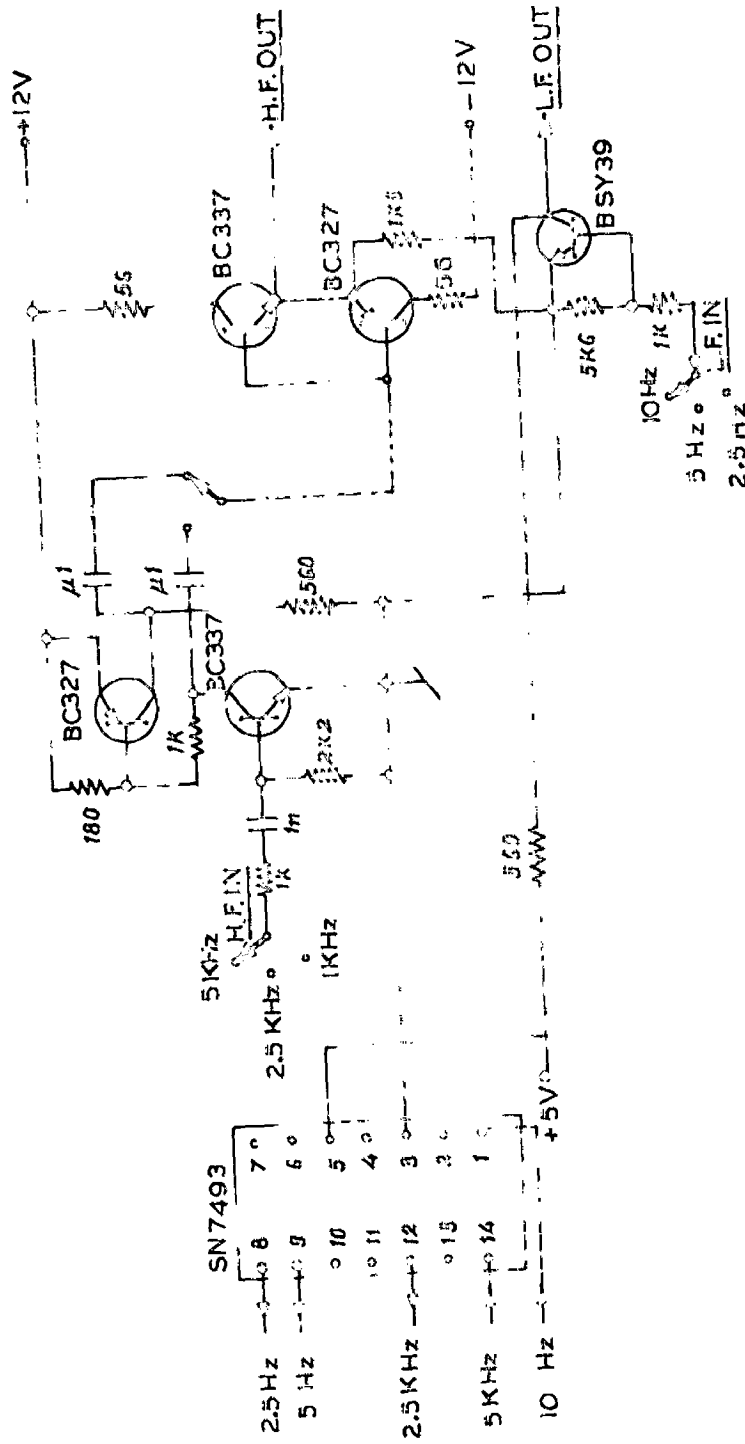
FIG. 3.11. EXTERNALLY GENERATED ADVANCING SIGNAL AND SQUARE WAVE GENERATOR
FOR TESTING CIRCUITS.

of the velocity spectra by a factor of two. To make the time resolution of velocity spectra double a binary frequency divider as suggested by Michelski et.al. |93| has been used. A detailed description of this has been presented else where | 94 |. An addo-X type printer was used as output coupling device of the MCA. The digital data from MCA is printed on a paper strip giving counts of one channel in one line. A low voltage power supply, unit NO. LV 236 with instrumentation bin, supplied by ECIL, India was used for providing a stabilized power to the preamplifier, linear amplifier and single channel analyser etc..

3.3 CALIBRATION

Like any other branch of spectroscopy one difficult but important experimental aspect of the Mössbauer spectroscopy is the accurate determination of the absolute velocity of the drive. A most commonly used method is to utilise the spectrum of a compound which has been calibrated as a reference. Various compounds and metal foils have received vide acceptance to be used as standard materials for the calibration of the Mössbauer spectrometer . During the whole measurements period the spectrometer was calibrated using the sodium nitroprusside $(Na_2 [Fe(CN)_5 NO].2 H_2O)$ of G.R. grade supplied by E.Merck AG. Darmstadt and natural iron foil, 1 mil thick supplied by Radio Chemical Centre, England, as the standard absorbers. The values of Mössbauer parameters for these absorbers given in Refs. |95, 52 | were used for the calibration purpose. For

deciding the zero velocity channel also the natural iron foil

was used and the middle point of the magnetic spectrum of

iron (6 finger pattern) was taken as zero velocity channel.

The negative and positive velocity sides were decided on the

basis of isomer shift values of standard stainless steel and

sodium nitroprusside absorbers with respect to iron.

The distance between the source and detector was kept

$\sim$ 12.5 cm while performing measurements at room temperature

and the absorber was kept in between the two. However, the

distance between the source and detector was kept little less

($\sim$ 10 cm) while performing temperature dependent studies. A

lead sheet of thickness 3 mm and having a hole of diameter

equal to the diameter of detector window was attached to the

detector window to minimise the scattered radiations and thus

signal to noise ratio was improved.

With all the above settings done a good and almost

linear (linearity better than 1 channel) spectrum was obtained.

Fig. 3.12 shows an example of the six fingered pattern for

1 mil thick natural iron foil taken on this spectrometer. The

outermost lines give 15% absorption and the full width at

half maximum (F W H M) is 0.29 mm/sec. The inner lines are

little more narrower while the intensity ratio is approximately

3:2:1:1:2:3

3.4 OTHER AUXILIARY SYSTEMS

The reported studies have been performed at various
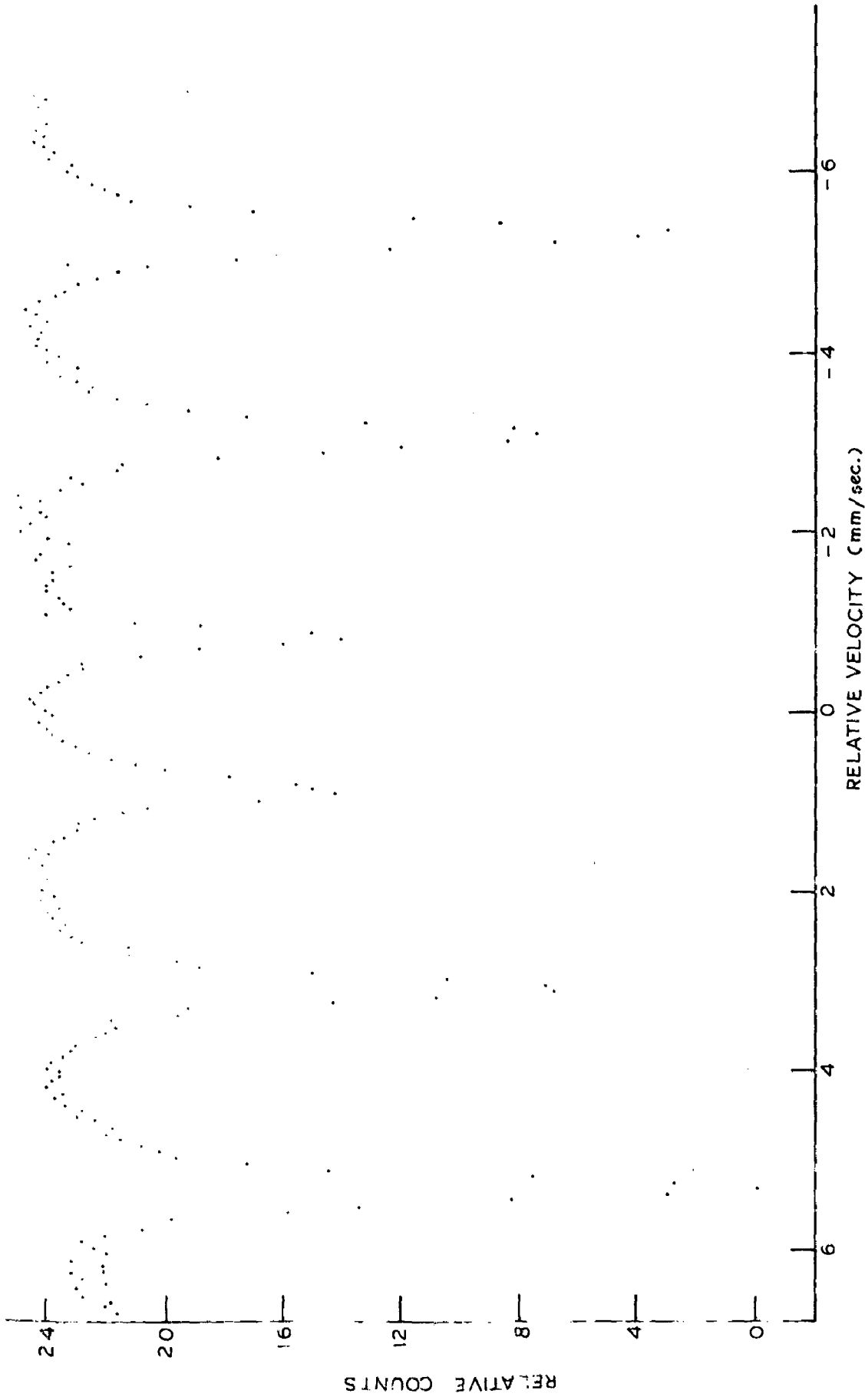
FIG. 3.12 - MÖSSBAUER TRANSMISSION SPECTRUM OF NATURAL IRON FOIL 1mil THICK TAKEN ON THE DISCUSSED SPECTROMETER (FWHM = 0.29 mm/sec.).

temperatures above   and below the room temperature. The system used for performing studies below room temperature is known as cryostat while for high temperature studies a furnace is used. The important consideration which one should keep in mind while designing the cryostat and furnace for Mössbauer spectroscopy are (a) there must be no vibrations inside the cryostat and furnace, and (b) γ-rays should pass through the system with minimum possible attenuation. In this section a brief description of the cryostat and furnace used have been presented while the details have been given else where |94|.

(A) CRYOSTAT

A continuous flow type crystat has been used for performing Mössbauer studies between the temperature range 300 K to 77 K. The temperature between room temperature and 77 K can be obtained by controlling the flow rate of liquid nitrogen. Edwards High Vacuum Ltd. Sussex needle valve was used for controlling the flow of nitrogen.

Fig. 3.13 shows the mechanical details of the cryostat. A gun metal chamber with Mylar windows for γ-ray transmission was used as vacuum chamber. Inside this chamber an absorber holder of copper on which copper pipe was wound (and welded with copper system to maintain proper contact) was used for producing the low temperature. This copper pipe was connected to the liquid nitrogen container through a German silver pipe. In this absorber holder of copper proper passage for gamma ray transmission was provided and the absorber in the form

HEATER AND
THERMO-COUPLE WIRES

O RING

COPPER PIPE

TO PUMP

POLISHED GUN METAL
CHAMBER

THERMO-
COUPLE

COPPER PIPE

ALUMINIUM
FOIL

COPPER
SPRING

ALUMINIUM FOIL

TO LIQUID NITROGEN

LEGS

VACUUM
VALVE
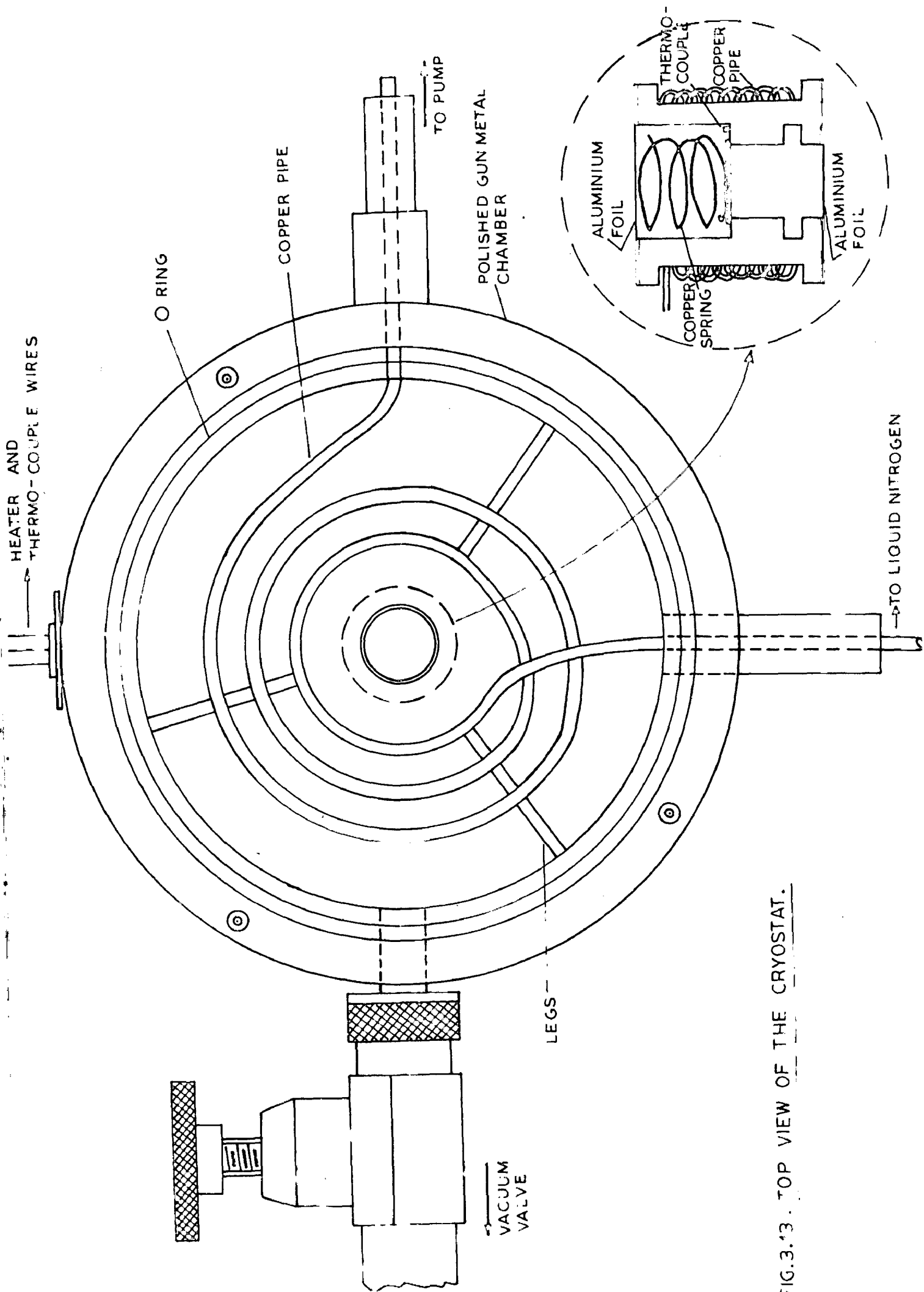
FIG. 3.13. TOP VIEW OF THE CRYOSTAT.

of pallet inside a copper ring was put in this system. To achieve homogeneous temperature inside the system it was covered with aluminium foils on both side having pin holes. The absorber holder was connected to outer gun metal chamber through three non metallic legs. It works as a vibration absorber while liquid nitrogen passes through the pipe and evaporates. The absorber was kept pressed in the cooled chamber with copper springs. Various other specifications are given below:

SPECIFICATIONS

Temperature range	77 to 300 K
Thermocouple	Iron-constantan
Heating element (for controlling temperature in the middle range).	Nichrome wire, $26\,\Omega$
Radiation transmission angle	20° Conical (maximum)
Dimensions of sample	16 mm dia.(outer)
Dimensions of cryostat	140 mm dia. 80 mm height
Main material	Gun metal
Windows	Transparent to low energy gamma rays (Mylar)

(B) FURNACE

A Recor type furnace has been used for high temperature studies and is shown in Fig. 3.14 . A small cylindrical furnace
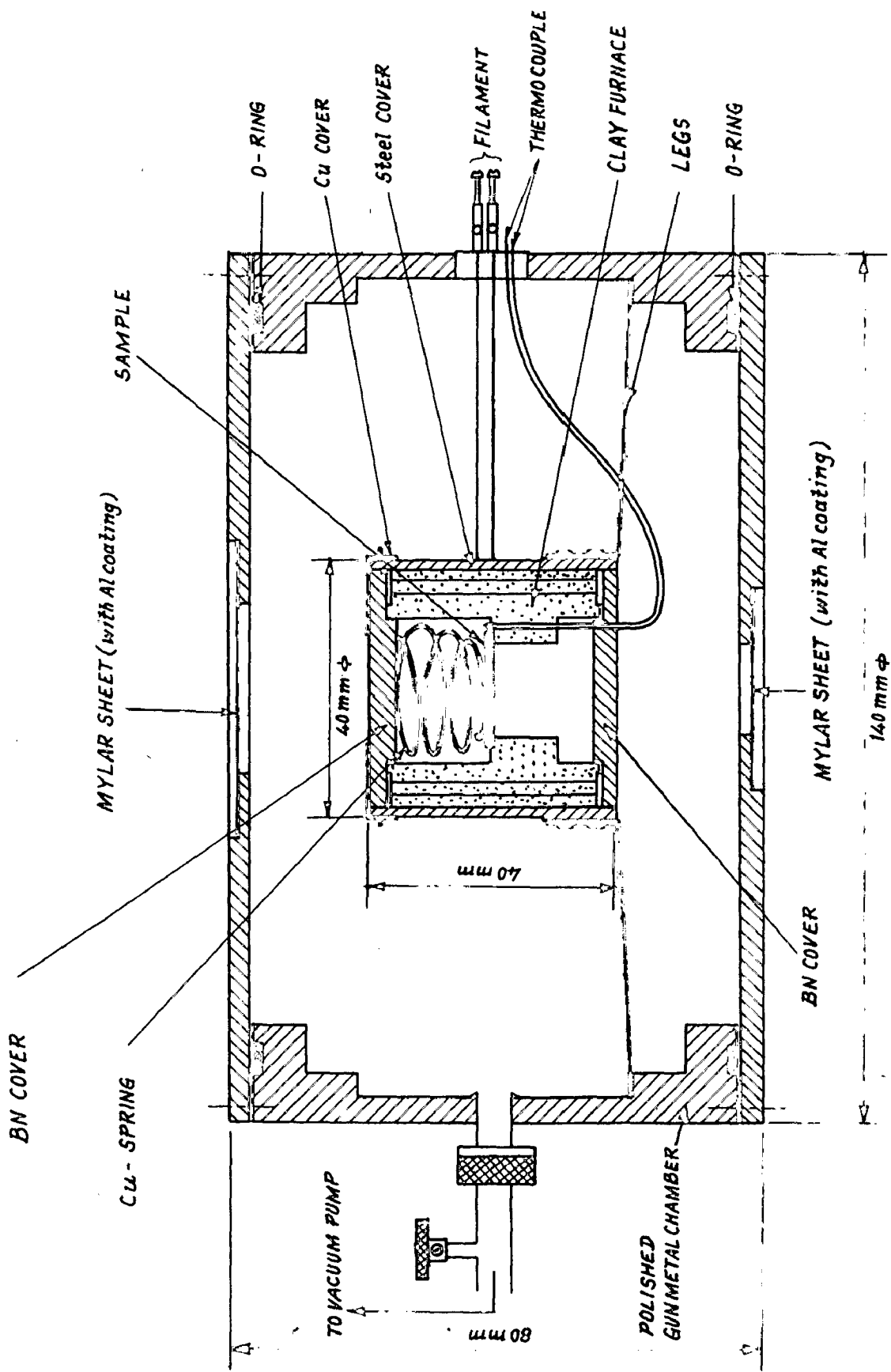
Sectional elevation of Mössbauer Furnace

FIG. 3.14

was constructed using nichrome as the heating filament. The vacuum chamber in this case was also of gun metal and Mylar windows were provided on this chamber for gamma ray transmission. The perfulite furnace was covered with boron nitride covers from both sides. This was done to make the temperature inside the furnace homogeneous. The furnace was put inside a steel cylinder and this cylinder was held by three thin stainless steel legs connected to the vacuum chamber. The upper boron nitride cover was of demountable type for changing the sample inside the furnace. The absorber was put in the form of pallet inside the furnace and was held fixed with a copper spring. The specifications are given below:

SPECIFICATIONS

Temperature range	300 - 900 K
Thermo-couple	Iron-constantan
Heating elements	Nichrome wire, 14 Ω ,
Radiation transmission angle	20° conical (maximum)
Dimensions of sample	16 mm dia.(outer)
Dimensions of the furnace	140 mm dia. 80 mm height
Main material	Gun metal
Windows	(For temperature 600 K Mylar was used)
Direction of radiation	Horizontal.

2.5   TEMPERATURE CONTROLLER

(A) INTRODUCTION : While performing temperature dependent

studies it is desirable to control the temperature very accura-

tely. In studies of critical phenomena near phase transitions

either through Mössbauer spectroscopy or susceptibility measu-

rements it becomes necessary to control the temperature of the

specimen with a high precision and over a fairly long time.

For instance, in some studies of ferromagnetic transition |96,97|

of iron, the entire region of interest is over a short range

of $\pm$ 0.3 K even though the temperature changes made may be

about 1000 K. In this short range, maintenance of temperature

accurate to within $\pm$ 0.05 K is required. This requirement of

temperature stability may be more stringent | 98| in some other

cases. Control with a precision better than one part in 10^4

is practicable, but its absolute measurement is not, in general,

possible to this accuracy and also is not generally required.

Here we report a temperature controller which can be used for

temperature regulation within the temperature range from liquid

nitrogen temperature to 900 K with an accuracy of $\pm$ 0.05 K

over a long length of time. The controller is devised to

control the temperature very accurately.

Various types of temperature controller have been

discussed in the literature | 99 - 102 |. Craig | 99 | cont-

rolled the temperature using a feedback unit capable of long

term regulation to 0.1 μV. Steyert et.al. |100| controlled

the temperature using a proportional regulator that delivers

a current proportional to the deviation from zero in the galva-nometer. The quiescent current was set with a 10 turn poten-tiometer and a regulation of the order of 0.01 K was obtained provided there was no major change in the sample temperature. Schurer |102| used a temperature stabilizing unit which was consisting of a proportional and differentiating amplifier. This proportional amplifier was used to increase or decrease the heating current proportional to the error signal and the diff-erentiater (in parallel with proportional amplifier) was used to change the heating current so that the rate of change of temperature decreases. All these controllers, however, suff-ered from a serious draw back of an inherently long thermal time constant due to the large thermal capacity of the system in which the control was required. The problem has been over-come by designing a dynamic type temperature controller |103| and is discussed below.

(B) PRINCIPLE: A thermo-couple has been used as a sensor. The thermo e.m.f. developed across this thermo-couple (iron-constantan in this case) is compared with a standard d.c. voltage (generated separately) and the difference of the two voltages, error signal, is amplified. In previous controllers, the temperature was controlled by switching the heater 'on' when the error was negative (the error signal negative means the e.m.f. developed was less than the standard d.c. voltage and positive error signal corresponds to the e.m.f. developed more than the standard d.c. voltage) and 'off' when it was positive.

But due to the large thermal capacity of the system, if the system is at a higher temperature then even after the heater is 'off' it will remain at a higher temperature for a long time and the reverse will happen at lower temperature i.e. it will remain at a lower temperature even after some time of the heater is on., the 'on' and 'off' cycle is too large. Further, the temperature will never be stabilized and it will be varying within the accuracy limits of the controlling unit. In the present controller, the heater is actuated at a preset rate (5 times /min) with the help of an external signal, the heater will be 'on' and 'off' within each cycle but the time of 'on' and 'off' within each cycle is controlled by the magnitude of error signal. Thus, if the error signal is positive then in one cycle the heater will be 'off' for longer time and 'on' for less time. This 'on' of the heater for longer time during the cycle will continue till the error signal goes towards zero. Thus when the temperature has been stabilized (error zero) then during each cycle heater will be 'on' and 'off' for equal time durations.

(C) CIRCUIT DESCRIPTION AND WORKING

(i) STANDARD D.C. VOLTAGE GENERATION CIRCUIT: The thermo e.m.f. developed across the thermo-couple is compared with some standard d.c. voltage, hence this d.c. voltage should be stabilized and should be of the order of e.m.f. developed across the thermo couple. The standard d.c. voltage is generated using an IC 7805 and is shown in Fig.3.16a. The

output voltage of this has been taken across a resistance so that the current of 1 mA may flow through the circuit. This resistance is kept fixed to keep the current in the circuit constant. Now according to the requirement a particular resistance ranging from 0 to 50 Ω is selected and thus a voltage of the order of 0 - 50 mV is obtained. All the resistances used in the output circuit and this resistance network were metal film (0.5 %, 100 ppm) resistances of low temperature coefficient. Thus the voltage will be fixed and particularly temperature independent. This voltage is divided on a band switch and a 10 turn helipot, so that a desired voltage in the range 0-50 mV can be obtained.

(ii) REFERENCE TRIANGULAR GENERATOR CIRCUIT: The reference triangular voltage, 1.4 V peak to peak (+ 0.7 to -0.7 V), 5 cycles/min. has been generated separately. The circuit is shown in Fig. 3.16b. Two operational amplifiers 741 have been used as an integCrator and comparator separately.

(iii) OPERATION: The complete block diagram of the temperature controller is shown in Fig.3.15 while the detailed circuit in Fig. 3.17. The standard d.c. voltage is compared with the thermo e.m.f. developed across the thermo-couple. The difference of the two voltages is designated as error in the text. This error signal is now preamplified 50 times using an instrumentation amplifier IC 725. The preamplified signal is given to a 5 Hz low pass filter with a gain of 10 to minimise 50 Hz
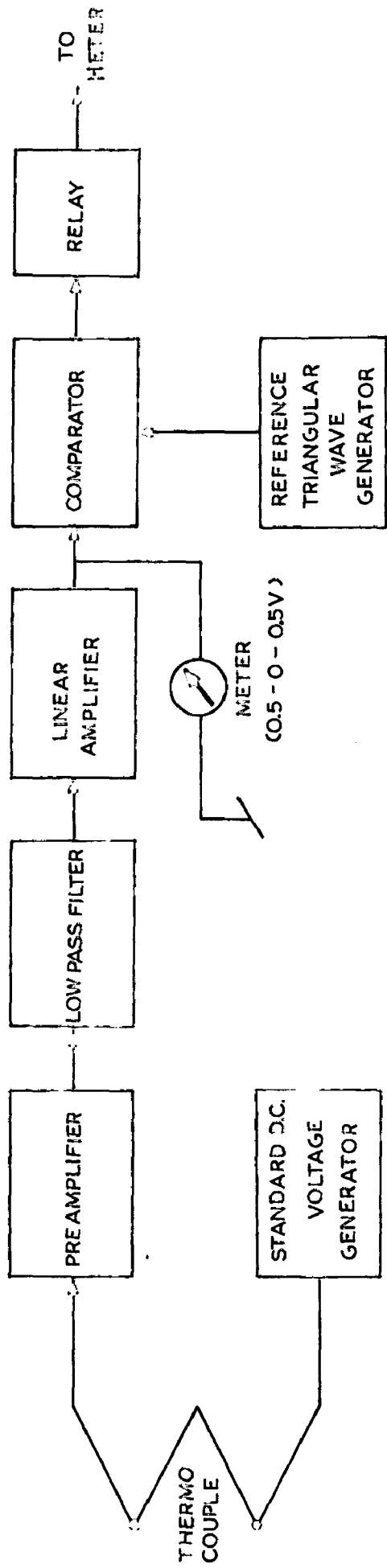
FIG. 3·5 BLOCK DIAGRAM OF THE TEMPERATURE CONTROLLER.
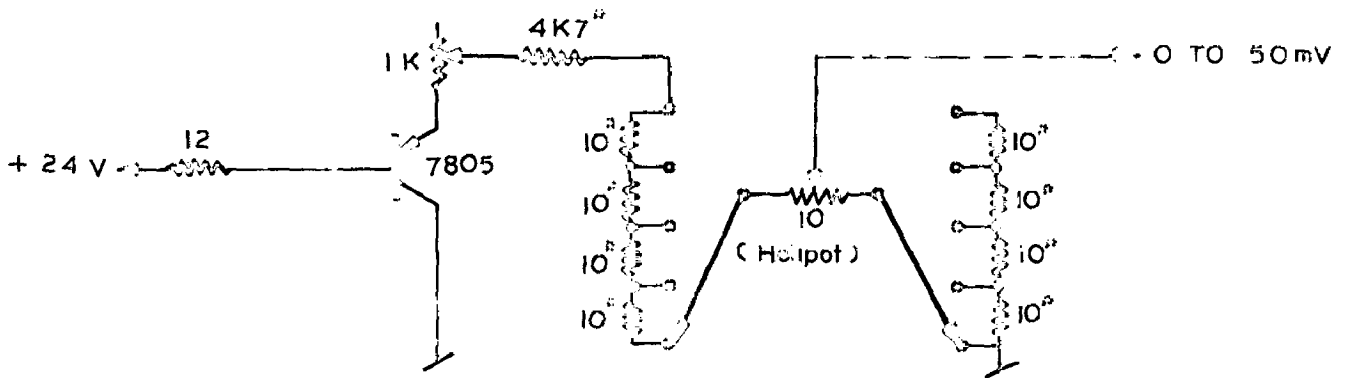
(* Metal film resistances 0.5 % 100 ppm)

FIG.3.16 (a) _ STANDARD D.C. VOLTAGE GENERATOR.
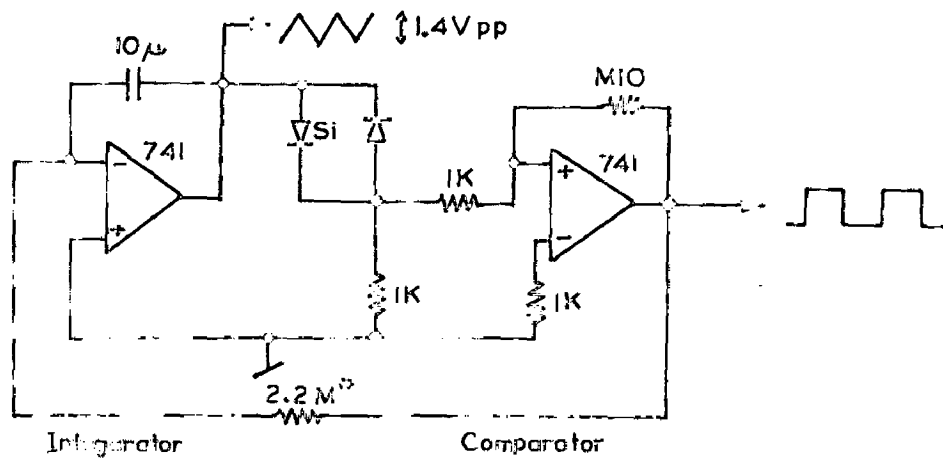
(* Metal film resistance 0.5 % 100 ppm)

FIG.3.16 (b)_ REFERENCE TRIANGULAR WAVE GENERATOR.

PRE AMP.   LOW PASS FILTER   LINEAR AMP.   VOLTAGE FOLLOWER
725   741   741   741

Thermo couple

Standard DC Voltage

Error

METER (0.5-0-0.5)

COMPARATOR 741

* Metal film resistances 0.5 % 100 ppm

Ref. tri.Input

+ 12V

+ 12 V (RAW)

AC127

AC127

To heater

Relay

Bulb
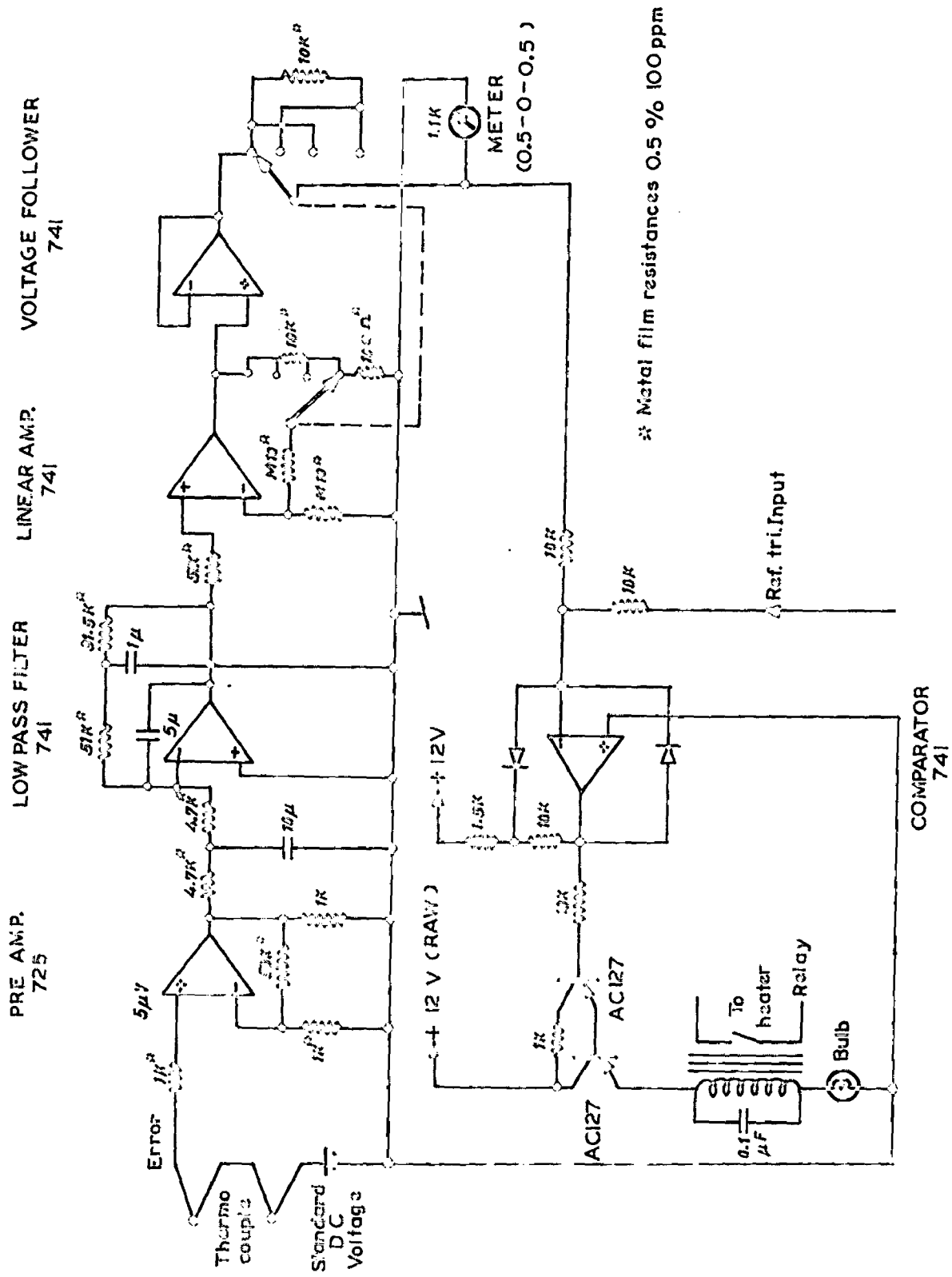
FIG. 3.17 - DETAILED CIRCUIT DIAGRAM OF THE CONTROLLER.

noise signal and other pick-ups that may be present around the thermo-couple. The bypassed signal is further amplified through a chain of linear amplifiers of gain 2 , 20 and 200. Thus in the most sensitive range, the total amplification of the circuit is 10^5 times. Since the amplification is too high and can not be obtained by a single operational amplifier so the amplification has been achieved in three stages to avoid instabilities and self oscillations. The maximum amplification obtained from a single operational amplifier is 200 which is within the safe limits. All the resistances used in feedback circuits and for amplification purposes were of low temperature coefficient, metal film resistances (0.5 % , 100 ppm). This amplified signal is finally passed through a voltage follower and is read on a voltmeter (range -0.5 - 0 - + 0.5). Thus if the initial error signal is of less than 5 μV value then after maximum amplification the deflection of voltmeter will be within the scale. This error corresponds to a temperature difference of .1^{0}C (because the thermo power of the used thermo-couple is 50 μV per degree). Since the voltmeter has 100 divisions (50 - 0 - 50) for .1^{0}C so at the maximum accuracy of the controller i.e. $\pm$ 0.05^{0}C the deflection of the meter should be within (25 - 0 - 25) divisions of the meter. To, obtain this much accuracy this amplified error signal was compared with a reference triangular voltage, 1.4 V peak to peak (+ 0.7 to-0.7V), 5 cycles/min. in a comparator. This comparator will give a gated output of frequency 5 cycles/min. The width of the gate will depend upon the magnitude of the resultant of amplified

error and reference triangular voltage. The relation between the gate width and the resultant of amplified error signal and reference triangular voltage is clearly shown in Fig. 3.18. Thus the gate opens when the resultant of the error signal and the reference triangular wave (instantaneous valve) is positive and the width of the gate depends as discussed above. The amplified error signal shown in Fig. 3.18 is opposite in polarity to the initial error signal due to one inverting amplifier used in the circuit. Thus a gated output (5 cycles/min.) of varying width is obtained which operates the relay after passing through the set of emitter follower used in Darlington pair configuration. The relay ultimately operates the heater.

(D) MERITS AND DEMERITS: The controller is designed not to measure the temperature precisely but rather to maintain its stability. In the most sensitive range ($5\mu V$), some unstabilities do come in at the time of switching events of relay but this problem has been overcome to a large extent using a separate power supply for the relay circuit and a Darlington pair of emitter followers for driving the relay. Further, it is also recommended that most of the current in the heater should be passed directly and only a small portion ($\sim 0.5A$) through the relay. This minimises the problems like spark, erosion of switching contacts, etc.. Also, if the whole current is passed through the heater it is very difficult to make the temperature constant because the controller heat energy will be too high to obtain equilibrium. A possible

REFERENCE TRIANGULAR WAVE

ERROR SIGNAL

GATED OUTPUT

FIG.3.18- RELATION BETWEEN THE GATE WIDTH AND THE RESULTANT OF AMPLIFIED ERROR AND REFERENCE TRIANGULAR VOLTAGE.
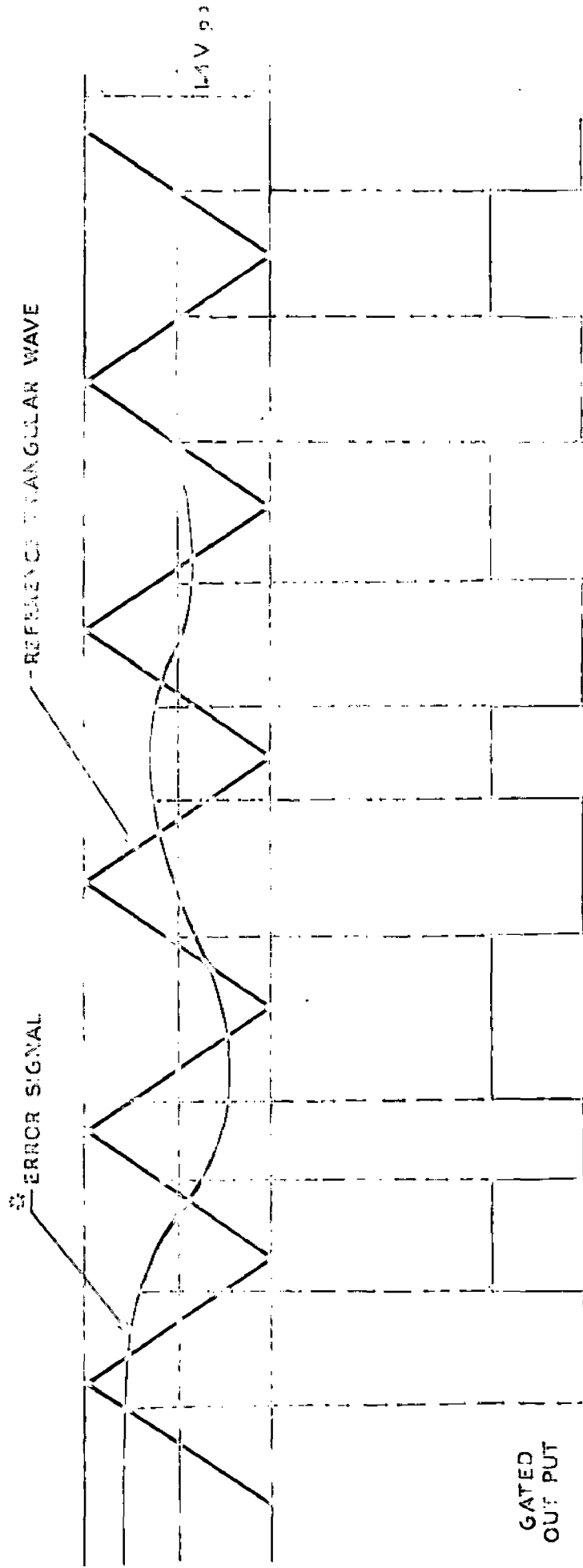
※ Error shown in this figure is opposite in polarity to the actual error

alternative for avoiding the problems of erosion etc. in the

relay contacts may be to replace it by silicon controlled

rectifiers, but this has not been used by us due to (i) the

nonavailability of a suitable SCR at the time of fabrication

of this unit and (ii) an SCR will need a more powerful d.c.

voltage supply for heating the filament which we did not prefer

to fabricate.

CHAPTER 4

STUDIES OF CORRODED STEELS

4.1 INTRODUCTION

The problem of corrosion in metals and alloys is very important and has been a subject of wide study since long. Corrosion is a general word and used for all the reactions taking place on the surface of metallic material with its environment. These reactions may provide the formation of any type of corrosion product i.e. solid, liquid or gaseous and depend on the type of environment present in the vicinity of material. In general a metal suffers from corrosion in the presence of acids, alkalis, pure water and also from atmosphere. Both the physical and chemical nature of the corrosion products are important since they frequently influence the subsequent rate of corrosion. The structure of the metal (or material) also plays a decisive role in deciding the corrosion behaviour. Crystal structure may determine the incidence of corrosion in two ways : (a) where planes of atoms cut the surface of a metallic article, the work needed to dislodge atoms from an incomplete layer is less than to start removal from a new layer, so that corrosion products facets related to crystal orientation (b) less work is needed to dislodge an atom at the boundary of two differently oriented crystals than to dislodge an atom from the interior of the lattice having all its neighbours similarly oriented; thus corrosion often starts at integranular boundaries. The above discussion reveals that a detailed study of corrosion phenomenon

needs the help of physicists, chemists and metallurgists. For
example, a physicist can help in measuring semi-conductivity of
corrosion products and thus idetify them, a chemist gives
information about electrochemical kinetics and a metallurgist
studies surface and dislocation arrangements. The literature
dealing with the basic principle, theory and the parameters
affecting the corrosion, prevention of corrosion etc. is exte-
nsive and some of these are listed as references |104-107|.

The wide applicability of Mössbauer effect has been dis-
cussed in chapter 2. It also covers the field of corrosion
science. Mössbauer effect is used for the identification and
composition determination of corrosion products and also gives
information about the growth of corrosion process. Other
physical techniques like X-ray, electron diffraction etc. have
also been used for the identification of corrosion products.
But in some cases where the different corrosion products have
roughly same lattice parameters and could not be identified
easily with the help of X-ray or electron diffraction, Mössbauer
spectroscopy clearly distinguishes, by determining the internal
magnetic field, isomer shift and quadrupole splitting values
and thus shows its superiority over the other methods listed
above. For example the invisible films formed on iron exposed
to air at $18^{o}C$ or slightly higher temperatures consist of cubic
oxide with end members of the series magnetite or γ-Fe_2O_3;
these members could not be differentiated with the help of
X-ray or .electron diffraction techniques |108| while Mössbauer

spectroscopy |1o9| identified it to be Fe_3O_4 on the basis of internal magnetic field values. Since iron, which is a most common metal, suffers from corrosion in its pure as well as alloying forms hence it has further enhanced the applicability of Mössbauer effect in the field of corrosion because Fe^{57} is the best suitable isotope for Mössbauer studies. There are two types of corrosion products formed on iron: One rust (the formation of hydrated oxides in the presence of oxygen and water) and the other scale (the formation of anhydrous oxides).

Mössbauer spectroscopy was first used by Suzdalev et.al. | 3 | to study the corrosion problem. Since then the technique has been used in both scattering and transmission geometry depending upon the character of the sample available.

The scattering geometry is used if one does not want to destroy the sample. As a rule, a Mössbauer scattering spectrum is a superposition of spectra of both the substrate and of the phases present in the film. For, oxide films thinner than $\sim 10\mu m$ the spectrum of the substrate will dominate over the film in the composite Mössbauer spectrum. The enhancement of oxide or corrosion film has been achieved in various ways: the enhancement of the substrate in Fe^{57} prior to film growth |110, 111|, the detection of 6.3 keV X-rays |109,112-114| and the detection of conversion electrons |111,114,115|. Various other authors |116-122| have also worked in scattering geometry and have drawn some important conclusions.

The application of the technique in transmission

geometry may also be made in two ways; one by using thin corroded foils directly and second by stripping the corrosion products from the surface and then performing studies on powder samples. The direct-measurement on the corroded foil is not possible if the foil is thick. Channing and Grahm |123,124| and channing, Dickerson and Grahm |125| made Mössbauer transmission measurements on thin oxidised iron foils and obtained some important quantitative and qualitative results. Dezsi et.al. |126,127| also used the same technique for the identification of corrosion products and suggest that Mössbauer studies may be helpful in giving an idea about the progress of corrosion and the intermediate products formed because these can supply information about the structure and composition of the products. Joye and Axtmann |128| made quantitative estimation of corrosion products formed on a thin iron foil in the atmosphere of H_2O , HCl and air using Mössbauer spectroscopy in transmission geometry. This quantitative interpretation of the Mössbauer spectra aided in a provisional identification of the corrosion product as Fe_2O_3. $2H_2O$. Bancroft et. al. |129| studied the structure of oxide films formed on iron due to the exposure to dry air and chromate solution _____ having pH value 4. Recently Volenik et.al. |130| used Mössbauer transmission spectroscopy for the study of oxide films (formed due to high temperature oxidation) stripped from the low carbon steels and suggested that the technique yielded information on the phase composition of films and on deviation from stoichiometry of iron oxides present in the films . Other problems like relaxation

phenomenon |131| and effect of ultrafine particles |132| in rust

products formed have also been studied using the Mössbauer spe-

ctroscopy. All the above studies deal with either oxidation

of iron in pure air or formation of rust layers in the presence

of H_2O, HCl and chromate solutions etc.. No study has been

performed till now on corrosion of structural steels in the

presence of reinforced cement and concrete (rcc) using Mössbauer

spectroscopy. This chapter reports |133| some Mössbauer spec-

troscopy measurements carried out in transmission geometry on

some low carbon structural steels corroded in the presence of

reinforced cement and concrete. Under such a situation the

steel rod will get both the water as well as oxygen (until the

cement dries up) and thus the corrosion should be of electro-

chemical type. For sake of completeness an introduction to

electrochemical corrosion is presented in the next section.

4.2 ELECTRO-CHEMICAL CORROSION OF IRON

The electrochemical mechanism of corrosion can be

understood by considering a piece of iron in some salt solution

e.g. NaCl. On a iron piece which is suffering from corrosion

there are both anodic and cathodic sites. These may be perma-

nently separated from each other but in many cases the whole

of the iron surface consists of anodic and cathodic sites

which are continuously shifting. At an anodic site an oxidation

process (loss of electrons) occurs and thus the iron goes into

the solution usually as ferrous iron, according to the electronic

equation.

$$2 \text{ Fe} - 4 \text{ electrons} \rightarrow 2 \text{ Fe}^{2+}$$
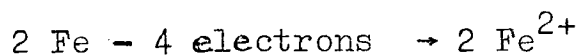
At the cathodic site the reduction process (gain of electrons) occurs and this will result in the reduction of dissolved oxygen. The equation can be represented as

$$O_2 + 4 \text{ electrons} + 2 \text{ H}_2O \rightarrow 4 \text{ OH}^- .$$
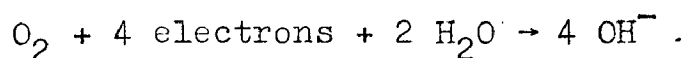
If the iron bar is partially immersed in a solution then there is often a permanent separation of the anodic and cathodic areas with the latter near to the water line where oxygen is readily available.

Since the sodium and chlorine ions are present in the solution, the cathodic product can be regarded as being sodium hydroxide and the anodic product as ferrous chloride. Both of these are freely soluble and thus will not suppress the attack. These two form solid substances where they meet; ferrous hydroxide $Fe(OH)_2$ may be momentarily precipitated, but if excess of oxygen is present then this product $Fe(OH)_2$ will be oxidised to ferric hydroxide |134|, this substance, commonly known as ferric rust, is $FeO(OH)$ or $Fe_2O_3 . H_2O$. If the supply of oxygen is limited, a green ferrosoferric hydroxide or black anhydrous magnetite, Fe_3O_4 may form. The product $FeO(OH)$ can be α - or γ - $FeO(OH)$, according as the pH value is high or low.

Thus it is clear that the electrochemical corrosion

ultimately brings about a combination of iron with oxygen (and usually with water) giving a product either oxide or hydroxide. It is different from the direct oxidation in the sense that the corrosion product formed forms at a point distant from the point of attack and thus can not stifle the action while in direct oxidation the product forms at the point of attack and thus act as a protector. This makes the electrochemical corrosion more dangerous than the direct oxidation.

4.3 EXPERIMENTAL

(i) HISTORY AND SAMPLE DESIGNATION

Two corroded structural steel bars which were kept in rcc for 7 years and 10 years, respectively, were taken. These samples were obtained from Roorkee University Civil Engineering Laboratory. The rust on these samples was loosely bound and it could be removed easily from the metal surface by mechanical process (filing) and hence the stripping procedure was not adopted. Further in mechanical removal process the rust is in general free from the substrate. The rust samples obtained from these corroded bars have been designated as R_1 and R_2, respectively, in the text. The rcc and steel used in these cases were as per civil engineering standard specifications.

Another sample corroded steel bar was taken from a building which collapsed only after 5 years of its construction. The steel bar taken from this building was heavily corroded and hence the rust was removed in such a way that two rust samples

could be obtained: one from the uppermost layer of the rust and this was obtained by scrapping the rust with filing and the second sample was prepared from the rust in between the uppermost rust layer and the substrate. These two rust samples from the uppermost layer and middle layer were designated as R_3 and R_4 respectively. After the removal of the rust each steel bar was cleaned till the shining surface due to metal appeared. From this clean surface, the steel for Mössbauer analysis was also obtained by filing with a very fine file. Since the structural steels are the mild steels having very low carbon concentration, no problem arose in filing. For the uniformity and suitable size of particles the steel filings were passed through a sieve of mesh No. 325. The three steel samples were marked as S_1, S_2 and S_3 respectively.

(ii) SAMPLE PREPARATION

The samples for Mössbauer studies were prepared in the pallet forms. The rust, weighing 15 mg /cm^2 (this gives a thickness roughly $\sim$ 10 mg/cm^2 of iron), from each specimen was thoroughly mixed with the required inert and light compound boron nitride. This was mixed to obtain a finite thickness and uniformity of the absorber sample. The choice of this compound was guided by the fact that it does not have any effect on the sample. This thoroughly mixed powder was pressed in a copper ring of inner diameter 1.4 cm and thickness 1 mm using a brass die. This method provides a compact and almost uniformly thick absorber. The same method was adopted for making

the steel absorber samples for Mössbauer studies. But in this case the amount of steel powder used was ~ 10 mg./cm^2.

(iii) MÖSSBAUER DATA RECORDING

. Mössbauer spectra were recorded at room temperature on a spectrometer described in chapter 3 using a source of 3.5 mCi Co^{57} in copper matrix. The spectra were recorded for sufficie-ntly long time to minimize the statistical error and at least 7×10^5 counts per channel were stored in case of each rust. The percentage statistical error at this much counts comes out to be .12 % and thus it improves the statistics to a satisfactory extent. For high temperature measurements the furnace discussed in chapter 3 was used.

4.4 RESULTS AND DISCUSSION

The qualitative chemical analysis of the concrete used was performed. It showed the presence of '' chloride'' ions in all the cases. Various concrete samples were taken from the building from which steel sample S_3 was obtained for study. The pH measurements were made and all the samples showed highly alkaline nature with pH value between 11 and 12.

Microstructure of the steel samples was viewed on a metallurgical microscope using a magnification of 200. Samples S_1 and S_2 showed a mild steel structure with a major portion of ferrite and little pearlite while S_3 was having more pearlite than S_1 and S_2.

As mentioned in the discussion of electrochemical

corrosion the corrosion products formed on a steel rod in the

presence of concrete may be either oxides or any hydroxides

of iron. Other impurities like chloride and sulphate may also

be very well attached with these if present. The oxyhydroxides,

FeO(OH), may be present in various modifications α and γ

depending upon the pH of the solution and β due to the presence

of chloride ions. Mellor, Cohen and Beck |135| identified an

association between chloride ion and γ-FeOOH . For the

present case the Mössbauer spectra of rust samples R_1 and R_2

are given in Fig. 4.1 and those of R_3 and R_4 in Fig. 4.2. The

spectra for the steels are projected in Fig. 4.3; since the

spectra of steels S_1 and S_2 were same only that of S_1 is shown

in the figure. The analysed rust products and their parameters

are given in Table 4.1.

Mössbauer spectra of rust samples R_1 and R_2 are the same

(except a very little difference in intensities of the patterns)

and consist of a simple non magnetic doublet pattern near

zero velocity. The values of quadrupole splitting and isomer

shift corresponding to the pattern are 0.624 mm/sec. and

0.312 mm/sec. respectively. The reported values of isomer

shifts are given with respect to iron. These values can be

assigned to the product β FeOOH. To further confirm the

identification of the product as β FeOOH, this rust product

was heated at 600 K in air where it oxidises to α Fe_2O_3 |136|.

The Mössbauer spectrum of the heated products gave values
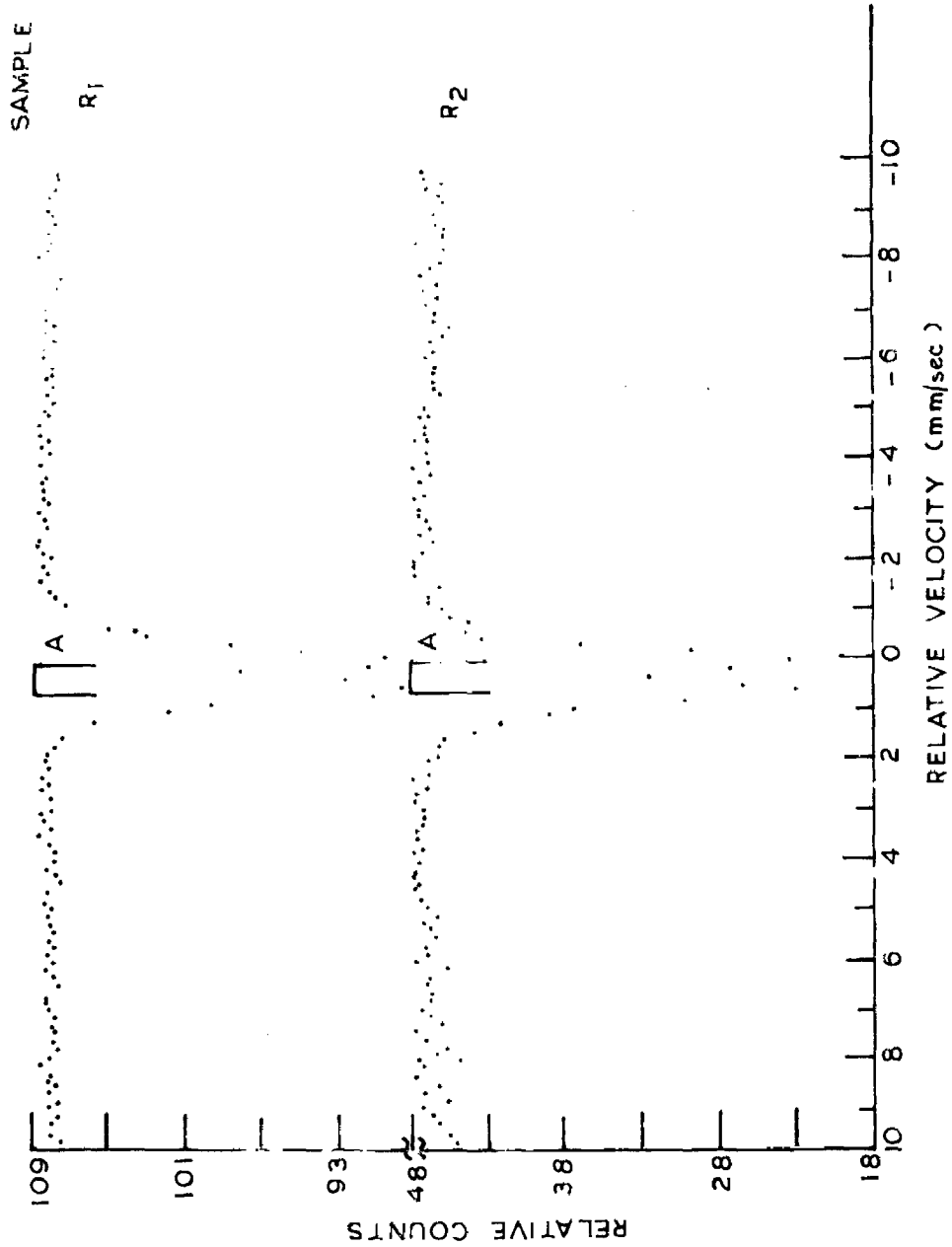
FIG.4'- MÖSSBAUER SPECTRA OF RUST SAMPLES R_1 AND R_2 AT 300K.

A : β FeOOH
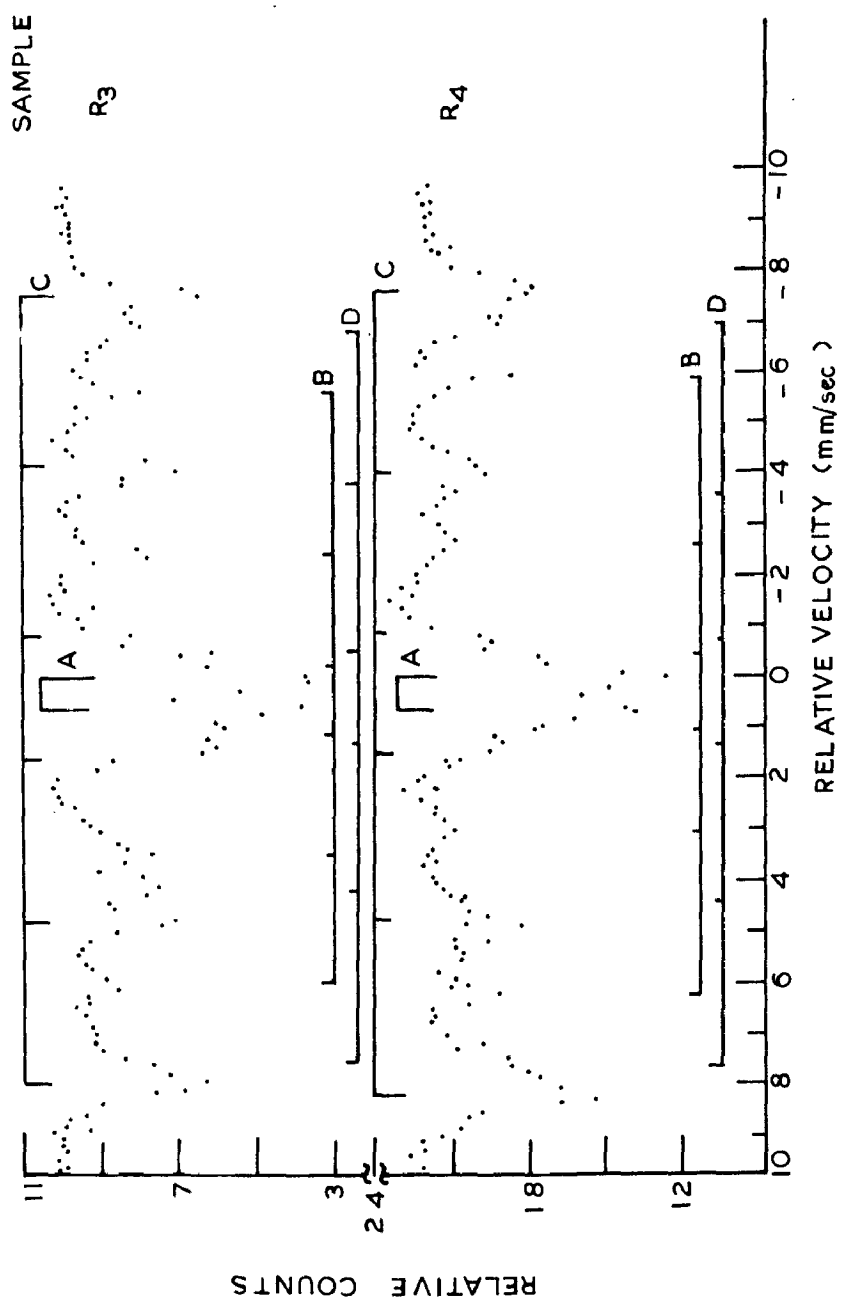
FIG.4.2.- MÖSSBAUER SPECTRA OF RUST SAMPLES R₃ AND R₄ AT 300K.

A : βFeOOH
B : ∝FeOOH
C : Fe₃O₄ (Tetrahedral site)
D : Fe₃O₄ (Octahedral site)
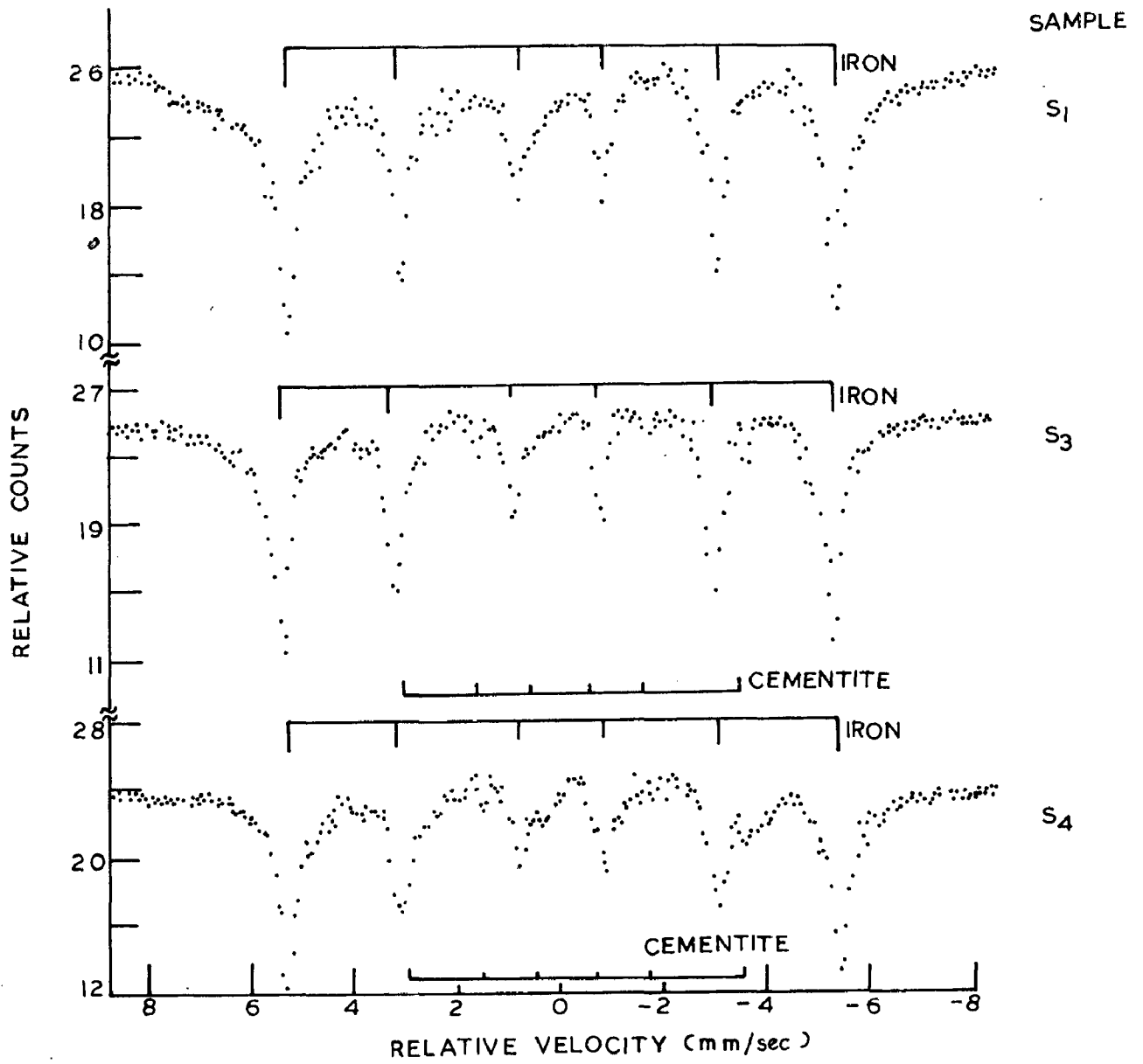
FIG.4.3 _ MÖSSBAUER SPECTRA OF STRUCTURAL STEELS AT 300K.

TABLE 4.1: MÖSSBAUER PARAMETERS OF RUST SAMPLES AT 300K

Sample	Products formed	Sites	Internal magnetic field(kOe)	Quad-split. (mm/sec.)	Isomer shift* (mm/sec.)
R_1	β FeOOH	A	—	0.624	+ 0.312
R_2	β FeOOH	A	—	0.624	+ 0.312
R_3	β FeOOH	A	—	0.624	+ 0.312
	α FeOOH	B	369	0.195	+ 0.312
	Fe_3O_4 Tet	C	490	0.078	+ 0.325
	Oct	D	455	0.117	+ 0.299
R_4	β FeOOH	A	—	0.624	+ 0.312
	α FeOOH	B	383	0	+ 0.209
	Fe_3O_4 Tet	C	495	0.039	+ 0.351
	Oct	D	461	0.078	+ 0.351
R_5	β FeOOH	A	—	0.624	+ 0.312
	Fe_3O_4 Tet	C	485	0.156	+ 0.182
	Oct	D	461	0	+ 0.653
	FeO	E	—	0.468	+ 0.780

* Isomer shifts have been measured w.r. to natural iron absorber.

corresponding to α Fe_2O_3. The values of β FeOOH are in close
agreement with those reported by Terrell and Spijkerman |114|.

Further the analysis shows that the last corrosion product
formed in this case is β FeOOH. The spectra due to R_3 and R_4
were quite complicated and were decomposed into four patterns
separately. One due to nonmagnetic doublet with the Mössbauer
parameters same as those due to the patterns of R_1 and R_2
(β FeOOH) and three magnetic patterns. One magnetic pattern
was assigned to α FeOOH and the other two to Fe_3O_4 Tetrahedral
and Octahedral sites. The identification was done on the basis
of the internal magnetic field, quadrupole splitting and isomer
shift values. The products formed in R_3 and R_4 have also been
identified to be the same. The value of the internal magnetic
field in the case of R_3 (upper layer rust) is less than that
for R_4 (rust layer between upper layer and substrate). The
low value of field in case of R_3 may be attributed to the
presence of impurities which are quite probable because the
upper surface is in direct contact with the concrete etc.and
hence the field values may be affected. The effect of impuri-
ties on the iron oxides has also been discussed in Refs.
|137, 138|. Moreover, there exists no other oxide or hydroxide
having field values as observed in case of R_3 and hence the
products can be attributed only to the corresponding oxides
as in R_4 with some impurities. The values of magnetic field
for Fe_3O_4 Tetrahedral and Octahedral sites were in close
agreement with the values of Fujio |109 |.

The Mössbauer spectroscopic analysis of steels shows a

difference between the two steels. The steels S_1 and S_2 show
iron spectrum while the steel S_3 gives the presence of extra
pattern along with the normal iron pattern. This extra pattern
was identified corresponding to the cementite on the basis of
internal magnetic field value $\sim$ 210 kOe.

A look on the identified corrosion products in various
rusts shows that β FeOOH is present in all rusts and it has been
assigned to the presence of '' chloride'' ions in the water
used. Terrell et.al. |114| also obtained the rust products
β FeOOH in case of steel surface rusted through exposure to the
fumes of Hydrogen chloride in air. The chemical analysis of
concrete has shown the presence of chloride ions and thus again
justify the formation of β FeOOH. Further the product Fe_3O_4
was found only in those cases where steels have more cementite.
The presence of greater amount of cementite in steel was evident
from the Mössbauer studies as well as microstructural analysis.
In this case the formation of Fe_3O_4 along with FeO(OH) suggest
the presence of some reducing atmosphere which partially
reduces FeOOH into Fe_3O_4. The presence of this reducing atmos-
phere in steels having more cementite may probably be considered
due to the availability of more cathodic area in this case and
thus producing a large reducing area or less oxidising area.
This explains the formation of both products Fe_3O_4 and
β FeOOH in the case of R_3 and R_4. Thus it appears that the
steels having more cementite end up with a corrosion product
Fe_3O_4. To further confirm the formation of Fe_3O_4 in steels

having more cementite, one steel sample (S_4 shown in Fig. 4.4)
having larger amount of cementite was kept in standard rcc for
40 days only. The rust products formed were analysed and the
Mössbauer spectrum of this rust R_5 is shown in Fig. 4.4. It
also contains Fe_3O_4 along with other identified products as
β FeOOH and FeO. The presence of α FeOOH in case of rusts
R_3 and R_4 was assigned to the presence of highly alkaline
atmosphere in this case. The chemical analysis of the concrete
used in this case has already shown the presence of highly
alkaline atmosphere and hence the presence of α FeOOH in this
case should not be surprising. On the basis of above analysis
of steels, the rust products and the rcc various factors may
be pointed out which might have probably accelerated the
corrosion in case of the 5 years old highly rusted sample:

(i) Presence of more cementite in steel. The presence of more
cementite in steel provides more cathodic area and thus more
hydrogen can be evolved causing the quick attack of corrosion.
The presence of cementite becomes more deteriorating in the
presence of some catalyst. Since '' chloride'' ion works
as a catalyst and hence the presence of both '' chloride'' ions
in water and cementite in steel simultaneously would have
accelerated the corrosion. The acceleration of corrosion in
steels having more cementite in presence of chloride ions
was also pointed out by Evans |105|.

(ii) Presence of highly alkaline atmosphere. The increased
value of pH though decreases the overall attack but at these

300K

SAMPLE

R5

RELATIVE COUNTS

92

84

76

RELATIVE VELOCITY (mm/S^{-1})

-10 -8 -6 -4 -2 0 2 4 6 8 10

IRON

A
E
D C
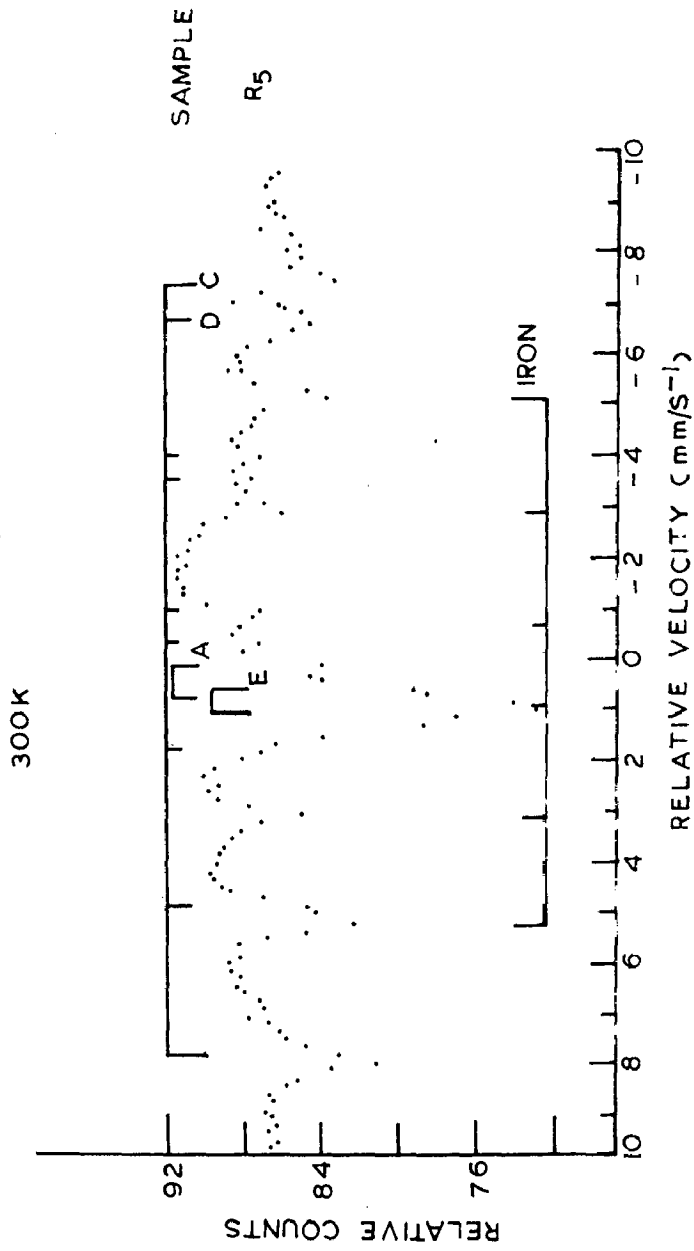
FIG.4.4. MÖSSBAUER SPECTRUM OF RUST SAMPLE R5.

A βFeOOH

C Fe_3C_4 (Tetrahedral site)

D Fe_3O_4 (Octahedral site)

E   FeO

values there is a real danger that the attack will be concentrated at a limited number of points and the depth of pitting may be very severe, particularly in the presence of aggressive ions such as chloride. Since in the reported case both the highly alkaline atmosphere and chloride ions are present simultaneously and thus pitting will be a severe problem.

4.5 CONCLUSIONS

The presence of β FeOOH in each rust studied was assigned to the presence of chloride ions in the water used for rcc. It was found that steels having more cementite end up with a corrosion product Fe_3O_4. The product α FeOOH in case of rust R_3 and R_4 was due to the highly alkaline nature of concrete. The accelerated corrosion in the case of 5 years old heavily corroded sample, obtained from a building, has been assigned to the presence of cementite in steel and highly alkaline atmosphere due to the concrete along with the chloride ions.

CHAPTER 5

EFFECT OF ALLOYING ELEMENTS IN

PLAIN CARBON STEELS

5.1 INTRODUCTION

Mössbauer spectroscopy is supposed to be the best available tool to understand the behaviour of the interstitial carbon atoms during and after transormation. X-ray spectroscopy can also be used but it supplies information indirectly through the lattice parameters. Other techniques are electron transmission microscopy and internal friction measurements method. The application of Mössbauer spectroscopy to study the iron based solid solutions, namely the substitutional ones, is extensive. It has also been employed to study the interstitial solid solutions mainly iron-carbon and iron nitrogen. Among these systems a considerable effort has been made to study the iron-carbon solid solution austenite and martensite because of their technological importance. The main object of the investigations on iron-carbon system and steels has been to study different phases and carbides formed and the structural changes occurring due to various thermal and mechanical treatments. A number of workers | 139-141 | have reviewed the metallurgical use of Fe^{57} Mössbauer effect in metallic iron and steels while the application of this technique in physical metallurgy has been discussed by Fujita | 142 | and Gonser |143|.

All the commercial steels (of metallurgical use) contain varying amounts of manganese, silicon, phosphorus and sulfur and often also varying amounts of elements such as nickel, chromium, molybdenum and vanadium (which are added intentionally) in addition to iron and carbon. The presence of these

alloying elements causes appreciable changes in the nature of phases present and the manner in which these phases are arranged to form the desired structure. This change in the phases improves various properties like increased strength, hardness, shock resistance, weldibility and corrosion resistance etc.. If the allyⁿing elements are present in very small amount roughly below 1 $^c/_o$ and the carbon concentration varies from 0 to 1.7 wt. $^a/_o$ then the steels are known as plain carbon steels. Since Mössbauer spectroscopy can be used to study both the interstitial and substitutional solid solutions and can detect even small changes occurring in the phases present, so its importance for studying the effect of alloying elements other than carbon in steels is quite obvious.

Mössbauer effect spectroscopy has been successfully applied to understand the effect of these alloying elements in martensitic and austenitic steels by many workers |144-147|. Galperin et. al.|148| discussed the influence of silicon on the properties of Fe-C alloys having carbon concentrations between 11 at.$^o/_o$ and 13 at. $^o/_o$ and found that for low concentration of silicon, it is used in ferrite formation but for a higher concentration, greater than 5 at. $^o/_o$ Si, it is used mainly in graphite formation. Lauermannova' and Žemčik |149| performed the Mössbauer measurements of hyperfine field in Fe-Ni-C martensite and found that the rate of change of hyperfine field with the carbon content was determined by the amount of nickel present. The type and degree of long range

ordering in Fe - Si steels was determined by Bogachev et.al.
|150| using Mössbauer effect technique. Bokshtein et.al.|151|
used the technique to find out intermediate phases in austenitic
Cr - Ni steels.

Very little work has been done of this nature in peailitic
steels. This chapter reports |152| the Mössbauer measurements
and their discussion on the effect of alloying elements silicon
and manganese in plain carbon steels of pearlitic nature. Along
with silicon and manganese other alloying elements which are
in general present in plain carbon steels are phosphorus,
sulfur. But both of these are in negligibly small amount and
hence their effect will be ignored. In the following section
first of all the general effect of these alloying elements is
given and then a brief introduction to the phase diagram (Fe-C)
is presented before discussing actual measurements and results.

5.2 GENERAL EFFECT OF THE ALLOYING ELEMENTS IN PLAIN CARBON STEELS

SILICON: A very small quantity of silicon, less than 0.2 percent,
is used in ferrite formation and does not have any significant
effect on the properties of steels. 0.2 to 0.4 percent of
silicon increases the ultimate strength of steel without an
appreciable decrease in ductility. Further increase in silicon
concentration decreases ductility while the concentrations
higher than 1 %, work as graphitising agent. This effect is
very pronounced in high carbon steels. Therefore the level

of silicon content must be kept to a minimum.

SULFUR : Normally it exists as sulfide (FeS) in steels. But in the presence of manganese it forms MnS instead of FeS due to its high affinity towards manganese the presence of FeS makes the steel brittle. Thus to neutralise the effect of sulfur the use of manganese is important and necessary.

MANGANESE: : It is the most important alloying element after carbon in most steels. In steels having less carbon contents manganese forms a solid solution with ferrite and has strengthening effects. In higher content carbon steels it exists as Mn_3C and forms the part of pearlite. The combination of cementite and manganese carbide has marked hardening effect on steel. Its usefulness in the presence of sulfur has been discussed above. In general upto 1% of manganese increases the strength but reduces ductility of the steel while hardenability is increased considerably.

PHOSPHORUS : It forms phosphide Fe_3P which exists in solid solution in the ferrite. If its concentration is more than 0.06 % , it has deteriorating effect since it leads to ferrite segregations during hot working.

5.3 PHASE DIAGRAM

Fig. 5.1 shows the phase diagram of the iron-carbon system for carbon concentrations (in weight percent) less than
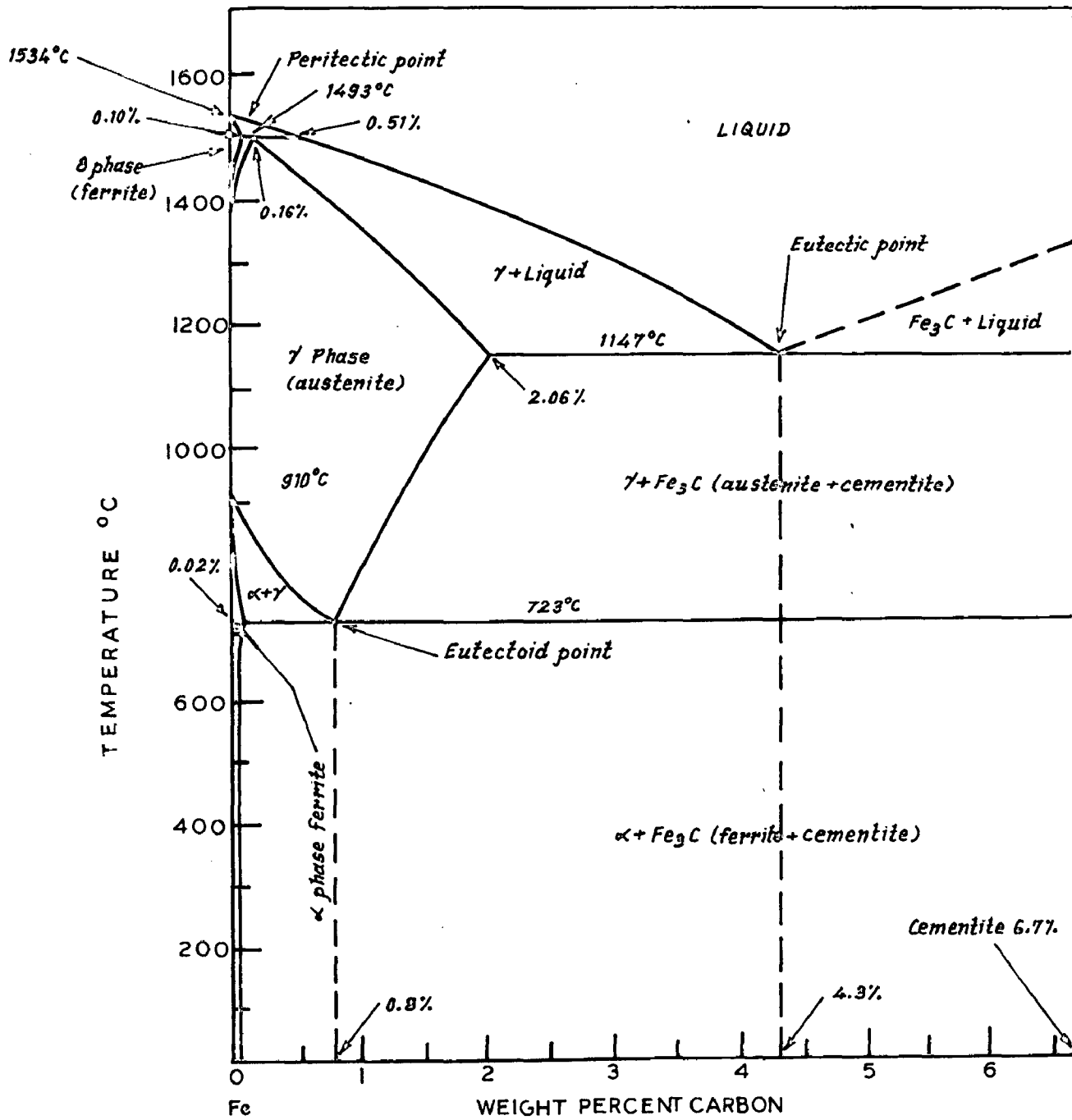
FIG.5.1 _ THE METASTABLE SYSTEM Fe - Fe₃C.

6.67 percent carbon, the composition of Fe_3C, or cementite;
the enlarged section of the eutectoid section is depicted in
Fig. 5.2 |153|. The iron-carbon system with carbon concentra-
tion upto 6.67 percent only has commercial significance and
therefore the phase diagram has been given for this part. It
is not a true equilibrium diagram since cementite is not an
equilibrium phase. This is because cementite under proper
conditions decomposes to form graphite. But this decomposition
has never been observed in ordinary steels because the nuclea-
tion of cementite in iron, supersaturated with carbon, occurs
much more rapidly than the nucleation of graphite and due to
this reason for all practical purposes it can be treated as an
equilibrium phase diagram. This diagram shows the formation
of various phases with change in composition. The diagram
is characterized by three invariant points; a peritectic point
at 0.16 percent Carbon and $1493^{\circ}C$, an eutectic point at 4.3
percent carbon and $1147^{\circ}C$, and an eutectoid point at 0.80
percent carbon and $723^{\circ}C$.

The austenite is face centered cubic solid solution
or gamma phase. The study of phase diagram shows that all
compositions with less than 2.06 percent carbon pass through
this austenitic region. And the alloys in this region are
called steels. The alloys with carbon concentration greater
than 2 % are called cast irons. Though these are not the simple
iron-carbon alloys but contain relatively large quantities of
silicon. The peritectic and eutectic points of the iron carbon
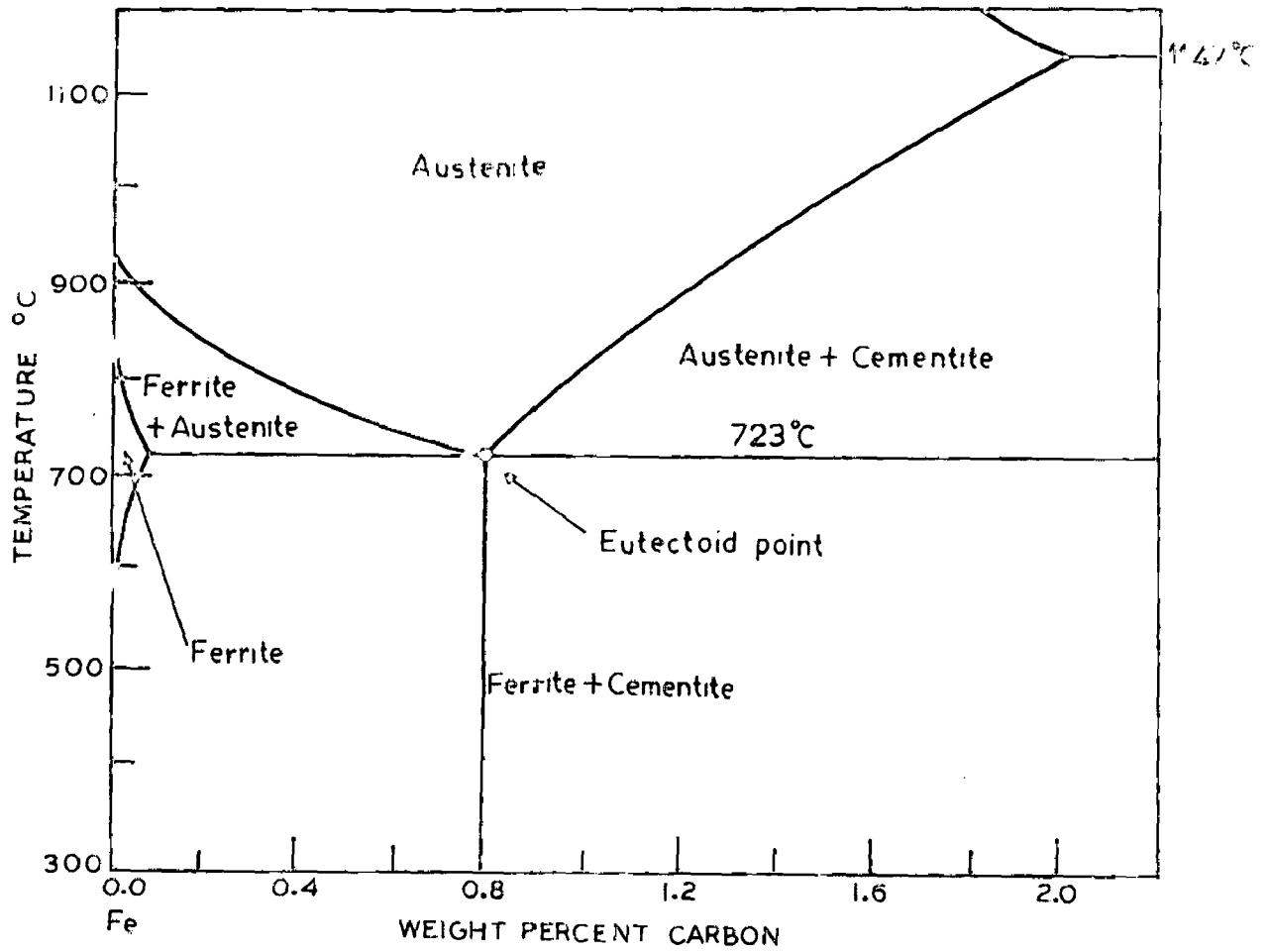
FIG. 5.2 _ THE EUTECTOID SECTION OF THE IRON ~ CARBON DIAGRAM.

system are not essential in the study of steels and the only point of importance is the eutectoid point. If any specimen is brought from a temperature above the eutectoid point to a temperature lower than the eutectoid point, austenite decomposes into two phases ferrite and cementite |154|. The ferrite is a soft and ductile solid solution of iron having very small amount of carbon upto 0.008 % at room temperature and cementite is a hard brittle interstitial compound formed between iron and carbon and contains 6.7 % carbon, the letter is generally denoted by the formula Fe_3C. If the specimen from the austenitic region is -quenched to room temperature it undergoes a martensitic transformation. The eutectoid structure formed by the mixture of stable phase ferrite and cementite is called pearlite and it consists of alternative plates of ferrite and cementite with ferrite continuous phase. When the austenite of eutectoid composition is reacted to form pearlite just below the eutectoid temperature, two phases appear in a definite ratio having 87.5 percent ferrite and 12.5 percent cementite.

5.4 CHEMICAL AND MICROSCOPIC INFORMATIONS

The steels studied were supplied by Metallurgical Services Laboratories Ltd., England. Chemical composition of steels, as specified by the manufacturer |155|, has been given in Table 5.1. The microstructural informations of the steels are given below while their microphotographs are shown in Fig. 5.3.
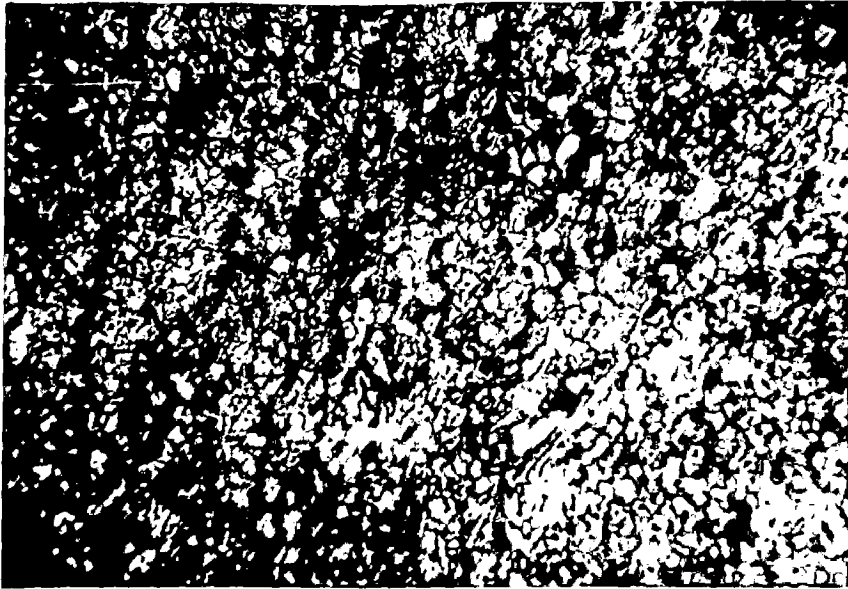
Microstructure of Steel N 25

Magnification   150
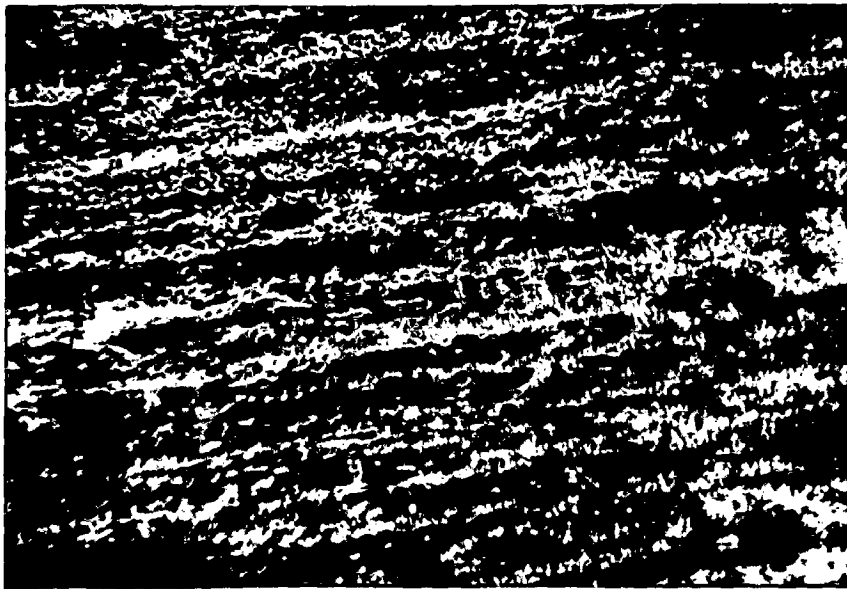
Enlarged   x 2

Microstructure of Steel N 15

Magnification   150

Enlarged   x 2

Microstructure of Steel N 20

Magnification 600

Enlarged   x 2
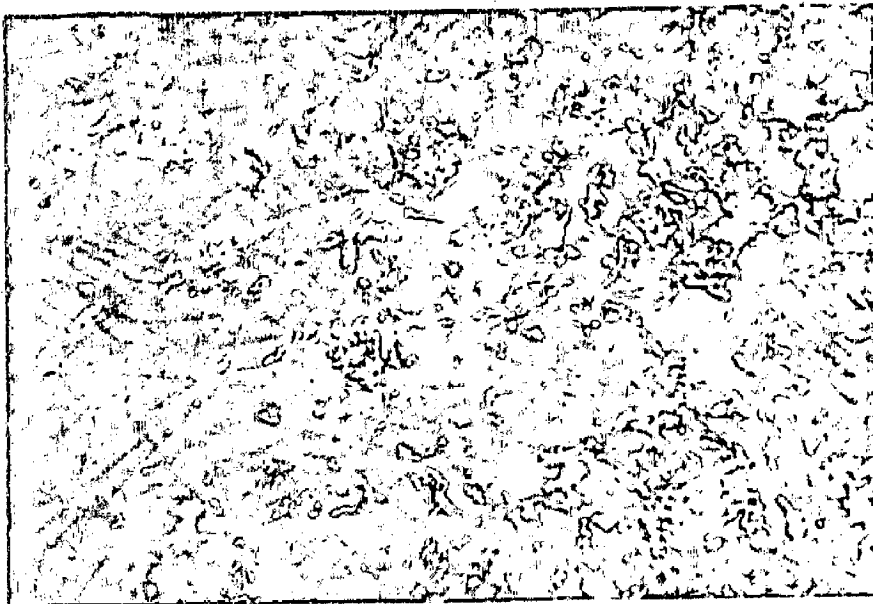
Microstructure of Steel N 24

Magnification 150

Enlarged   x 2

FIG. 5.3 MICROSTRUCTURE OF STEELS

TABLE 5.1: <u>CHEMICAL COMPOSITION OF STEEL IN WEIGHT</u>
<u>PERCENT</u>

Specimen no.	Type of material	C	Si	Mn	S	P	Total atomic percent of Si+Mn
N-25	0.1 percent C steel	0.11	0.21	0.85	0.02	0.015	1.27
N 15	0.3 percent C steel	0.31	0.29	0.84	0.038	0.03	1.42
N 20	0.7 percent C steel	0.66	0.33	0.84	0.034	0.038	1.50
N 24	1.3 percent C tool Steel	1.31	0.25	0.35	0.007	0.01	0.85

N.25 : The structure consists of equiaxial grains of ferrite together with about 10 % pearlite. The pearlite is generally distributed in bands following the rolling direction, although the ferrite grains are not elongated. Atleast 50 % of the pearlite is resolved with a 4 mm objective.

N 15 : A rough comparative index of ferrite content indicates the presence of 65 % ferrite. The pearlite is unresolvable by a 4 mm objective. An oil immersion objective helps in partial resolution of the pearlite.

N 20 : Here the structure is pearlite with a thin partial network of about 10-15 % ferrite. On polishing and etching first time, the structure is mainly unresolvable under a 4 mm objective. Repolishing and reetching makes the structure mainly resolvable using oil immersion objective.

N 24 : It consits of pearlite with a thin net work of cementite. The pearlite is partly resolved with a 4 mm objective and the resolution increases more when oil immersion objective is used. The carbide net work is only properly distinguished under oil. The etching with picrate makes the resolution more clear.

5.5 RESULTS AND DISCUSSION

The microscopic information on steels suggest their pearlitic nature. As discussed in section 5.3 pearlite is a eutectoid of two stable phases ferrite and cementite. Since steels N 25, N 15 and N 20 have carbon contents less than 0.8 % , which is eutectoid point, these steels must have ferrite

along with some pearlite. The ratio of the two phases depends on the carbon concentration. At the eutectoid composition (0.8 wt. $^o/_o$ carbon) the steel structure should be completely pearlitic. The N 24 steel is having 1.3 wt. $^o/_c$ carbon which is well above the eutectoid composition and hence in this region the steel structure should consist of pearlite and cementite. The optical microscopic studies are inadequate to confirm the above said phases conclusively. Further, due to the presence of Mn in the steels, the formation of Mn_3C is possible as discussed in section 5.2. The microscopic studies do not, as well , show any difference between the appearance of Mn_3C and cementite while Mössbauer spectroscopy distinguishes between the two. Further, the alloying elements forming solid solution with ferrite and replacing Fe in Fe_3C can also be detected. Thus Mössbauer spectroscopy can give both quantitative and qualitative informations more reliably.

Mössbauer spectra of steels N 25, N 20 and N 24 taken at room temperature and 500 K are shown in Fig. 5.4 and 5.5 respectively while the derived parameters are given in Table 5.2 and 5.3.

Due to the pearlitic nature of steels Mössbauer spectra should show a composite pattern due to ferrite and pearlite or more precisely due to ferrite and cementite. The ferrite spectrum, in the case of a steel having no alloying element, should be same as that of pure iron which is a well established six finger pattern showing field of 330 kOe. This is because

TABLE 5.2: MÖSSBAUER PARAMETERS OF STEELS AT 300K

Specimen	Site	Internal magnetic field kOe (Error = ± 2 kOe	Quadrupole splitting mm/sec. (Error = ±0.01 mm/sec	Isomer* shift mm/sec. (Error = ± 0.01 mm/sec.)
N 25	P(0)	331	0	0
	P(1)	304	0	+0.015
N 15	P(0)	331	0	0
	P(1)	304	0	+0.015
N 20	P(0)	332	0	0
	P(1)	304	0	+0.015
N 24	P(0)	332	0	0
	P(1)	Not separable	-	-

* Isomer shift values are reported with respect to iron.

TABLE 5.3: MÖSSBAUER PARAMETERS OF STEELS AT 500K

Specimen	Site	Internal magnetic field kOe (Error = ± 2 kOe	Quadrupole splitting mm/sec. (Error = ± 0.01 mm/sec.	Isomer* shift mm/sec. (Error = ± 0.01 mm/sec.
N 25	P(0)	314	0	-0.130
	P(1)	282	0.028	-0.116
N 15	P(0)	314	0	-0.130
	P(1)	282	0.028	-0.116
N 20	P(0)	314	0	-0.130
	P(1)	283	0.028	-0.116
N 24	P(0)	314	0	-0.130
	P(1)	Not separable	–	–

* Isomer shift values are reported with respect to iron.

ferrite contains very small amount of carbon (0.008 % C) and so would not have any observable effect of carbon. The cementite has also been studied extensively using Mössbauer spectroscopy |156-158|. It is an interstitial solid solution of carbon in iron and is ferromagnetic below $T_c \cong 210^{\circ}C$, the magnetic field being ~ 208 kOe and at room temperature; the chemical isomer shift is + 0.19 mm/sec. above that of α-Fe |156, 157|. Thus, the spectra of both phases ferrite and cementite show their specific parameters. Now if impurities e.g. Mn and Si (which are present in our case) are added as alloying elements may enter in the steel in three ways: (i) form solid solution with ferrite (ii) substitute for iron in Fe_3C (iii) form some carbides (like Mn_3C etc.). The first two types of effects will cause the change in Mössbauer parameters of the ferrite and cementite phases and thus should appear as satellites in the spectrum of main phases (ferrite and cementite). However, in the third case, it can not be directly detected with the help of Mössbauer spectroscopy. Its indirect detection will be manifested in the decrease of other phases. Thus, it should be possible to understand the behaviour of the alloying elements by observing the change in various phases.

Due to the small amount of carbon in these samples, we could not observe Mössbauer pattern of cementite (or carbide) at room temperature upto the total storage of counts 3×10^5 per channel Fig. 5.4. Since microscopic study revealed these steels to be pearlitic in nature and thus, should contain
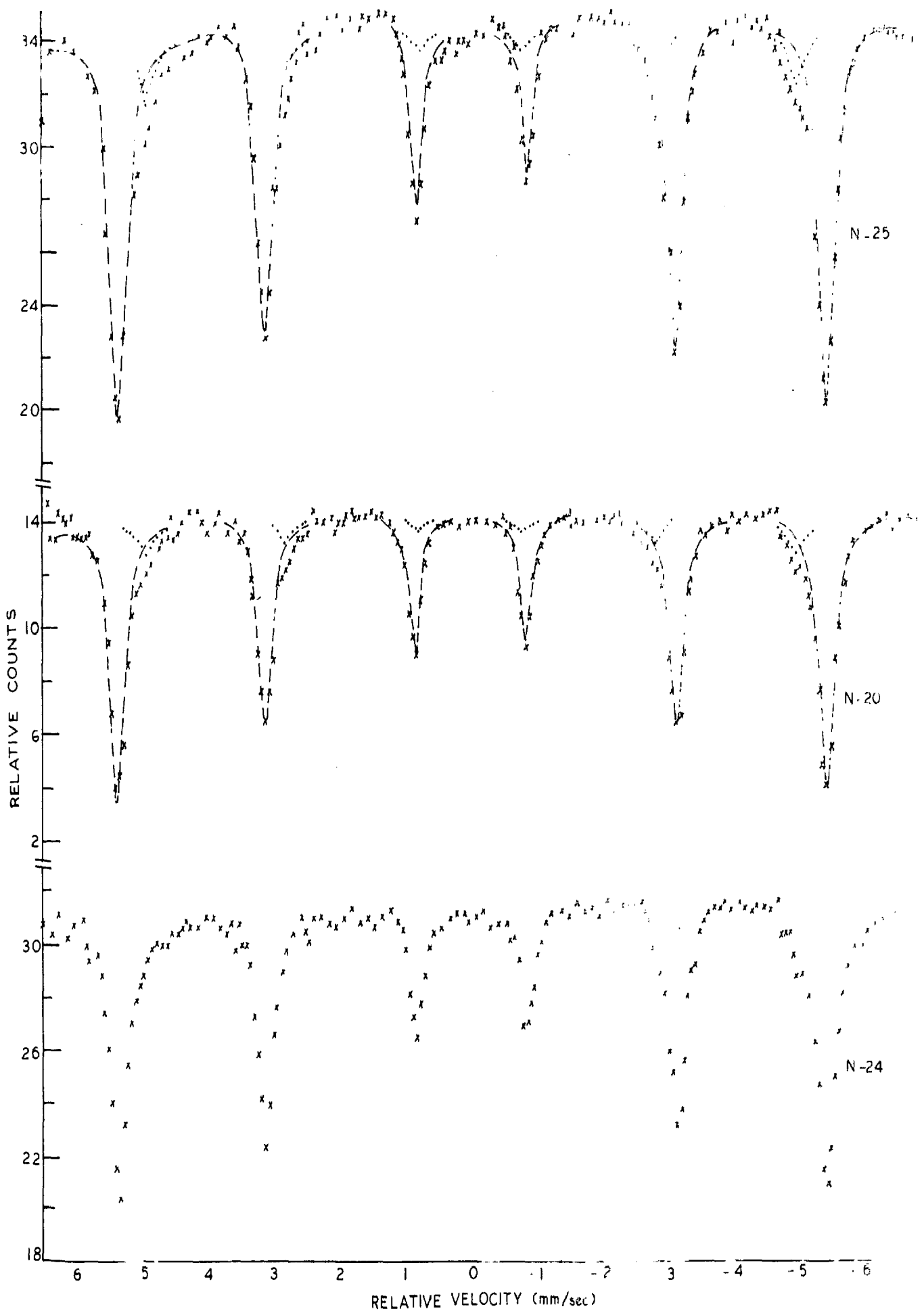
FIG.5.4 _ MÖSSBAUER SPECTRA OF STEELS AT 300K.

xxxx Experimental points
– – – Separated pattern due to P(0)
• • • • Separated pattern due to P(1)

some amount of cementite. To check this through Mössbauer spectroscopy the spectra were recorded at 500 K which is well above the Curie temperature of cementite. At this temperature cementite manifests its presence by lowering of the middle portion of the spectrum Fig. 5.5 and confirms the pearlitic nature of steels through Mössbauer spectroscopy too. The presence of cementite becomes clear at this temperature due to its transformation from magnetically ordered state to paramagnetic state and thus the Mössbauer spectrum is a doublet so the total absorption which was first divided in six peaks is now limited to two peaks only and this increase in absorption per peak indicates the presence of cementite. Such a lowering of the spectrum was not observed in N 25 steel, which is not surprising because it contains only 0.1 percent carbon.

Mössbauer spectra of N 25, N 15 and N 20 steels show clear satellites in their 1st, 2nd, 5th and 6th peaks atleast. This satellite structure in outer two or four lines was first of all observed by Stearns | 59 | and Wertheim et.al. | 62 | and was attributed to the iron sites having impurities in their neighbourhood. The observation of zero quadrupole splitting for the iron site having impurities in their neighbourhood (Table 5.2) suggests that the impurities have gone substitutionally | 62, 159 |. Vander Woude and Sawatzky | 63 | in their review article have also mentioned that for dilute iron alloys the quadrupole splitting is negligible. Thus it shows that in this case the impurities have gone substitutionally. To understand the behaviour of alloying elements in these steels
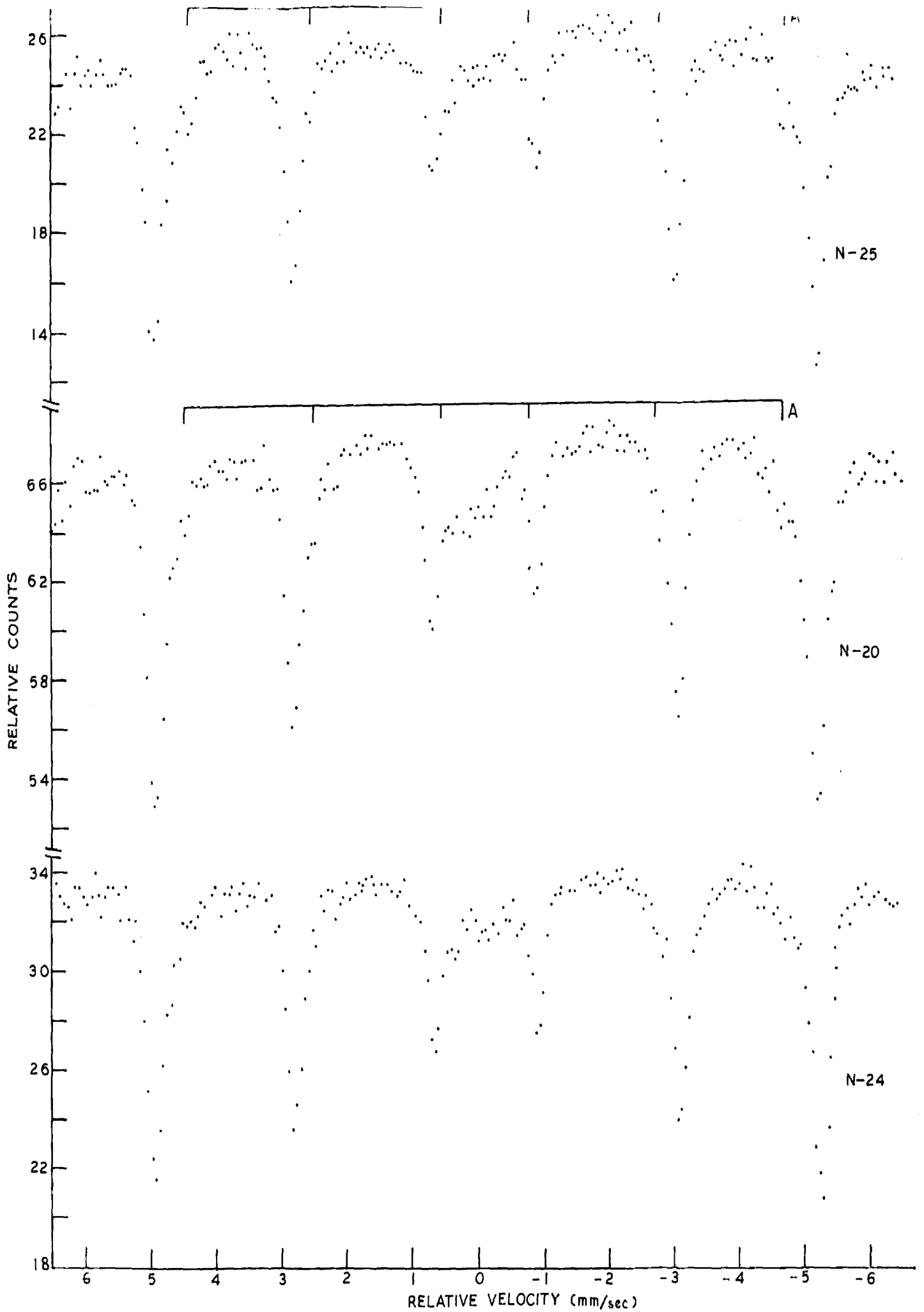
FIG.5.5 - MÖSSBAUER SPECTRA OF STEELS AT 500K.

A : Pattern due to site P(1)

with the concentration of carbon, the following procedure was adopted. If the impurities have gone only substitutionally then the intensity of the satellites should increase as the impurity concentration increases.

To estimate the probabilities of various sites the following assumptions were made:

(1) Both the impurities (Mn and Si) in the first nearest neighbour cause the same effect | 160, 161 | on the hyperfine pattern of iron nucleus.

(ii) In this low concentration range of impurities, the distribution of impurities is random.

Further, the probabilities for only those sites were calculated which give , the probabilities sum close to unity. The probability of finding an iron atom in a particular configuration (m, n) is given by

$$P(m,n) = \binom{8}{m} \binom{6}{n} C^{m+n} (1-C)^{14-m-n}$$

where C is the total impurity concentration; m and n are the number of impurity atoms in the nearest neighbour (nn) and next nearest neighbour (nnn) respectively. The iron lattice is b.c.c and it has nn and nnn 8 and 6 respectively. Calculation for probability were done for the configurations P(0) and P(1) since these give the total probability greater than 0.99. The contribution from the other sites will therefore be too little to be detected and thus the observed spectra were

separated into two patterns due to P(0) and P(1) sites having
zero and one impurity atom in the nearest neighbour shell
respectively.

The calculated and observed probabilities are given
in Table 5.4. The estimation of the observed probabilities
P(0) and P(1) was made as follows. The total area instead of
intensities ratios of peaks was considered. This was done
because due to the distortion in line shape and broadening
in line width caused by impurities, it is the area not the
depth of the peaks which should be considered as discussed in
chapter 2. Then the measured area under the two patterns P(0)
and P(1) was normalised to the total area 100. From this total
area 100 the separate percentage of the two patterns was esti-
mated. The comparison of the calculated and observed occurrence
of the two patterns (Table 5.4) gives following information:

(i) The observed and calculated occurrence of the patterns P(0)
and P(1) are of the same order in N 25 steel.

(ii) The observed occurrence of P(1) goes on decreasing as
the carbon concentration increases.

(iii) The observed occurrence of P(1) is undetectably small in
N 24 steel (having 1.3 % carbon).

The roughly equal order of calculated and observed
occurrence of P(1) in the case of N 25 steel leads to the
conclusion that all the impurities (total Mn and Si) have been
utilized in solid solution formation with ferrite. The less

TABLE 5.4: CALCULATED PROBABILITIES AND OBSERVED AREA OF VARIOUS SITES.

Specimen no.	Site	Calculated probability percent -	Observed relative areas (Total area taken to be 100)
N 25	P(0)	90.28	91.6
	P(1)	9.30	8.4
N 15	P(0)	89.18	92.1
	P(1)	10.30	7.9
N 20	P(0)	88.60	92.2
	P(1)	10.80	7.8
N 24	P(0)	93.40	Not Separable
	P(1)	6.40	

observed occurrence of P(1) in the case of N 15 and N 20 in comparison with N 25 while these have more impurity contents may be understood as follows:

The impurities Si and Mn exist in two forms. Firstly in the form of solid solution with ferrite and secondly in the form of carbides. Thus, in these steels N 25 to N 24, as the carbon concentration increases more and more impurity atoms will be utilized in the formation of carbides. Therefore, samples N 15 and N 20, although have little more impurity concentration than N 25, will have rather less number of these atoms available for solid solution formation with ferrite due to increased concentration of carbon in these samples (Table 5.1). This explains the reduction of satellite intensities in these samples. The formation of carbides with impurity atoms may further be argued from the spectrum of N 24 steel. Here although carbon is 1.3 wt. $\%$ but no iron carbide, e.g., cementite could be detected at room temperature, Therefore, it appears that in this case part of the carbon has been utilized in the formation of carbides with other elements e.g. silicon which is a good graphitizing agent and also may be manganese which forms Mn_3C as discussed in sec. 5.2 and the rest forms carbides with iron. This iron carbide was so small that it could be detected only at 500 K above the Curie temperature of cementite.

5.6 CONCLUSIONS

These studies show that for the low carbon concentration in steels most of the alloying elements form solid solution

with ferrite. As the carbon concentration increases the alloying
elements exist in two forms: one in the solid solution with
ferrite and second in the form of carbides. The latter was
concluded indirectly from the undetectable presence of cementite
in N 24 steel where it has sufficient amount of carbon present
(1.3 wt. %).

CHAPTER 6

PART A : AN INVESTIGATION OF BINARY SYSTEM FeSe

A.6.1 INTRODUCTION

Selenium is an element from VI group of periodic table with electronic configuration $|Ar|\ 3d^{10}4s^24p^4$. It forms compounds in formal oxidation states IV and VI along with divalent species and the coordination number is not limited to four because d orbitals may be utilized in bonding. Cotton and Wilkinson |162| have remarked that selenium shows non-metallic covalent chemistry. Lower electronegativity of this element lessens the ionic character of the compounds that are formed analogous to those of oxygen.

Selenium finds a number of applications in modern technology. Along with its application in photoelectric devices it has also been greatly used in glasses. It has been in use as a decolourizer for Fe containing glasses for last eight decades and as a colourant even longer, but the chemistry of selenium in glass is not completely understood. Since the boiling point of elemental selenium is about $700^{\circ}C$, well below the temperature of commercial glass furnaces. As a result, selenium is lost — continuously during the melting process. Some selenium does remain in the melt. The remaining selenium in the glass can be in any of the different valence states (Se^0, Se^{-2}, Se^{+4}, Se^{+6}), some providing colour while others are colourless. Elemental selenium and Se^{-2} (present in the form of various selenide compounds such as Na_2Se, $CdSe$, $FeSe$ etc.) provide colour to the glass while Se^{+4} in the presence of an oxidising agent such as As_2O_3 or Na_2NO_3 or in an oxidising atmosphere ·produce various selenite compounds

such as Na_2SeO_3 which helps in making the glass colourless. Se^{+6} is a rare valency for selenium and exists under extreme oxidising conditions and also helps in decolourizing the glass. Selenium is also used as a constituent in heat absorbing glasses. In a heat absorbing glass the infrared portion, which is 50% of the total solar load, is absorbed and thus making the transmittance of the visible portion roughly 100 percent. This is obtained by adding Fe_2O_3 ($\sim$ .5 wt. %), most of which is in Fe^{2+} state. The visible transmittance can also be reduced by proper combination of selenium, CoO and Fe^{3+} and thus producing a neutral grey colour.

A small amount of selenium when added to carbon steels affects the inclusions present and hence the machineability of steels. Since small amount of selenium has such pronounced effect on iron bearing systems, it becomes very interesting to study the iron-selenium system. Further, binary alloys of iron, especially chalcogenides, form interesting systems for a comparative study of the Mössbauer effect.

The phase diagram of iron and selenium giving the liquid phases does not exist. Fig. A 6.1 taken from Ref.|153| gives the equilibria at elevated temperatures between various products and compositions. It shows that Fe forms two types of selenides FeSe (58.75 wt. % Se) | 163-166| and $FeSe_2$ (73.87 wt. % of Se) |167|. Other selenides have also been reported in the literature but their identification has been precluded by the absence of homogeneous phases |163,168|.
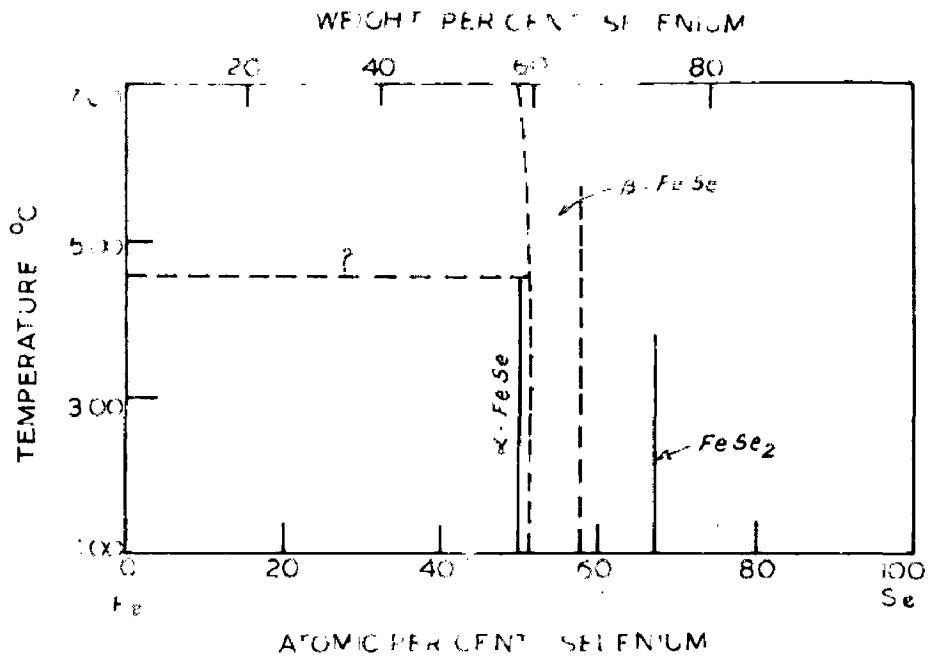
FIG. 6.1. Fe-Se SYSTEM.

X-ray analysis of Hägg and Kindstrom |166| showed that FeSe

exists in two forms (i) α-FeSe having the PbO (B10) type tetra-

gonal structure and (ii) β-FeSe, isotypic with NiAs (B8) ,

|165,166|. In the NiAs type structure each iron atom is surr-

ounded octahedrally by six selenium atoms, but is also approached

fairly closely by two other metal atoms. These metal-metal

distances are responsible for their alloy like or semimetallic

type character. Hirone and Chiba |169| performed magnetic

susceptibility measurements on $FeSe_x$ system with NiAs structure

and concluded that ferrimagnetism in this system originates from

β-FeSe, and the α phase with PbO structure is weakly paramagnetic

or antiferromagnetic. This β phase is stable in stoichiometric

form only at higher temperatures while at room temperature it

is only stable in nonstoichiometric form having more selenium

content. Ferrimagnetism was also established in β-FeSe by

Hirone and Maeda |170| and Maxim |171| on the basis of magnetic

susceptibility measurements. Mössbauer studies on this system

β-FeSe with NiAs type structure were performed by Ono et.al.

|172| and Kasper and Drickamer |173|. The former workers

obtained a single line Mössbauer spectrum while the latter a

doublet and thus got information about the paramagnetic beha-

viour of the compound. Hirone and Chiba |169| also observed

another modified form of β-FeSe phase known as ϒ-FeSe while

studying the system $FeSe_x$ (x=1.00 to 1.30) and found that

this system $FeSe_x$ is a mixture of two phases α and β, which

transform into the third phase ϒ by eutectoidal reaction at

$350^{\circ}C$. Mössbauer studies performed by Reddy and Chetty |174|

on this γ phase showed it to be non-magnetic. The compound Fe_7Se_8 has also been extensively studied because of its interesting crystallographic transformation and ferrimagnetic properties |175-180|. Two types of crystallographic superstructures |175,177| of ferrimagnetic Fe_7Se_8 have been proposed. One of these is triclinic superstructure (4c structure) having a unit cell length along the c axis four times as long as that of the unit cell of the fundamental NiAs structure. The other is the orthorhombic superstructure (3c structure). Magnetic properties of Fe_7Se_8 have been studied by neutron diffraction method |178| and by magnetic torque and magnetic measurements |176, 179|. These measurements suggest that magnetic moments of iron atoms at high temperatures are parallel to the c plane and parallel to each other on the same atomic layer, while they are antiparallel to those on the next layer. Mössbauer studies have been performed by Ok and Lee |181| and Boumford and Morish |182| to understand the magnetic properties of the system and also to confirm the change in spins direction which these two modifications undergo at lower temperatures. -The spin direction changes from c plane to parallel to c axis. The other selenide $FeSe_2$ having the marcasite structure (a structure very similar to the pyrite but some what less regular) was studied by Temperley and Lefevre | 183 | through Mössbauer spectroscopy. Recently Reddy and Chetty |174| reported findings of Mössbauer studies on the system FeSe. But there are no reports which pertain exclusively to the investigation of α-FeSe. This chapter reports the results of the system

FeSe |184| with selenium concentration only upto 25 at.%.

According to Troften and Kullerud |185|, in this range FeSe

system has two phases Fe and α-FeSe. The objective of the

presently reported experiments was to check the formation of

the above said phases and to understand the bonding mechanism

of FeSe existing in the α-form.

A. 6.2 STRUCTURE

X-ray measurements of Hägg and Kindstrom |166| showed

that α-FeSe has a tetragonal structure of PbO (B10) type. The

PbO structure is well known. According to Wells |186| it has

a layer structure in which the metal atom is bonded to 4 O atoms

which are arranged in a square to one side of it, with the lone

pair of electrons presumably occurring at the apex of tetrago-

nal bipyramid |187|. All the four bond lengths are same 2.30 A°.

In this structure the lead atoms lie at positions (1/2, 0, u)

and (0, 1/2, $\bar{u}$) while oxygen atoms at positions (0,0,0) and

(1/2,1/2, 0). The exact nature of the structure for PbO type

compounds depends on the values of u and c/a. Janusz Leciejewicz

|187| performed neutron diffraction measurements to determine

the crystal structure of tetragonal PbO and found the parameters

a = 3.96 ± 0.01 , c = 5.01 ± 0.01 A° , c/a = 1.27 and u = .237

± 0.002. These measurements tally with the X-ray measurements

of Bystrom |188| who found a= 3.964 A° , c = 5.008 A° and

u = 0.2385.

In view of the observations made by Hägg and Kindstrom

|166| that the structure of α-FeSe is similar to that of PbO

the Fe atoms will occupy the positions (1/2, 0, u) and

(0, 1/2, $\bar{u}$) and Se atoms will be at (0,0,0) and (1/2,1/2,0).

In this case a = 3.77 $\overset{o}{A}$, c = 5.53 $\overset{o}{A}$, c/a = 1.47. The

observed bond length |174| is 2.37 A^o which – corresponds to

u $\sim$ .26. The elementary tetragonal cell contains two atoms

each of Fe and Se. Since in this case the c/a and u values are

different from that of PbO and thus the structure will also be

different. On the basis of above data the structure of α-FeSe

is given in Fig. A 6.2 (i). Here also the structure is a

layered structure with only Fe-Fe contacts between the layers.

The arrangement of bonds from a metal atom is shown in

Fig. A 6.2 (ii), where the two dots represents the 'inert pair'

of electrons. The most probable space group assigned to

α-FeSe is D_{4h}^{7} – P_4/nmm while the point group symmetry of

Fe site is C_{4v}.

A. 6.3 <u>EXPERIMENTAL</u>

(i) <u>SAMPLE PRAPARATION</u>: The samples were prepared using the

solid diffusion technique. The melting method is not applicable

because of the large difference in melting and boiling points

of iron and selenium. FeSe samples were prepared for

4,6,8,10,15,20 and 25 at.$^o/_o$ Se. The calculated amounts of

the two constituents iron and selenium (minimum 99.99 $^o/_o$

pure) were thoroughly mixed in an agate mortar (dry mixing

was preferred to avoid the possibility of formation of any
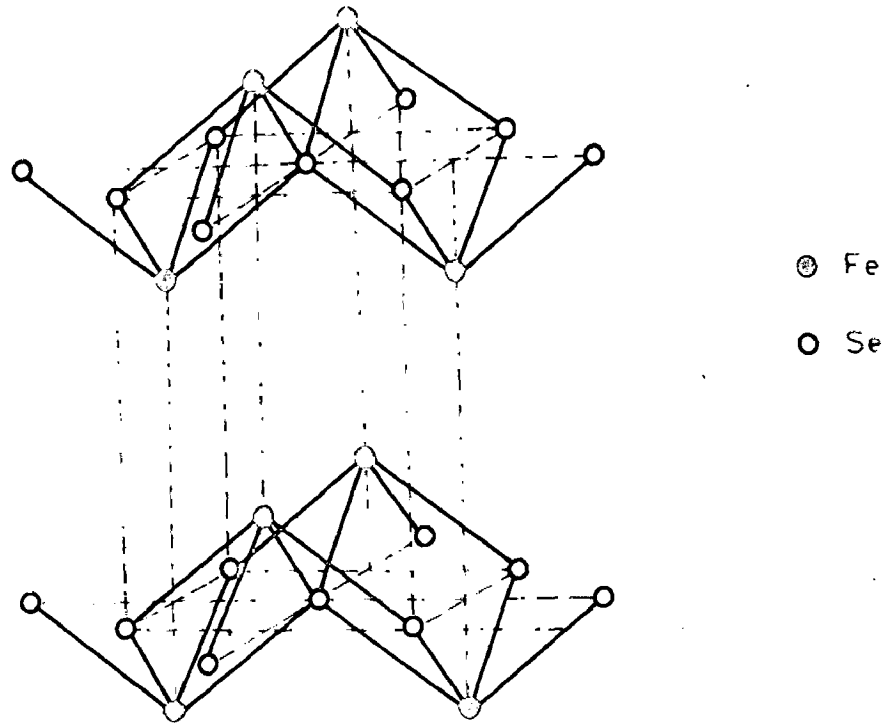
FIG.A.6.2(i) CRYSTAL STRUCTURE OF
TETRAGONAL Fe Se .

⊛ Fe

O Se
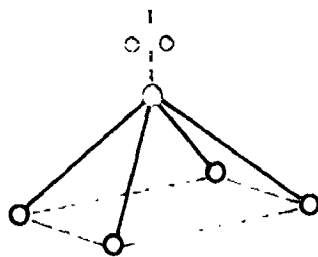
FIG.A.6.2(ii) ARRANGEMENT OF BONDS FROM A
METAL IN FeSe ɔ—► LONE ELECTRON.

oxide or hydroxide) for a long time to ensure the complete mechanical mixing. The mechanical mixtures of different compositions were compressed by a hydraulic press with a press - ure of 5 tons/sq.inch. This compacting of the powder mixtures helps in increasing contact area and therefore increasing in the diffusion rate. The compressed pallets (2.5 ~3 gms) were vacuum sealed in silica tubes and heated at a temperature of $300^{\circ}C$ for one week. These were then cooled to room tempera- ture, powdered and repalleted. This process again helps in making the diffusion fast and homogeneous. The repalleted samples were again vacuum sealed in silica tube and given the heat treatment at $400^{\circ}C$ for a week. The same process was repeated for $500^{\circ}C$. Samples having 6 and 20 at. % selenium were quenched from $500^{\circ}C$ and others with 4,8, 10,15 and 25 at. % selenium were heated at a temperature of $650^{\circ}C$ for a week and then quenched. The oil quenching was preferred.

(ii) <u>X-RAY ANALYSIS</u> : The sintered compacts were crushed to get the fine powder. Lindamann glass capillary with 0.5 mm diameter was used for holding the samples. The X-ray powder diffraction photographs were taken on a Russian X-ray unit of YPC make using iron target and Debye Scherrer camera of diameter ϕ 57.3 mm. The operating voltage was 30 kV, current 18 mA and exposure time 6 hours. The pattern revealed the α-FeSe phase with lattice parameters a = 3.77 $\overset{o}{A}$, c = 5.53 $\overset{o}{A}$ and c/a = 1.47.

A. 6.4 IONICITY CALCULATION USING SANDERSON METHOD OF EQUALISATION OF ELECTRONEGATIVITIES.

The concept of electronegativity has been of wide interest as it can be used at least relatively, to estimate the polarity of bonds and hence the conditions of the atoms in the combined state. However, it can not be defined precisely and different workers have given different quantitative measures of electronegativity. The magnitudes based on the relative compactness corrected in the light of trends in electron densities have been found to reproduce various experimental data quite reliably.

When two or more atoms having different electronegativities combine together, they share the electron clouds in such a way that their electron densities are changed to give an intermediate electronegativity in the compound. In order to determine this intermediate value, both arithmetic and geometric means have been investigated and the latter appears to be more acceptable. Thus the electronegativity E of the compound is given by

$$E = \left| E_1^{n_1} \, E_2^{n_2} \, \ldots\ldots\ldots E_k^{n_k} \right|^{1/n_1 + n_2 + \ldots + n_k}$$

where E_i is the electronegativity of ith type of the element whose n_i atoms are present in the compound. This constitutes the principle of equalisation of electronegativities and can be used to find the change in electronegativity of a particular atom due to compound formation.

$$\Delta E_i = E - E_i$$

A change in electronegativity corresponds to a change in the electron density around the atom and thus knowing the change in electronegativity due to addition or removal of an electron (unit charge), one can find the partial charge resulting from the change in electronegativity of the given atom.

Partial charge on atom: ΔQ =

$$= \frac{\text{Actual change in electronegativity of atom } \Delta E_i}{\text{Electronegativity change } \Delta E_i(1) \text{ due to addition or removal of one electron}}$$

Sanderson |189| has tabulated the values of electronegativity change corresponding to addition or removal of unit charge such that the experimental values of dipole moments are faithfully reproduced, and some of these numbers for typical elements are also listed in Table A 6.1, along with the electronegativities defined on the compactness scale. The partial charge is associated with the bond polarity resulting from the difference in electronegativities of the combining atoms and this quantity divided by the valency of that atom gives the ionicity due to this factor. Consequently, 1-ionicity may be regarded as measure of all other factors like covalency, overlap etc. which determine the charge distribution in the compound. This method of finding partial charge through equalisation of electronegativity, introduced by Sanderson |189|, has been found to give good agreement between calculated

TABLE A 6.1: ELECTRONEGATIVITY AND CHANGE IN ELECTRONEGA-
TIVITY PER UNIT CHARGE FOR A NUMBER OF
ELEMENTS.

Element	Electronegativity E	Change in Electronegativity per unit charge $\Delta E(1)$
H	3.55	3.92
C	3.79	4.05
N	4.49	4.41
O	5.21	4.75
S	4.11	4.22
Cl	4.93	4.62
K	0.56	1.56
Fe	2.10	3.01
Se	4.25	4.29

and experimental values of dipolemoments of a large number of molecules |189,190|. Recently Vishwamittar and Puri |191| used this method to compare 1- ionicity factors for many compounds/systems and got reliable information from this data.

We have also calculated 1-ionicity for FeSe and some other compounds and compare these with the observed isomer shift values for the compounds Table A 6.2. To illustrate the steps involved in these calculations we give below the details for FeSe, the system under consideration, and for $K_4Fe(CN)_6$, which has reasonably large number of atoms.

CALCULATION OF IONICITY

(i) FeSe

$$E_{Fe} = 2.10 \quad , \quad E_{Se} = 4.25$$

$$E_{FeSe} = \sqrt{2.10 \times 4.25} = 2.99$$

$$\Delta E_{Fe} = E_{FeSe} - E_{Fe} = 2.99 - 2.10 = .89$$

So, partial charge on Fe $= \dfrac{\Delta E_{Fe}}{\Delta E(1)} = \dfrac{.89}{3.01} = .30$

ionicity of Fe $= \dfrac{\text{Partial charge on Fe}}{\text{Valency}} = \dfrac{.30}{2} = .15$

Thus covalency and overlap factor $= 1-$ ionicity

$$= 1- .15 = .85$$

(ii) $K_4Fe(CN)_6$

$$E_K = 0.56 \quad , \quad E_{Fe} = 2.10, \quad E_C = 3.79, \quad E_N = 4.49$$

TABLE A 6.2: COMPARISION OF CALCULATED VALUES OF 1-IONICITY AND OBSERVED ISOMER SHIFTS FOR SOME IRON COMPOUNDS.

Element	1- Ionicity of Fe	Isomer shift* mm/sec.
$FeCl_2$	0.73	1.083 |Ref. 194|
FeO	0.80	0.96 |Ref. 109|
Fe_2O_3	0.83	0.696 |Ref. 192|
FeSe	0.85.	0.47 |Ref. 184|
FeS	0.86	0.35 |Ref. 195|
$K_4Fe(CN)_6$	0.94	-0.032 |Ref. 193|

* with respect to iron.

$$1/17$$

$$E = |(.56)^4 \times (2.10) \times (3.79)^6 \times (4.49)^6|$$

$$= 2.48$$

$$\Delta E_{Fe} = 2.48 - 2.10 = .38$$

So partial charge on Fe $= \dfrac{\Delta E_{Fe}}{\Delta E(1) \text{ for Fe}} \approx \dfrac{.38}{3.01} = .126$

ionicity $= \dfrac{\text{partial charge}}{\text{valency}} = \dfrac{.126}{2} = .063$

covalency and overlap factor $= 1 - .063 = 0.937$

A. 6.5 RESULTS AND DISCUSSION

Mössbauer spectra of FeSe with 4,6,8,10,15,20 and 25 at. % selenium were recorded at room temperature. The spectra due to 4,6 and 8 at. % selenium show iron spectrum with some unidentified lowering in the middle part. This lowering of spectrum in the middle was assigned to the presence of FeSe in small quantity. For higher concentrations of selenium, this lowering becomes clear and the spectrum was a composite spectrum due to iron and α-FeSe. The X-ray diffraction results confirm this FeSe to be in PbO type form. Thus it clearly shows that in the lower concentration range of selenium a two phase system between Fe and α-FeSe exists and support the findings of Troften and Kullerud |185| obtained through X-ray and thermal studies. Since the Mössbauer effect spectroscopy is a more sensitive technique than others e.g. X-ray and thermal studies,

and can detect a phase present in a very small quantity, thus may be used to estimate the formation of various phases in the low concentration range of selenium. In Mössbauer spectroscopy the presence of phases in very small quantities is reflected in the change in peak intensity ratios or line shapes and width of the main phases. The effect of various thermal treatments was also seen. This study shows that in the lower concentration range of selenium the heating temperature is not very much important and selenium is insoluble in iron. The samples having 6 and 20 at. % of selenium were given a heat treatment only upto $500^{\circ}C$ while the others upto $650^{\circ}C$. But the Mössbauer patterns in both the cases were same in nature. Such two patterns corresponding to 20 and 25 at. % selenium, which were given different heat treatments, are shown in Fig. A 6.3 and Fig. A 6.4 as typical examples. In order to obtain a more reliable data for α-FeSe the spectrum of 20 at. % selenium was run at lower velocity and is given in Fig. A 6.5.

The phase identified as α-FeSe gives the values of isomer shift (I.S.) and quadrupole splitting (Q.S.) as 0.48 mm/sec. and 0.23 mm/sec., respectively (Table A 6.3). The only values reported earlier for this compound are those of Reddy and Chetty |174| who found I.S. to be 0.39 mm/sec. and Q.S. as 0.45 mm/sec.. A close examination of their spectra gives line width of peaks of the order of 0.9 mm/sec., which is obviously too high for a single phase and thus makes their fitting of curves doubtful. On the other hand, in our case the line width of α-FeSe lines is of the order of .35 mm/sec.

300 K

RELATIVE VELOCITY (mm/sec)

RELATIVE COUNTS
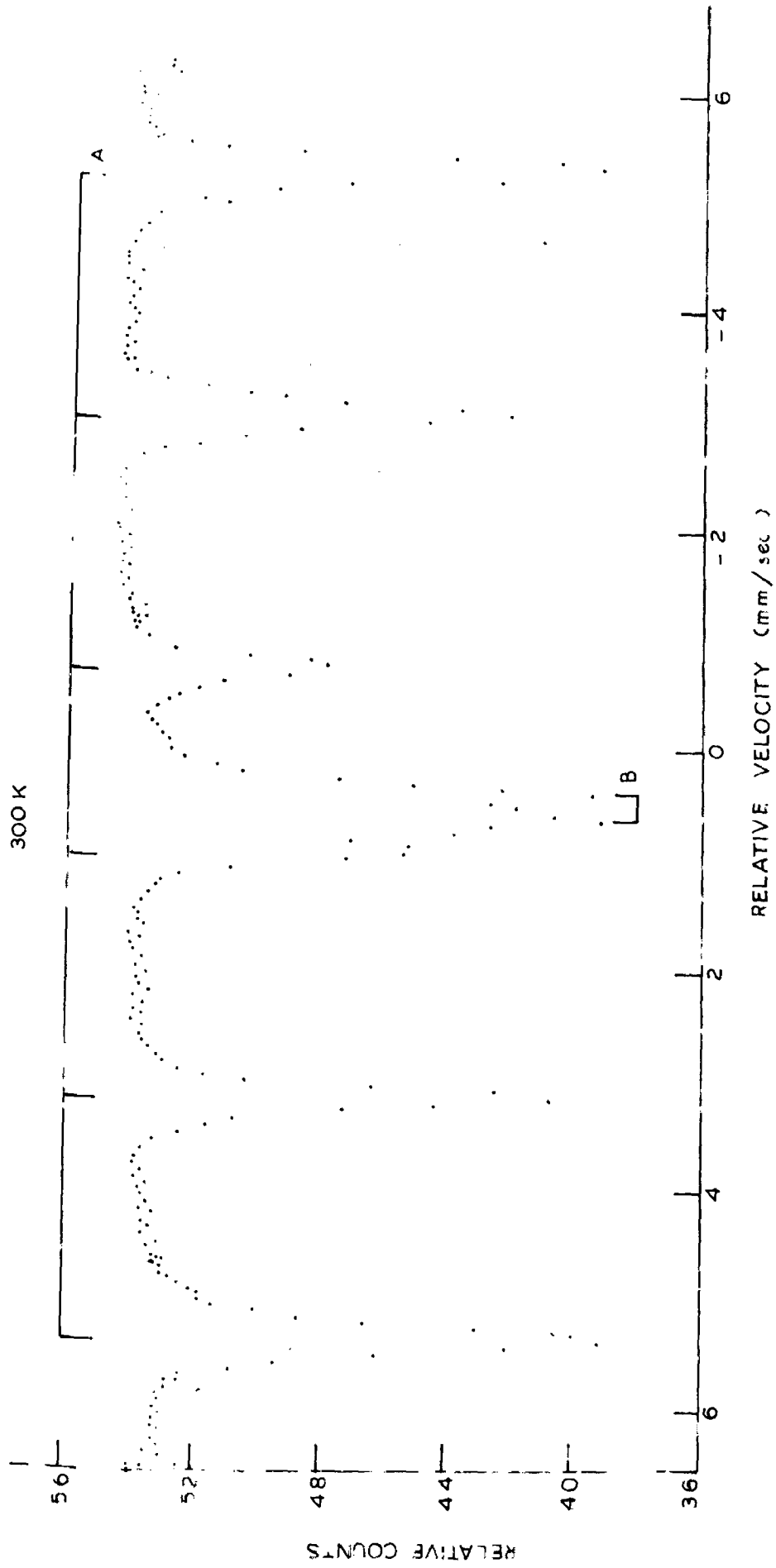
FIG.A.6.3 . MÖSSBAUER SPECTRUM OF Fe-Se (20at.% Se) QUENCHED FROM 500°C.

A : Fe
B : ∝ Fe Se

300 K
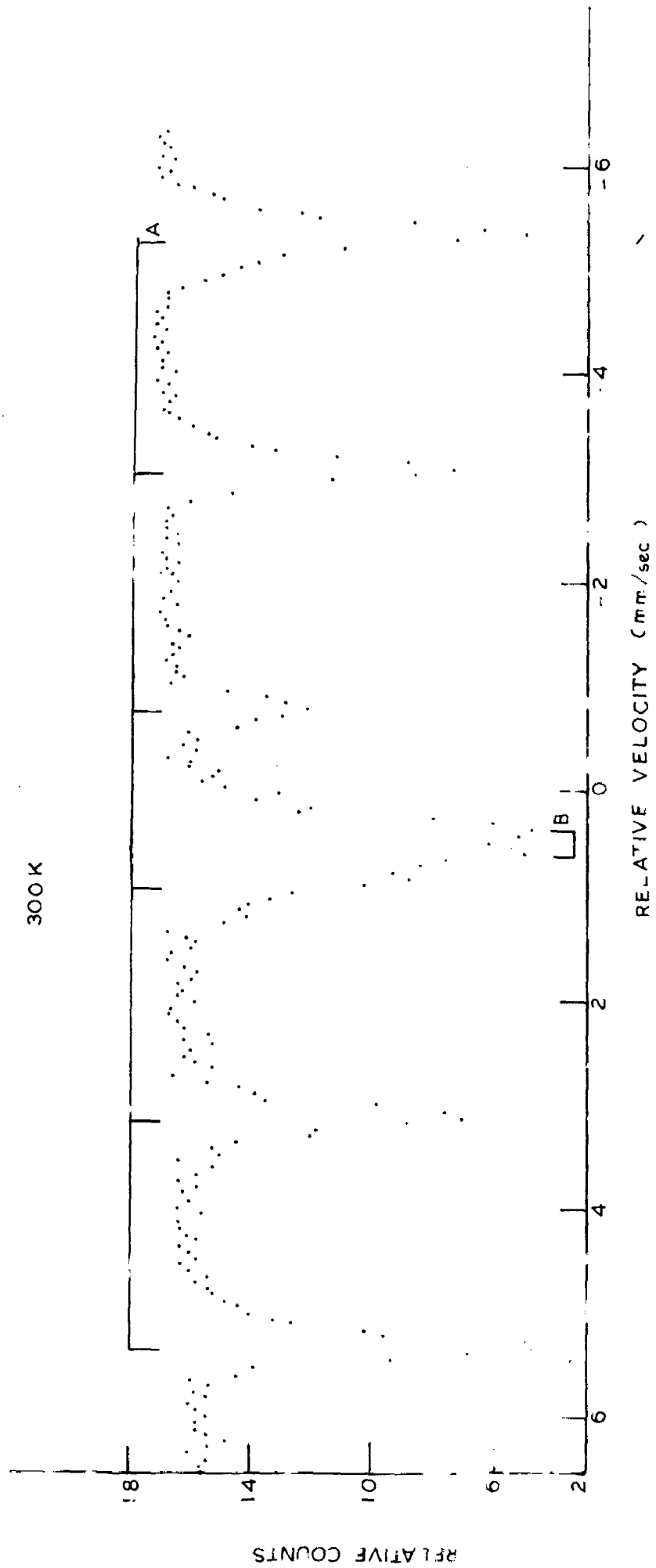
FIG. A.6.4. MÖSSBAUER SPECTRUM OF Fe-Se (25 at.% Se) QUENCHED FROM 650°C.

A : Fe

B : ∝ FeSe

RELATIVE VELOCITY (mm/sec)

RELATIVE COUNTS
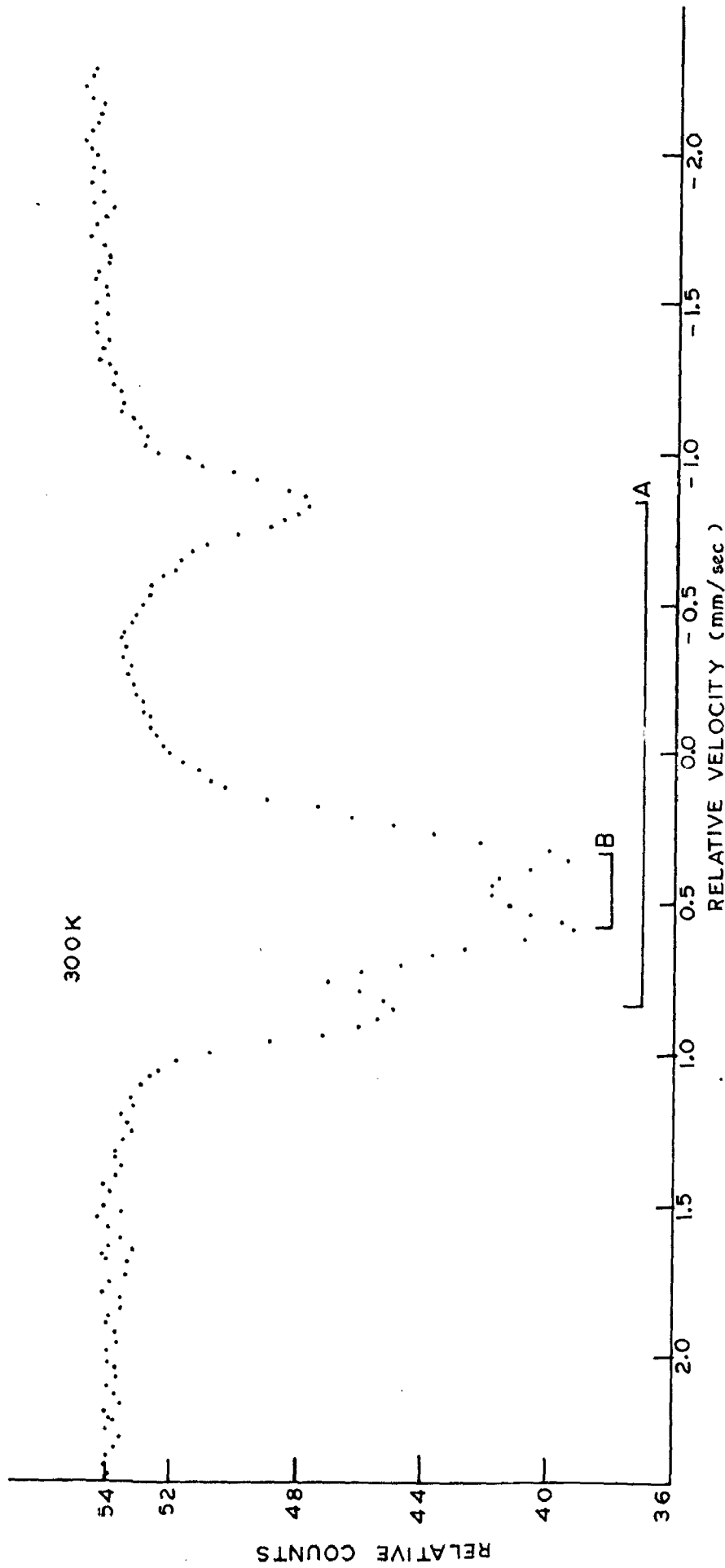
FIG.A.6.5 _ MÖSSBAUER SPECTRUM OF FeSe WITH 20at.% Se AT A LOWER VELOCITY.

A   inner peaks of ∝Fe
B   ∝FeSe

TABLE A 6.3: MÖSSBAUER PARAMETERS OF α-FeSe
ALONG WITH SOME REPORTED DATA

Compound	Thermal Treatment	Temperature	† I.S.(δ) mm/sec.	Q.S. mm/sec.
α-FeSe*	Quenched from 500°C	RT	0.48±0.02	0.23±0.02
α-FeSe*	Quenched from 500°C	LNT	0.57±0.02	0.29±0.02
α-FeSe**	Quenched from 650°C	RT	0.48±0.02	0.23±0.02
α-FeSe***	Quenched from 1000°C	RT	0.46±0.02	0.25±0.02
α-FeSe*	Annealed at 400°C	RT	0.47±0.02	0.18±0.02
FeS (tet.) |Ref.195|		RT	0.35	0.00
α-FeSe |Ref 174|		RT	0.39±0.03	0.45±0.03
FeSe(hex.) |Ref. 173|		RT	0.78±0.03	Not reported

* α-FeSe in the FeSe sample containing 20 at. % Se.

** α-FeSe corresponding to FeSe sample having 25 at. % Se.

*** α-FeSe separated from the FeSe sample with 20 at. % Se.

† I.S. reported with respect to iron metal .

and the intrinsic line width of the spectrometer is of the order of .29 mm/sec.. Further in the range studied by Reddy and Chetty |174| both the phases α and β FeSe are formed and hence the misfit in values of the different phases is quite possible. Kasper and Drickamer |173| performed high pressure studies of iron compounds with group V and VI, elements having either orthorhombic (c-18) marcasite or hexagonal (B-8) NiAs structure and observed a quadrupole splitting in case of FeSe hexagonal β-type while Reddy and Chetty |174| reported only isomer shift. This further lessens the faith in their parameters. The compound tetragonal FeS, which has the same basic lattice structure as α-FeSe, (Fe^{2+} is tetrahedrally coordinated) was studied by Bertaut et.al.|195| and the values of I.S. and Q.S. were found to be as 0.35 mm/sec. and 0.00 mm/sec. respectively. The comparison of the data for FeS and α-FeSe led us to believe that in α-FeSe there is a large distortion from tetrahedral symmetry. The observed value of I.S. of α-FeSe suggests that iron ions exist in the 2+ oxidation state with a major covalent contribution. This value of I.S. is less than the value of FeSe hexagonal and is in agreement with the general trend followed by iron chalcogenides i.e, $\delta(Fe^{2+})$ tet $<$ $\delta(Fe^{2+})$oct where δ denotes the I.S. The covalent and overlap contribution are also clear from the ionic distances. In FeSe the observed Fe- Se distance is 2.37 A° |174| in comparison to the ionic separation (when no overlap occurs) r_c+r_a = 2.65 A°. And thus it also throws

light on the highly covalent and overlap behaviour.

The covalency and overlap factors have been calculated in sec.A6.4 using Sanderson |189| method of equalisation of electronegativities . The calculations give the covalency and overlap factors as 0.85 and 0.86 for FeSe and FeS respectovely. Since FeSe is less covalent then FeS so the observation of more I.S. for α-FeSe in comparision to the I.S. of αFeS observed by Bertaut et.al. |195| is justified. The covalency and overlap factors for some typical compounds are given in Table A.6.2 along with their reported I.S. values. This table shows that the I.S. values are generally in accordance with the calculated covalent contribution. The highly ionic $FeCl_2$ shows maximum I.S. while the minimum I.S. is observed for $K_4Fe(CN)_6$ which shows a highly covalent behaviour. The covalency between the iron ions and their ligand neighbours plays an important role and the stronger the covalent bonding of iron ions, the small is the value of quadrupole splitting. Thus, in the present case also the low value of quadrupole splitting suggests the increased covalent character of the compound.

The possible hybridization schemes considering only σ. bonding has been discussed in Appendix A1. It was concluded that only d^3s type of hybridization is possible in this compound. Berlaut |196| had also discussed d^3s type hybridization in tetragonal FeS. Since Fe ion exists in 2+ oxidation state so it will have 6 d electrons four of these will form hybrid orbitals with four selenium atoms and the remaining

two electrons will constitute the lone electrons. Since, the structure of α-FeSe is a layered structure so, the bonding between iron- iron will be through the lone electron. One electron will remain unpaired and this will give rise to a net magnetic moment making the substance paramagnetic or feebly antiferromagnetic in accordance with the results of magnetic measurements performed by Hirone and Chiba |169|. Further, this unpaired electron gives rise to a quadrupole splitting in general of the order of .2 or .3 mm/sec.. The observed value in our case also is of the same order. Since this d^3s hybridization is also found in tetrahedral system so only on this basis it may be said that in this compound α-FeSe iron exists as Fe^{2+} in a tetragonal (tetrahedrally bonded) structure, Nonetheless the actual structure will be as shown in Fig. A 6.2. The crystal field splitting of 3d levels for α-FeSe has been discussed in Appendix A2.

The Mössbauer spectra of α-FeSe at liquid nitrogen temperature Fig. A 6.6 give I.S. = 0.57 mm/sec. and Q.S.= 0.29 mm/sec.. The increase in I.S. is due to the decrease in second order Doppler shift and is less than the increase in I.S. in pure iron. This suggests that at liquid nitrogen temperature also there is no change in chemical bonding etc. Further, liquid nitrogen data shows that in α-FeSe magnetic ordering does not arise even at liquid nitrogen temperature. This may be due to the increased covalent character. The very little increase in quadrupole splitting at liquid nitrogen temperature
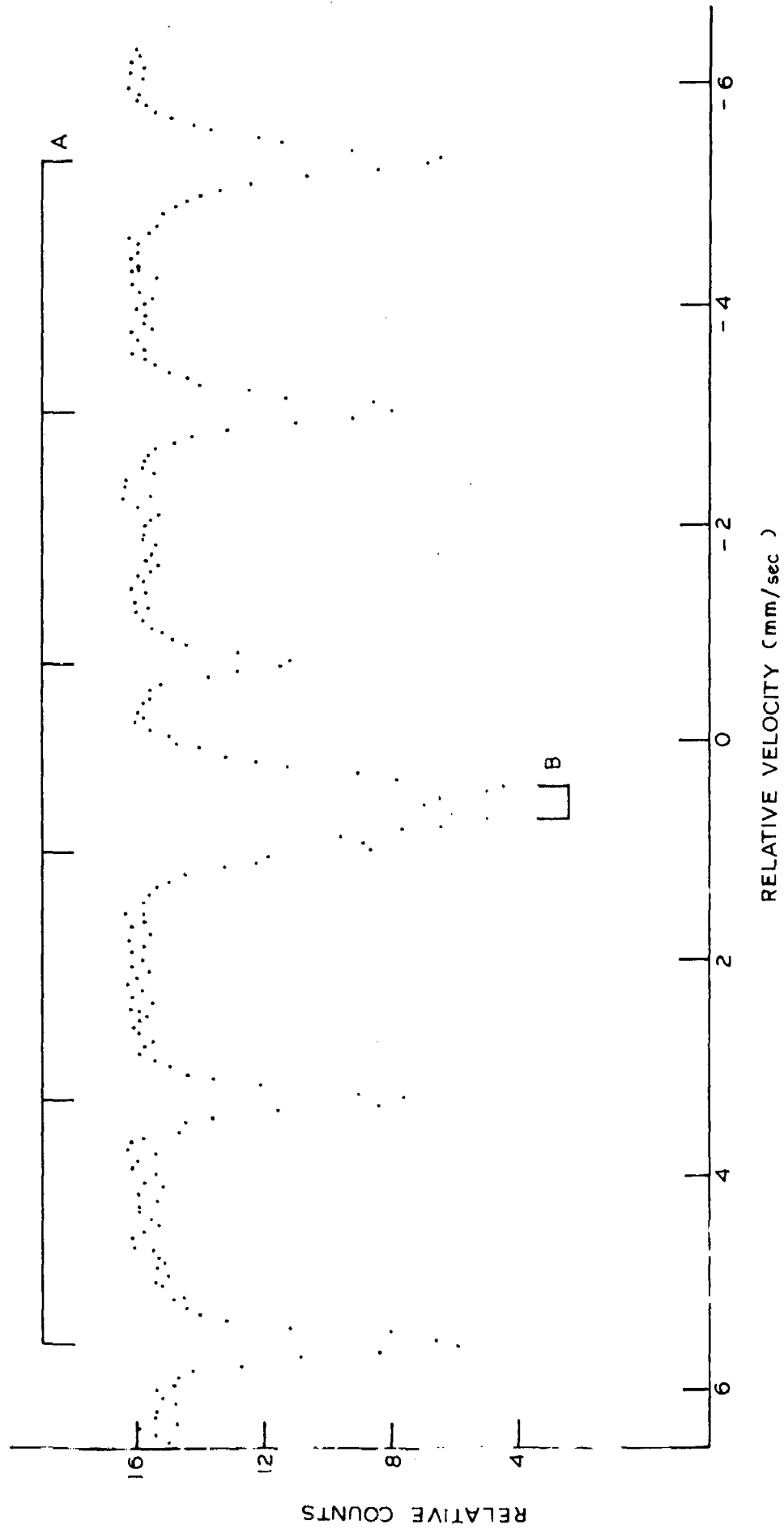
FIG.A.6.6 - MÖSSBAUER SPECTRUM OF Fe-Se (20 at.% Se), QUENCHED FROM 500°C.

A : Fe
B : α FeSe

also supports the highly covalent character of the compound.

This slight increase in Q.S. at liquid nitrogen temperature may be attributed to the locking of d electrons at lower temperature. While at higher temperature the extra d electron will give an average electric field gradient at the nucleus. And thus a less quadrupole splitting will be observed at higher temperatures.

Various annealing and quenching studies also have been performed. The oil quenching of the sample from $1000^{\circ}C$ or above separates $\alpha FeSe$ from iron. It is because the crystallization of $\alpha-FeSe$ takes place at this temperature and thus $\alpha-FeSe$ separates out from the other phase, pure iron. Thus. it provides a method for obtaining $\alpha-FeSe$ as a single phase. The Mössbauer spectrum of this separated $\alpha-FeSe$ is shown in Fig. A 6.7 and the observed values of I.S. and Q.S. are of the same order as those of $\alpha-FeSe$ in composite spectrum. The slow cooling from $1000^{\circ}C$ does not show the appearance of any other new phase but a little amount of iron remains attached on $\alpha-FeSe$ (on the surface).

Few samples were vacuum sealed in silica tubes and were annealed at $400^{\circ}C$ for 4 days and then furnace cooled. Mössbauer spectrum for one of these with 20 at. $\%$ selenium recorded at room temperature is shown in Fig. A 6.8. The values of I.S. and Q.S. obtained are 0.465 mm/sec. and 0.18 mm/sec. respectively. These values indicate that the annealing process leaves the I.S. unchanged while the Q.S. is decreased

300K

B

RELATIVE VELOCITY (mm/sec)
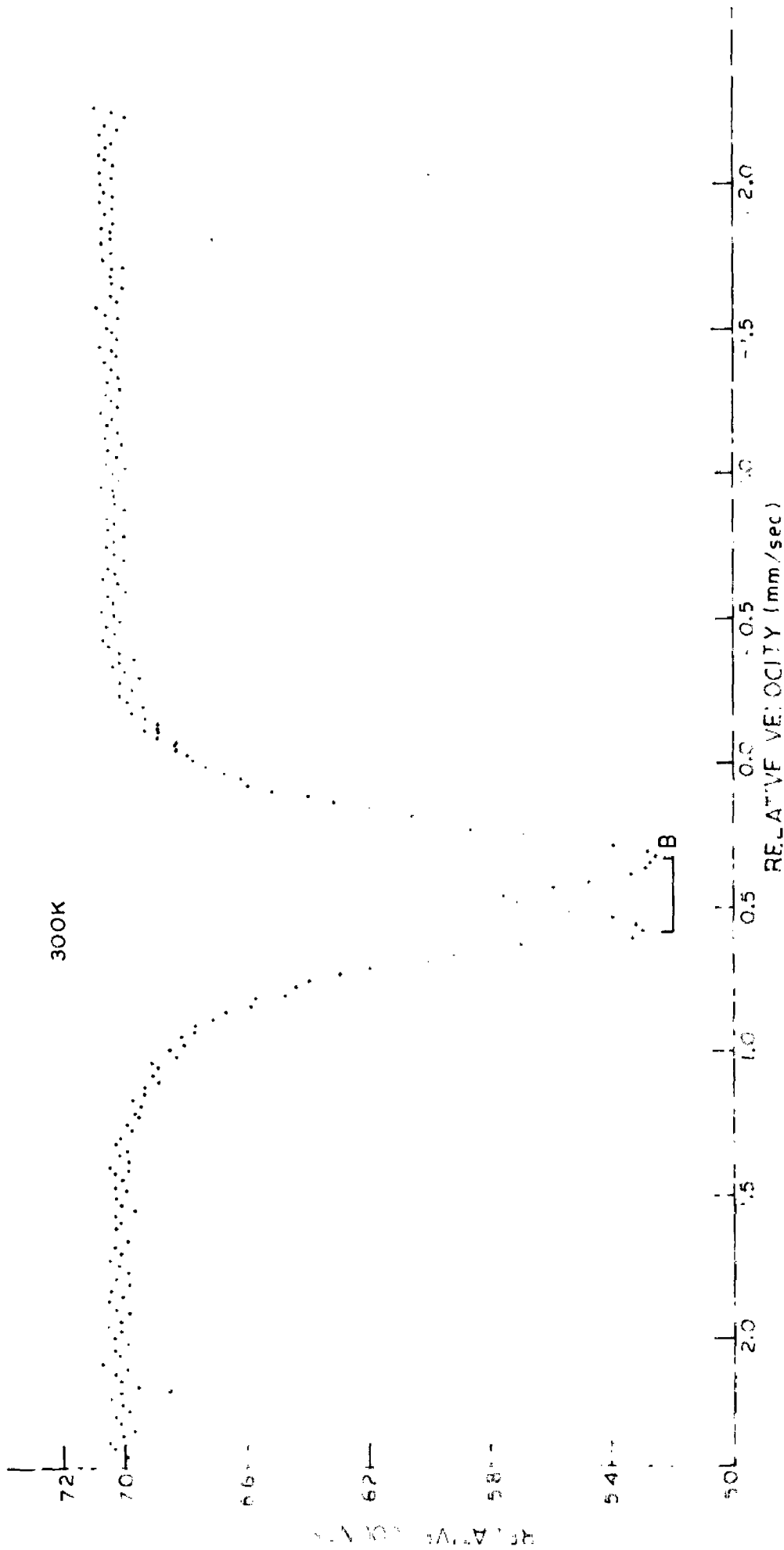
FIG.A.6.7. MÖSSBAUER SPECTRUM OF α FeSe SEPARATED FROM 2 at.% Se COMPOSITE SAMPLE

a. α FeSe separated
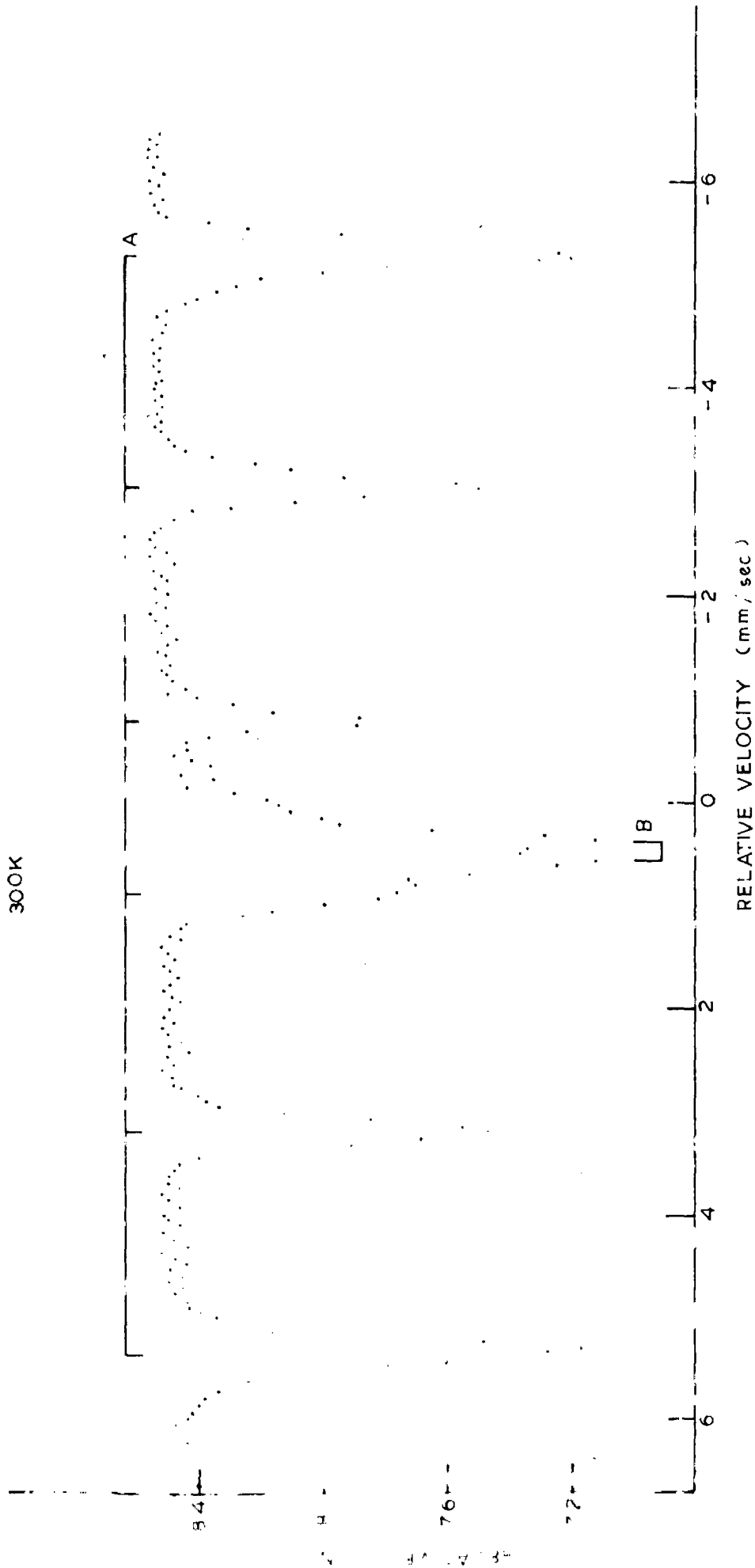
FIG.A.6.8. MÖSSBAUER SPECTRUM OF Fe—Se (20at.%Se) ANNEALED AT 400°C FOR 4 DAYS.

A: Fe

B: α FeSe

The same value of I.S. suggests that annealing at this temperature causes no change in the chemical behaviour of the compound while the decrease in Q.S. indicate a possible restoration of symmetry.

A.6.6 CONCLUSIONS

The studies reported in this chapter show the existence of a two phase system Fe and FeSe in the low concentration range of selenium (upto 25 at. %) and that Se does not dissolve in Fe. The FeSe has been assigned the α form having PbO type tetragonal structure. In α-FeSe iron exists in.2+ oxidation state with a major covalent contribution, which has been calculated to be 0.85. The I.S. and Q.S. values have been discussed in the light of the covalency factor. The possible hybridizations have been discussed and it is found that the d^3s type hybridization is the most probable. It is also found that α-FeSe separates out at a temperature higher than $1000^\circ C$ due to the crystallization of α-FeSe and thus it provides a method of separation of α-FeSe.

B 6.1 INTRODUCTION

The antimonides of transition elements of 3d group in the periodic table have been subject of wide interest due to remarkable changes in their magnetic properties in going from left to the right of the transition group elements. For instance, CrSb is a well known antiferromagnet with the Neel temperature 713K |197| where as $Fe_{1+\delta}Sb$ is paramagnetic at room temperature while MnSb is ferromagnetic. The system (Cr, Fe) Sb was studied by Schmid |198| and ferromagnetism was established above liquid nitrogen temperature.

According to the iron-antimony phase diagram |199| the system $Fe_{1+\delta}Sb$ crystallizes into a single phase having NiAs type structure where δ has the values $0.08 \leqslant \delta \leqslant 0.38$. The compositions outside this range do not exist as a single phase. Magnetic measurements on the system $Fe_{1+\delta}Sb$ were made by Ito et.al. |200| and Yamaguchi et.al. |201|. Ito et.al. |200| reported that $Fe_{1+\delta}Sb$ is paramagnetic above 77 K while Yamaguchi et. al. |201|, on the basis of neutron diffraction and Mössbauer measurements, suggested the onset of magnetic ordering below 197 K. Later on, detailed study of the magnetic properties on the systems $(Cr_{1.01}Sb)_{1-x}(Fe_{1.22}Sb)_x$ and $(Cr_{1.01}Sb)_{1-x}$ $(Co_{1.13}Sb)_x$ were made by Yamaguchi et.al. |202| and ferromagnetism was established in both these systems for intermediate values of x. The system $Fe_{1+\delta}Sb$ was undertaken for the detailed susceptibility measurements by Yamaguchi et.al.|203| who observed a maximum at 20 K and attributed it to the ordering

of excess Fe atoms going to interstitial sites. On the basis
of $Fe_{1.22}Sb$ Mössbauer measurements they showed that at and
below liquid nitrogen temperature the system is antiferromagnetic
and ascribed this ordering to the regular site Fe atoms.

Here we report the Mössbauer measurements carried out
on the system ϵ FeSb(which can be assigned the formula Fe_3Sb_2
|204|). The objective is to investigate the effect of excess
iron atoms on the magnetic properties of this system and to
compare with the findings on $Fe_{1.22}Sb$. Since Fe_3Sb_2 does not
exist as a single phase, a two phase system corresponding
to $FeSb_2$ and ϵ iron antimonide was prepared and studied.

B 6.2 PHASE DIAGRAM

The iron antimony phase diagram is shown in Fig. B 6.1.
It shows that in the concentration range of our present interest
(50 and 60 at. % Sb), a two phase system with ϵ and η phases
will be formed. The ϵ phase is supposed to be a solid solution
of Sb in the compound Fe_3Sb_2 |204|. The results of various
other workers |153| show that the homogeneity range in the
compound ϵ Fe-Sb, is shifted with decreasing temperature to
higher Sb contents. The ϵ phase is isotypic with NiAs (B8)
type and its lattice constants depend upon the Sb contents.
For 40 at. % Sb, the lattice parameters are a = 4.13 $\overset{o}{A}$,
c = 5.17 $\overset{o}{A}$, c/a = 1.252 ; at 43 at. % , a = 4.11 $\overset{o}{A}$,
c = 5.15 $\overset{o}{A}$, c/a = 1.253 and at 50 at. % Sb, a = 4.07 $\overset{o}{A}$,
c = 5.14 $\overset{o}{A}$, c/a = 1.263. The increase in lattice parameters
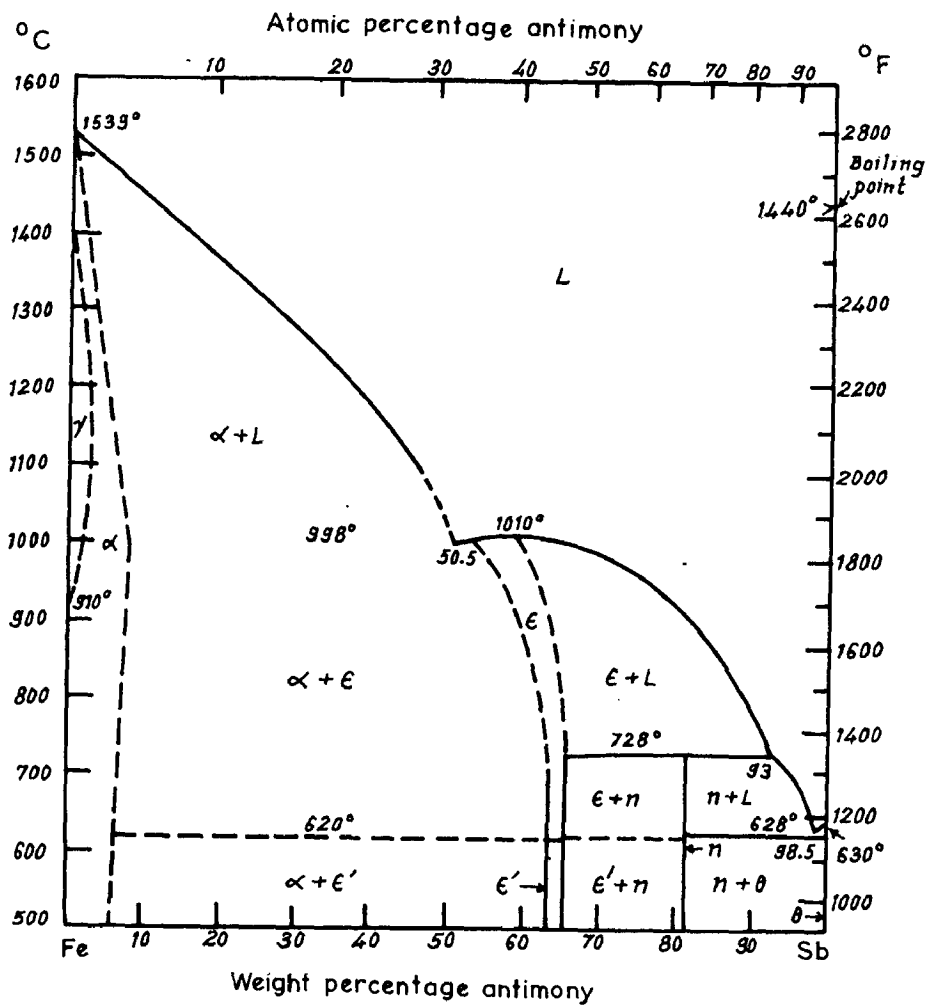
FIG.B.6.1 _ Fe - Sb SYSTEM

with increase in Fe contents suggests that the excess Fe atoms are located in the interstices of the NiAs lattice. The phase ($FeSb_2$) is isotypic with marcasite FeS_2 (C 18) structure having a = 3.195 A^O, b = 5.831 A^O, c = 6.53 A^O.

B 6.3 SAMPLE PREPARATION

Iron and antimony used in the preparation of samples were of 99.99%/purity. Two types of samples were prepared; one corresponding to 50 at. % Sb (68.5 wt. % Sb) and the other 66 at. % Sb (81.35 wt. % Sb). These have been designated as samples S_1 and S_2 respectively. For the preparation of sample S_1 calculated amounts of the two constituents were very thoroughly mixed in an agate mortar and the mixed powder was pressed into the form of capsules. These capsules were vacuum sealed in silica tubes and kept at 720^OC for two weeks and then oil quenched. The treatment was repeated to ensure the homogeneity and completeness of the reaction. For sample S_2 the heat treatment was given at 700^OC for one week and then furnace cooled. To obtain the phase $FeSb_2$ it was annealed at a temperature of 350^OC for one week.

X-ray studies revealed the presence of two phases ϵ and η in both the samples.

B 6.4 RESULTS AND DISCUSSION

Mössbauer spectra for samples S_1 and S_2 recorded at room temperature are given in Fig. B 6.2 and B 6.3 respectively

RELATIVE VELOCITY

32

24

6

8

0

2.5 2.0 1.5 1.0 0.5 0.0 - 0.5 - 1.0

RELATIVE VELOCITY (mm/sec)

FIG.B.6.2 - MÖSSBAUER SPECTRUM OF SAMPLE S_1.

a : $Fe_3 Sb_2$ (ϵ phase)
b : $Fe Sb_2$ (η phase)

300 K

RELATIVE COUNTS

36

32

28

24

2.5 2.0 1.5 1.0 0.5 0.0 - 0.5 - 1.0

RELATIVE VELOCITY (mm/sec)
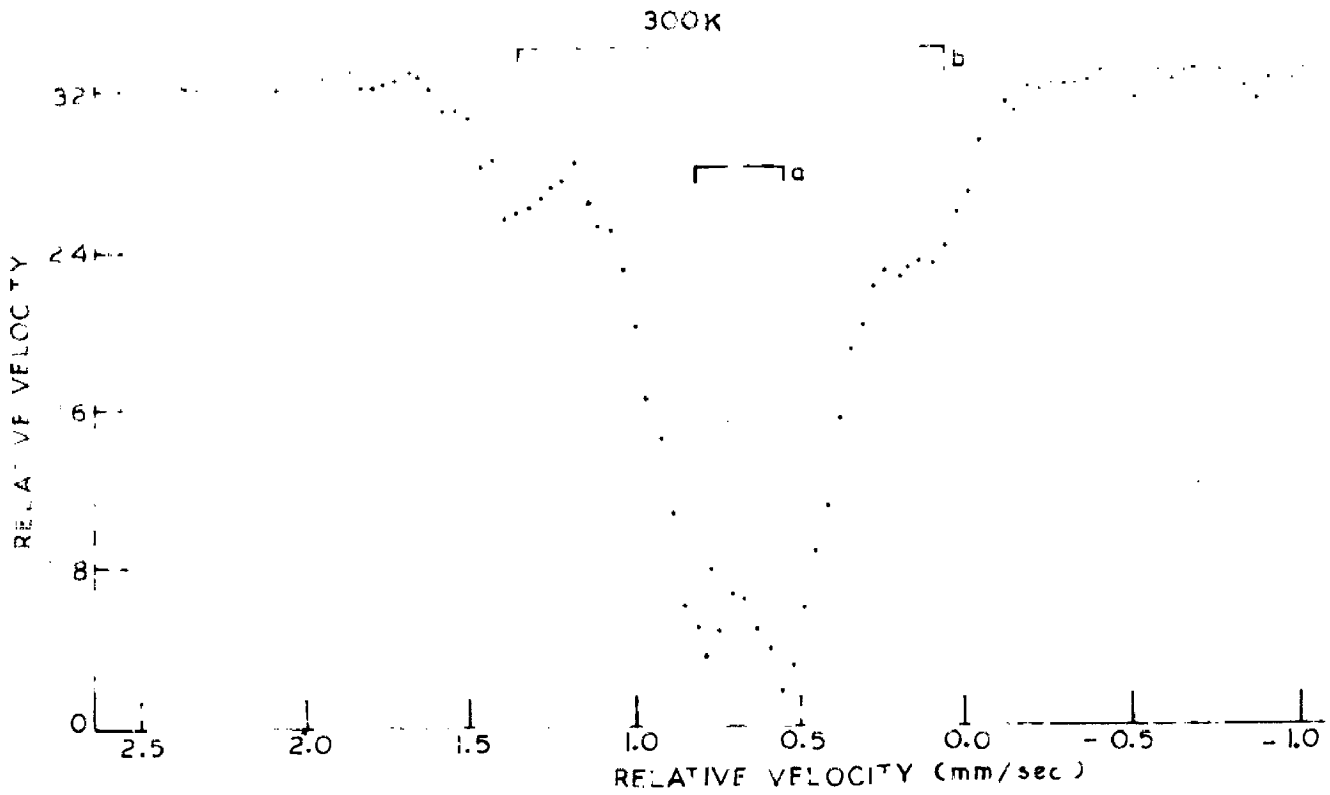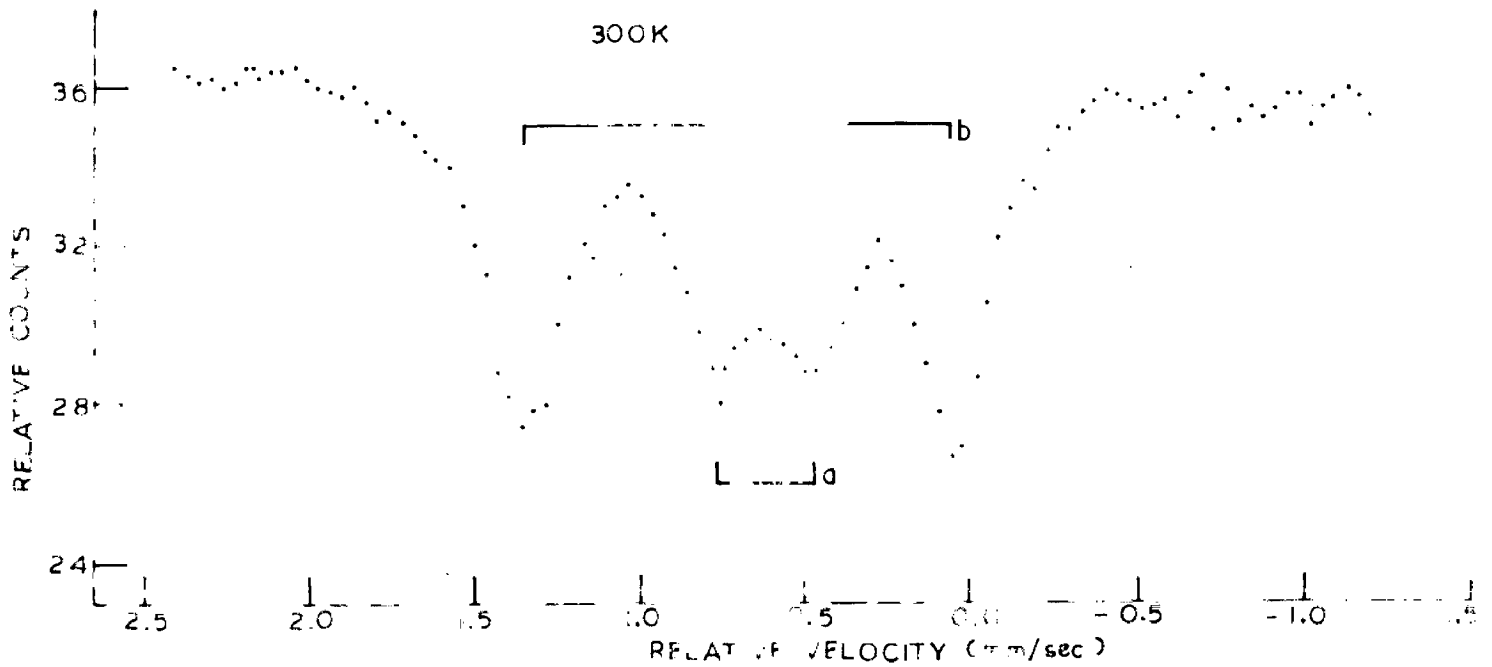
FIG.B.6.3 MÖSSBAUER SPECTRUM OF SAMPLE S_2.

while the analysed parameters along with some reported values
are given in Table B 6.1.

The spectrum due to sample S_1 indicates the presence
of two phases, ε phase (Fe_3Sb_2) and η phase ($FeSb_2$). The
Mössbauer parameters for η phase are Q.S. (Δ EQ) = 1.288
mm/sec. and I.S. (δ) = 0.699mm/sec.. These are in close
agreement with the values of Steger and Kostiner |205|

ΔEQ = 1.268 mm/sec. and I.S. (δ) = .710 mm/sec. This agreement
further confirms the formation of η phase. The ε phase
(Fe_3Sb_2) has ΔEQ = .285 mm/sec. and I.S. = .61 mm/sec. While
in the case of $Fe_{1.22}Sb$, which has the same basic structure
as Fe_3Sb_2, a single line pattern having I.S. = 0.6 mm/sec.
was observed by Yamaguchi et.al. |203|. The appearance of
Q.S. in ε phase at room temperature may be assigned to the
lattice distortion caused by additional filling of interstitial
sites by the extra Fe atoms in comparison to $Fe_{1.22}Sb$. In
the case of $Fe_{1.22}Sb$ the lattice distortion due to the excess
Fe atoms going at the interstitial sites was not sufficient
to give observed Q.S. at room temperature. But it has been
detected at liquid helium temperature (2ΔEQ = 0.3 mm/sec.)
|203|. The liquid nitrogen temperature spectrum due to the
sample S_1 is given in Fig. B 6.4. This spectrum was splitted
in two patterns; one due to the $FeSb_2$ paramagnetic pattern
with parameters ΔEQ = 1.58 mm/sec. and δ = .912 mm/sec. and
the other, due to Fe_3Sb_2 is a magnetic pattern. The parameters
of the $FeSb_2$ phase at liquid nitrogen temperature are in
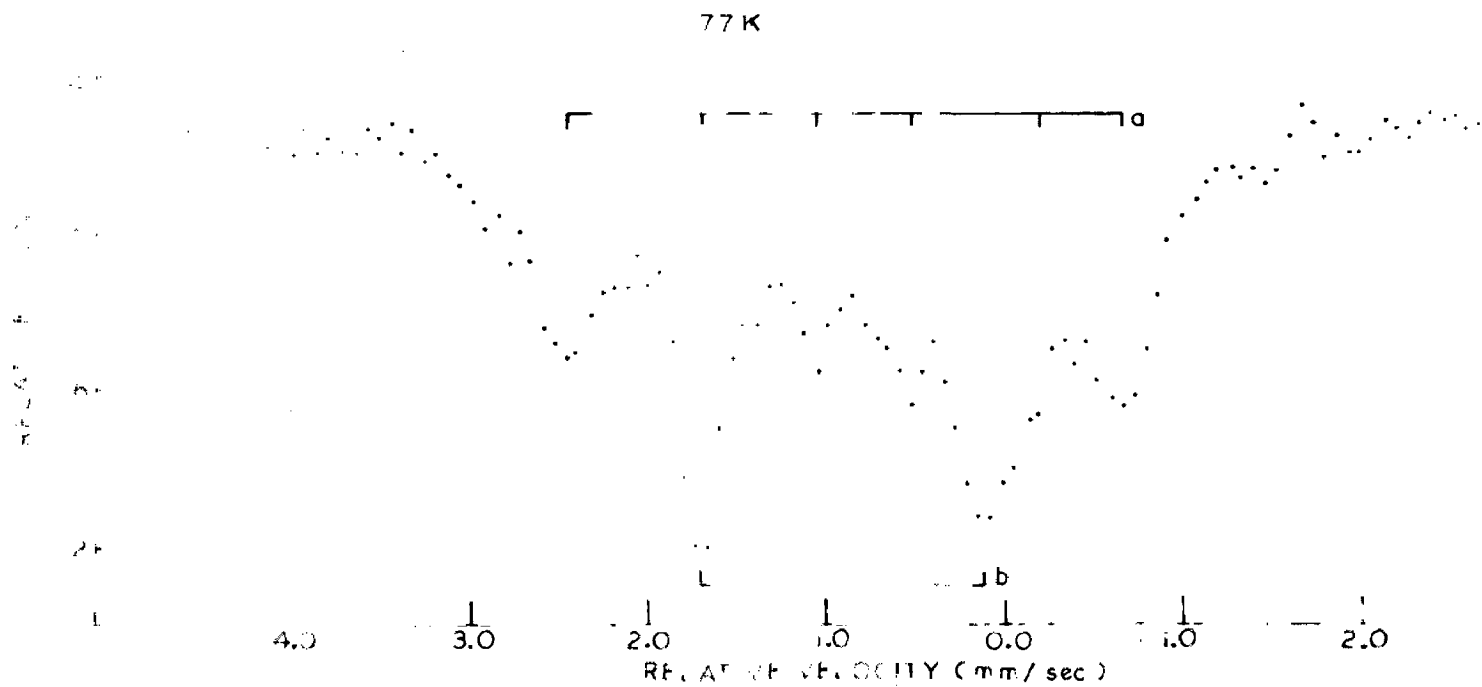
FIG. B.6.4 _ MÖSSBAUER SPECTRUM OF SAMPLE S₁ .

a: Fe₃Sb₂ (ε phase)

b: FeSb₂ (n phase)

TABLE B 6.1: MÖSSBAUER PARAMETERS OF ϵ AND η PHASES OBSERVED AND REPORTED.

Speciman	Temp.	I.S.* mm/sec. Error ± 0.02 mm/sec.	Q.S. mm/sec. Error ± 0.02 mm/sec.	Magnetic field B_{eff} kOe Error ± 4 kOe
Fe_3Sb_2	500 K	0.533	0.306	—
	300 K	0.610	0.285	—
	77 K	0.897	0.298	98
$FeSb_2$	500 K	0.554	1.028	—
	300 K	0.689	1.288	—
	77 K	0.912	1.580	—
$Fe_{1.22}Sb$	300 K	0.600	—	—
|203|	77 K	0.800	—	98
$FeSb_2$|205|	500 K	0.558	1.102	—
	300 K	0.710	1.268	—
	77 K	0.826	1.557	—

* The Isomer shift values are given with respect to sodium nitroprusside.

agreement with those reported in Ref. |205|. ϵ phase shows a magnetic pattern with B_{eff}= 98 kOe . The lines are broader at this temperature, which may be due to two reasons: One the transition is not complete and the other due to those regular site Fe atoms which have different number of excess Fe atoms as neighbours. The same order of effective internal fields in Fe_3Sb_2 and $Fe_{1.22}Sb$ suggests that the increased number of Fe atoms on interstitial sites in Fe_3Sb_2 do not have any observable effect on the magnetic field of the pattern observed with Mössbauer studies. These observations lead us to conclude that the ordering observed with the help of Mössbauer effect is due to the regular site iron atoms. This can further be argued that if the increased iron atoms at interstitial sites (in going from $Fe_{1.22}Sb$ to Fe_3Sb_2) cause an appreciable effect on the regular site iron atoms then they should themselves show their own pattern due to excess iron atoms. But no such pattern is observed. Thus it appears that the increased number of iron atoms would not have any observable effect on the magnetic field of the regular site iron atoms. The liquid — helium temperature Mössbauer measurements on this sample S_1 may throw some light in this regard but could not be done by us due to the lack of such facilities. Since at this temperature the iron atoms going at the interstitial sites may also show their ordering behaviour, as observed in susceptibility measurements |203|.

The spectrum of sample S_2 mainly consists of the spectrum

due to η phase ($FeSb_2$). The ϵ phase is also present in very small amount. The parameters for these two phases are same as those of sample S_1 and thus it confirms that the phases formed in the two samples are same and are in accord with the iron antimony phase diagram |199|. The spectrum of sample S_2 was also recorded at 500 K. The parameters of the phases $FeSb_2$ are $\triangle EQ$ = 1.028 mm/sec. and I.S. = .554 mm/sec. and are again in agreement with the reported earlier |205|. The ϵ phase Fe_3Sb_2 shows $\triangle EQ$ = .306mm/sec. and I.S. = .533 mm/sec. The decrease in I.S. at 500 K in case of Fe_3Sb_2 is due to the second order Doppler shift while the Q.S. shows a very little increase in its magnitude and this probably is due to more number of iron atoms going to interstitial sites at higher temperatures and hence causing a larger distortion.

B 6.5 CONCLUSIONS

The measurements show that ϵ phase is paramagnetic at room temperature with $\triangle EQ$ = 0.285 mm/sec. and antiferromagnetism sets in at and below liquid nitrogen temperature. Further, the present study confirms that the ordering appearing at and below liquid nitrogen temperature is due to regular site Fe atoms.

APPENDICES

A 1 HYBRIDIZATION SCHEMES FOR σ ORBITALS IN α-FeSe

In α-FeSe, there are 4 Se atoms on one side of the Fe atom and these are arranged in a square planar form. A perusal of various symmetry operations shows that this system will have only E, $C_4^{(1)}$, $C_4^{(3)}$, C_2, $\sigma_v^{(1)}$, $\sigma_v^{(2)}$, $\sigma_d^{(1)}$ and $\sigma_d^{(2)}$ as the possible group elements. There is neither inversion point nor an inproper axis. Accordingly the point symmetry of Fe site is C_{4v}. The σ bonds between Fe and Se will form a reducible representation of the point group C_{4v}. In order to determine the representation we mark the σ-- bonds as radius vectors r_1, r_2, r_3 and r_4, Fig. A 1.1, and study their transformation under various group operations.

The identity operation leaves the systems same i.e.

$r_1 \rightarrow r_1 + Or_2 + Or_3 + Or_4$

$r_2 \rightarrow Or_1 + r_2 + Or_3 + Or_4$

$r_3 \rightarrow Or_1 + Or_2 + r_3 + Or_4$

$r_4 \rightarrow Or_1 + Or_2 + Or_3 + r_4$

In the matrix form it can be represented as

$$\begin{pmatrix} 1 & 0 & 0 & 1 \\ 0 & 1 & 0 & 0 \\ 0 & 0 & 1 & 0 \\ 0 & 0 & 0 & 1 \end{pmatrix}$$
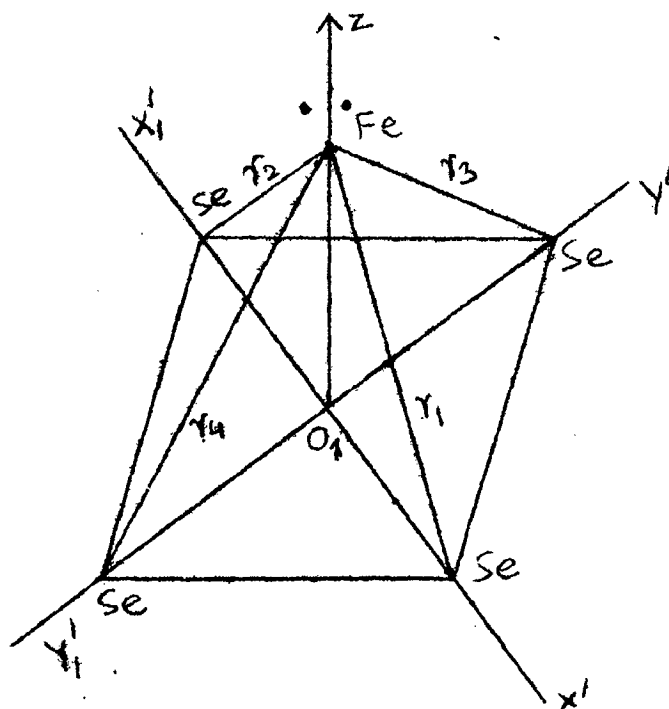
Fig A 1.1.

so that $\chi(E) = 4$.

Similarly the rotations about the proper axes yield:

$$c_4^1 : \quad r_1 \to r_4, \quad r_4 \to r_2, \quad r_2 \to r_3, \quad r_3 \to r_1$$

and $\chi(c_4^1) = 0$.

$$c_4^3 : \quad r_1 \to r_3, \quad r_2 \to r_4, \quad r_3 \to r_2, \quad r_4 \to r_1$$

with $\chi(c_4^3) = 0$.

$$c_4^2 \text{ or } C_2 : \quad r_1 \to r_2, \quad r_2 \to r_1, \quad r_3 \to r_4, \quad r_4 \to r_3$$

with $\chi(C_2) = 0$.

Carrying out the reflections in various planes we get the following transformations:

$$\sigma_v^{(1)} : \quad r_1 \to r_1, \quad r_2 \to r_2, \quad r_3 \to r_4, \quad r_4 \to r_3$$

with $\chi(\sigma_v^{(1)}) = 2$.

$$\sigma_v^{(2)} : \quad r_1 \to r_2, \quad r_2 \to r_1, \quad r_3 \to r_3, \quad r_4 \to r_4$$

with $\chi(\sigma_v^{(2)}) = 2$.

$$\sigma_d^{(1)} : \quad r_1 \to r_3, \quad r_2 \to r_4, \quad r_3 \to r_1, \quad r_4 \to r_2$$

with $\chi(\sigma_d^{(1)}) = 0$.

$$\sigma_d^{(2)} : \quad r_1 \to r_4, \quad r_2 \to r_3, \quad r_3 \to r_2, \quad r_4 \to r_1$$

with $\chi(\sigma_d^{(2)}) = 0$.

Thus the reducible representation for σ bonds is

	E	$2C_4$	C_2	$2\sigma_v$	$2\sigma_d$
C_{4v}	4	0	0	2	0

With the help of the character tables for point group C_{4v} (Ref. 206) we see that this representation is equivalent to

$$A_1 + B_1 + E$$

This means that the four atomic orbitals which are used to form four hybrid orbitals can be obtained by using the possible combinations of A_1, B_1 and E. The character table gives the wave functions corresponding to these as follows

A_1	B_1	E
s	dx^2-y^2	px,py
pz	dx^2-y^2	dxz,dyz
dz^2	dx^2-y^2	–

Accordingly the possible hybridization schemes are. sp^2d, sd^3, p^3d, pd^3, p^2d^2 and d^4. The symmetry point of view allow all these possible combinations for obtaining four hybrid orbitals. But the energy consideration rules out few of these. Here we are considering the central atom to be Fe^{2+} having six 3d electrons. The 4s, 3d, and 4p orbitals will be used in hybridization. Since 4p lies at a higher energy than 3d so the orbitals formed with 4p orbitals will be less stable.

The only stable hybrid orbitals will thus be d^3s and d^4. But d^4 gives a case of purely ionic type and hence it can also be ruled out leaving the only probable hybridization d^3s. Out of the six electrons available, four electrons will go to these four hybrid orbitals and the remaining two will constitute the lone pair. Hence the possible hybridization scheme is d^3s.

A.2 CRYSTAL FIELD SPLITTING OF 3d LEVELS IN α-FeSe

As discussed in chapter A6, , the ligation of Se to Fe may be indicated as shown in the Fig. A 2.1. Defining the coordinate system with origin at Fe and x and y axes parallel to the lines joining 1 and 2, and 3 and 4, respectively, the spherical polar coordinates of various ligands can be written as

ligand	r_i	θ_i	ϕ_i
1	a	θ	0°
2	a	θ	90°
3	a	θ	180°
4	a	θ	270°

where $a = 2.37$ Å and θ is given by $\cos \theta = \dfrac{uc}{a} = 0.602.$
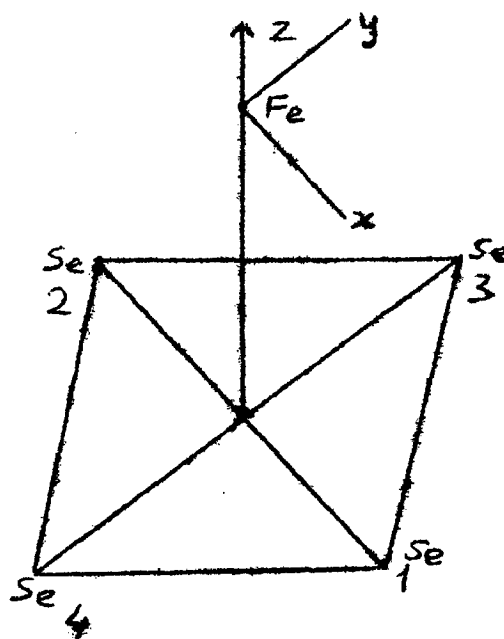
Fig. A2.1

Treating the ligands as point charges we get the interaction potential for 3d-electrons to be

$$V = 4\sqrt{\pi}\ ze^2 \left[(3 \cos^2\theta - 1)\frac{r^2}{\sqrt{5}\ a^3}\ Y_2^0 + \frac{r^4}{12a^5}\left\{ (35 \cos^4\theta \right.\right.$$

$$\left.\left. - 30 \cos^2\theta + 3)\ Y_4^0 + \frac{\sqrt{35}}{2}\ \sin^4\theta\ (Y_4^4 + Y_4^{-4}) \right\}\right]$$

The calculated values of various matrix elements for d wave functions can be written as

$$\int (0)^* \ V(0) \ d\tau \ = \ \frac{4}{7} A + \frac{1}{7} B$$

$$\int (\pm 1)^* \ V(\pm 1) \ d\tau \ = \ \frac{2}{7} A - \frac{2}{21} B$$

$$\int (\pm 2)^* \ V(\pm 2) \ d\tau \ = \ \frac{-15\pi}{256} A + \frac{1}{42} B$$

$$\int (\pm 2)^* \ V(\mp 2) \ d\tau \ = \ \frac{5}{6} C$$

where

$$A = \frac{ze^2 \langle r^2 \rangle}{a^3} (3 \cos^2\theta - 1)$$

$$\dot B = \frac{ze^2 \langle r^4 \rangle}{a^5} (35 \cos^4\theta - 30 \cos^2\theta + 3)$$

$$C = \frac{ze^2 \langle r^4 \rangle}{a^5} \sin^4\theta \qquad .$$

Therefore the secular determinant becomes

	2	1	0	-1	-2
2	$\frac{-15\pi}{256}A + \frac{1}{42}B - E$	0	0	0	$\frac{5}{6}C$
1	0	$\frac{2}{7}A - \frac{2}{21}B - E$	0	0	0
0	0	0	$\frac{4}{7}A + \frac{1}{7}B - E$	0	0
-1	0	0	0	$\frac{2}{7}A - \frac{2}{21}B - E$	0
-2	$\frac{5}{6}C$	0	0	0	$\frac{-15\pi}{256}A + \frac{1}{42}B - E$

which leads to the following positions of the energy levels:

$$|0\rangle \quad \text{at} \quad E = \frac{4}{7}A + \frac{1}{7}B$$

$$|1\rangle \quad \text{and} \quad |-1\rangle \text{ at } E = \frac{2}{7}A - \frac{2}{21}B$$

$$|2\rangle \quad \text{and} \quad |-2\rangle \text{ at } E = \frac{-15\pi}{256}A + \frac{5}{6}C + \frac{1}{42}B$$

$$\text{and} \quad E = \frac{-15\pi}{256}A - \frac{5}{6}C + \frac{1}{42}B$$

using the conventional symbols for d-wave functions i.e.

$$dxy = \frac{1}{\sqrt{2}}\left[\,|2\rangle - |-2\rangle\,\right]$$

$$dxz = \frac{1}{\sqrt{2}}\left[\,|1\rangle + |-1\rangle\,\right]$$

$$dyz = \frac{1}{\sqrt{2}}\left[\,|1\rangle - |-1\rangle\,\right]$$

$$dz^2 = |0\rangle$$

$$dx^2-y^2 = \frac{1}{\sqrt{2}}\left[\,|2\rangle + |-2\rangle\,\right]$$

we get the crystal field splitting in FeSe as given below :

orbital	Energy		
dxy	$\frac{-.005 \; ze^2\langle r^2\rangle}{a^3}\pi$	$- \frac{.078 \; ze^2\langle r^4\rangle}{a^5}$	$- \frac{.339 \; ze^2\langle r^4\rangle}{a^5}$
dz^2	$\frac{+0.050 \; ze^2\langle r^2\rangle}{a^3}$	$- \frac{.468 \; ze^2\langle r^4\rangle}{a^5}$	
dx^2-y^2	$\frac{-.005 \; ze^2\langle r^2\rangle}{a^3}\pi$	$- \frac{.078 \; ze^2\langle r^4\rangle}{a^5}$	$+ \frac{.339 \; ze^2\langle r^4\rangle}{a^5}$
dxz, dyz	$\frac{.025 \; ze^2\langle r^2\rangle}{a^3}$	$+ \frac{.312 \; ze^2\langle r^4\rangle}{a^5}$	

The relative ordering of the energy levels and their population, is shown in Fig. A 2.2. The figure gives only the order of energy levels, not the magnitude of splitting.

$$\underline{\quad \uparrow\uparrow \quad} \quad \text{d}xz, \text{d}yz$$

$$\underline{\quad \uparrow \quad} \quad \text{d}x^2\text{-}y^2$$

$$\underline{\quad \uparrow \quad} \quad \text{d}z^2$$

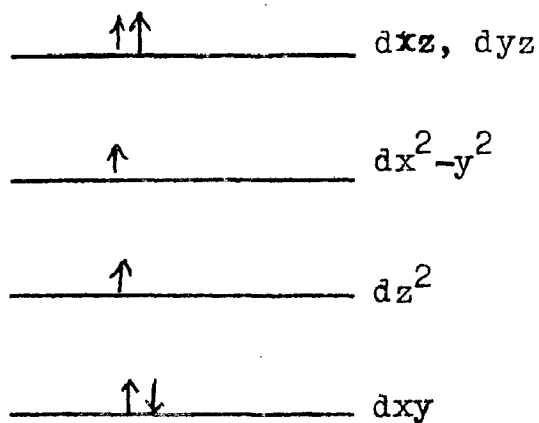$$\underline{\quad \uparrow\downarrow \quad} \quad \text{d}xy$$

FIG. A 2.2: RELATIVE ORDER OF CRYSTAL FIELD SPLIT d LEVELS IN FeSe (C_{4v} SITE SYMMETRY).

REFERENCES

1. R.L.Mössbauer; Z. Physik 151, 124 (1958).

2. R.L.Mössbauer: Naturwissenschaften 45, 538, (1958); Z. Naturforsch 14a, 211 (1959).

3. I.P. Suzdalev, E.F.Makrov and E.Ya. Gazanov: Kinet. Catal. (USSR) 6, 1002 (1965).

4. R.L.Mössbauer Les Prix Nobelen 1961 (Nobel foundation Stockholm 1962) p.136; and Science 137, 731 (1962).

5. International Atomic Energy Agency, Applications of the Mössbauer Effect in Chemistry and Solid State Physics, Technical Reports Series No. 50, IAEA, Vienna (1966); Mössbauer Spectroscopy and Its Applicat-ions, Proceedings of a Panel Vienna, 1972.

6. A.H.Muir Jr., K.J. Ando and H.M. Coogan; Mössbauer Effect Data Index, 1958-65. (Inter-Science, New York, 1966); and 1966-68.

7. J.G. Stevens and V.E. Stevens; Mössbauer Effect Data Index 1969-75 (Adam Hilger, London).

8. I.J. Gruverman (Ed.): Mössbauer Effect Methodology, Vols. 1-9 (Plenum Press, New York, 1965-74).

9. H. Lustig: Am. J. Phys. 29, 1 (1961).

10. R.L.Mössbauer: Ann. Rev. Nucl. Sci. 12, 123 (1962).

11. G.K. Wertheim: Am. J. Phys. 31, 1 (1963).

12. J.F. Duncan and R.M. Golding: Quart. Rev. (London) 19, 36 (1965).

13. R.H. Herber: Ann. Rev. Phys. Chem. 17, 262 (1966).

14. H.G. Drickamer, V.C. Bastron, D.C.Fisher and D.C. Grenoble: J. Solid State Chem. 2, 94 (1970).

15. N.N. Greenwood: Int. Cent. Nat. Rech. Sci. 191, 105 (1970).

16. R.L. Cohen: Science 178, 828 (1972).

17. G.K. Wertheim: Proc. of Conf. on 'Phase transitions and their applications in materials Science' (Pergamon Press, New York, 1973) pp.243.

18. C.E. Johnson: J. Phys. (Paris) Collog C1, 35 (1974).

19. H. Frauenfelder: 'The Mössbauer Effect' (W.A. Benjamin, New York, 1962).

20. V.I. Goldanskii: ' The Mössbauer Effect and its Applications to Chemistry' (Consultant Bureau, New York, 1964).

21. G.K. Wertheim: ' Mössbauer Effect: Principles and Applications (Academic Press, New York, 1964).

22. L. May (Ed.): ' An Introduction to Mössbauer Spectroscopy' (Plenum Press, New York, 1971).

23. V.I. Goldanskii and R.H. Herber,(Eds.): ' Chemical Applications of Mössbauer Spectroscopy' (Academic Press, New York, 1968).

24. N.N. Greenwood and T.C. Gibb: ' Mössbauer Spectroscopy' (Chapman and Hall London, 1971).

25. G.M. Bancroft ; ' Mössbauer Spectroscopy: An Introduction for Inorganic Chemists and Geochemists', (McGraw-Hill Book Company (U.K.) Ltd., 1973).

26. V.G. Bhide; ' Mössbauer Effect and its Applications (Tata McGraw-Hill Publishing Co., Ltd. New Delhi, 1973).

27. W.M. Visscher: Ann. Phys. 9, 194 (1960).

28. S. Margulies and J.R. Ehrmann: Nucl. Instr. Methods 12, 131 (1961).

29. G.K. Wertheim: Physics Today 20, 131 (1967).

30. J.W.G. Wignall: J. Chem.Phys. 44, 2462 (1966).

31. H.H. Wickman and G.K. Wertheim:Ref. 23, p. 556: Phys. Rev. 148, 211 (1966) see also H.H. Wickman: Ref.8 Vol.II (1966) p.39: G.K.Wertheim and J.P. Rameika:'Nuclear Magnetic Resonance and Relaxation in solids'L. Van Gervan, (Ed.), (North Holland Publ. Co., Amsterdam, 1965) p.1.

32. M. Blume: Phys. Rev. Letters 14, 96 (1965); ibid 16 (1967); M.Blume and J.A. Tjon: Phys. Rev. 165, 446 (1968); J.A. Tjon and M. Blume: ibid, 165, 456 (1968).

33. K. Albrecht and H. Neuwirth: Z. Physik 203, 420 (1967).

34. F.J. Lynch, R.E. Holland and M. Hamermesh: Phys.Rev. 120, 513 (1960).

35. U. Gonser and H. Wickdersich: J. Phys. Soc. Jap. 18, Suppl. II, 47 (1963).

36. P. Zory: Phys. Rev. 140A, 1401 (1965).; K.Chandra and S.P. Puri: Phys. Rev. 169, 272 (1968); V.K. Garg and S.P.Puri: J. Chem. Phys. 54, 209 (1971).

37. V.I. Goldanskii, E.F. Makarov,I.P. Suzdalev and I.A. Vinogradov: Phys. Rev. Letters 20, 137 (1968); S.V. Karyagin: Dokl, Akad. Nauk. SSSR 148, 1102 (1963).

38. S. Margulies, P. Debrunner, and H. Frauenfelder: Nucl. Instr. and Meth. 21, 217 (1963).

39. A.J. Freeman and R.E. Watson: ' Magnetism' G.T. Rado and H.Suhl. (Eds.) (Academic Press, New York, 1965) Vol.IIA p.167.

40. E. Matthias and D.A. Shirley, (Eds.): Hyperfine Structure and Nuclear Radiations North-Holland Publ. Co., Amsterdam, 1968 (Proc. Intern. Conf. on Hyperfine interactions detected by Nucl. Radiations, Asilomer Conf. grand, Pacific grove, California, U.S.A. August 25-30, 1967).

41. D.A. Shirley: Rev. Mod. Phys. 36, 339 (1964).(3rd International conf. on Mössbauer Effect Cornell Univ., Itaca, N.Y., (1963) A.J.Bearden (Ed.).

42. R.V. Pound and G.A. Rebka, Jr.: Phys. Rev. Letters 4, 274 (1960).

43. O.C. Kistner and A.W. Sunyar: Phys. Rev. Letters 4, 412 (1960).

44. E. Fermi and E. Segre: Z. Physik 82, 729 (1933); S.A. Goudsmit: Phys. Rev. 43, 636 (1933).

45. C.W. Kimball: Mössbauer Effect Methodology 3, 3 (1967).

46. P. Raj and S.K. Kulshrestha; J. Phys. Chem. Solids. 31, 9 (1970) Ref. 23 p.31.

47. E.L. Sprenkel - Segal and S.S. Hanna: Mössbauer Effect Methodology 2, 113 (1966); ibid Geochem Cosmochem. Acta 28, 1913 (1964); R.M. Housley, R.W. Grant, M. Abbel Gawad and E. Elander: Science 167, 688 (1970).

48. R.W. Vaughan and H.G. Drickamer: J. Chem. Phys. 47, 1530 (1967); R.V. Pound, G.B. Benedek and R. Drever: Phys. Rev. Letters 7, 405 (1961); R. Ingalls, H.G. Drickamer and G. Depasquali: Phys. Rev. 155, 165 (1967).

49. E. Fluck: Advances in Inorganic Chemistry and Radiochemistry, H.J. Emoleus and A.G. Sharpe, (Eds.), (Acad. Press, New York, 1964), Vol.6, p.278.

50. W.J. Nicholson, G.Burns: Phys. Rev. 129, 2490 (1963).

51. V.I. Goldanskii, E.F. Makarov and V.V. Khrapov: Soviet Phys. JETP 17, 508 (1963); Phys. Lett. 3, 344 (1963).

52. R.S. Preston, S.S. Hanna, and J. Heberle: Phys.Rev. 128, 2207 (1962).

53. L.W. Fagg and S.S. Hanna: Rev. Mod. Phys. 31, 711 (1959).

54. E.M. Condon and G.H. Shortley: " Theory of Atomic Spectra", (Cambridge University Press, 1935).

55. W. Marshall and C.E. Johnson: J. Phys. Rad. 23, 733 (1962).

56. F. Fermi: Z. Physik 60, 320 (1930).

57. R.M. Sternheimer: Phys. Rev. 86, 316 (1952).

58. A.J. Dekker and F. Van der Woude: Physica 33, 195 (1967).

59. M.B. Stearns: Phys. Rev. 129, 1136 (1963).

60. P.A. Flinn and S.L. Roby: Phys. Rev. 124, 34 (1961).

61. G. Shirane, C.W. Chen, P.A. Flinn and R. Nathans: Phys. Rev. 131, 183 (1963).

62. G.K. Wertheim, C. Jaccarino, S.H. Wernick and D.N.E. Buchanan: Phys. Rev. Letter, 12, 24 (1964).

63. F. Van der Woude and G.A. Sawatzky: Physics Reports 12C, 337 (1974).

64. M.B. Stearns: Phys. Rev. 6B, 3326 (1972).

65. P.J. Schurer, G.A. Sawatzky and F. Van der Woude: Phys. Rev. Letts. 27, 586 (1971).

66. P.J. Schurer, K.W. Maring, F. Van der Woude and G.A. Sawatzky: Proc. of the Conf. on Mössbauer Spectroscopy Dresden 1971, p.228.

67. P.J. Schurer, K.W. Maring, F. Van der Woude and G.A. Sawatzky Inter. J. Magnetism 4, (1973).

68. P.J. Schurer, K.W. Maring, F.Van der Woude and G.A. Sawatzky: Inter. J. Magnetism 4, (1973).

69. M.B. Stearns: J. Appl. Phys. 25, 1095 (1964).

70. T.E. Cranshaw, C.E. Johnson, M.S.Ridout and G.A. Murray: Phys. Lett. 21, 481 (1966).

71. T.E. Cranshaw: J. Phys. (F): 2, 615 (1972).

72. M.B. Stearns and S.S.Wilson: Phys. Rev. Letters, 13, 313 (1964).

73. F.N. Rhines: Phase Diagrams in Metallurgy Their Development and Application (McGraw-Hill Book Company, INC, New York, Toronto, London, 1956).

74. N. Benezer-Koller : in '' Chemical Applications on Mössbauer Spectroscopy'' V.I. Goldanskii and R.H. Herber (Eds.) (Academic Press, New York and London, 1968).

75. G.K. Wertheim, W.P. Kingston and Herber: J. Chem. Phys. 37, 687 (1962); R.H. Herber and G.K. Wertheim: J. Chem. Phys. 38, 2106 (1963).

76. V.G. Bhide and M.S. Multani: Phys. Rev. 149, 289 (1966); V.G. Bhide and G.K. Shenoy: Phys. Rev. 143, 309 (1966); J.D. Siegworth: Phys. Rev. 155 , 285 (1967); H.J. Guggessheim and G.K. Wertheim: Chem. Phys. 42, 3873 (1965); J.G. Mulley: Phys. Rev. 131, 1415 (1963).

77. L. May and D.K. Snediker; Nucl. Instr. and Meth. 55, 183 (1967).

78. A.J. Bearden, P.L. Mattern and P.S. Noble: Am. J. Phys. $\underline{32}$, 109 (1964); G. DePasquali, H. Frauenfelder, S. Margulies and R.N. Peacock: Phys. Rev. Letters $\underline{4}$, 71 (1960); D.A. Shirley, M. Kaplan, and P. Axel: Phys. Rev. $\underline{123}$, 816 (1961).

79. K.P. Mitrofanov: Instr. Expt. Tech.(USSR) (Eng.Trans) . $\underline{3}$, 526 (1965); A.J. Bearden, M.G. Hauser and P.L. Mattern: Ref. 8 Vol.1 (1965) p.67; R.L. Mössbauer: Proc. Second Intern. Conf. on the Mössbauer Effect Saclay, France (1961), p.38 (John Wiley and Sons, New York, 1962) D.M.J. Compton and A.H. Schoen (Eds.).

80. R. Booth and C.E. Violet; Nucl. Instr. Method $\underline{25}$, 1 (1963); R.H. Nussbaum, F. Gerstenfeld, and J.K.Richardson: Am. J. Phys. $\underline{34}$, 45 (1966).

81. S.S. Hanna, J. Herberle, C. Littlejohn, G.J. Perlow, R.S. Preston and J.H. Vinscent: Phys. Rev. Letters $\underline{4}$, 177 (1964).

82. A.D. Adler and M. Hane: Am. J. Phys. $\underline{34}$, 189 (1966).

83. J.G. Dash, R.D. Taylor, N.E. Nagle, P.P. Craig and V.M. Visscher: Phys. Rev. $\underline{122}$, 1118 (1961); R.L. Mössbauer and W.H. Wiedemann: Z. Physik. $\underline{159}$, 33 (1960).

84. J.G. Mullen: Phys. Rev. $\underline{131}$, 1410 (1963).

85. L. CSER et.al. 1966 Report of Hungasian Academy of Science, Central Research Institute for Physics.

86. P. Flinn: Rev. Sci. Instr. $\underline{34}$, 1422 (1963); P. Flinn; Ref. 8 Vol. 1 (1965) p.75 .

87. R.C. Knauer and J.G. Mullen: Rev. Sci. Instr. $\underline{38}$, 1624 (1967).

88. E. Kankeleit: Rev. Sci. Instr. $\underline{35}$, 194 (1964).

89. E. Kankeleit: Ref. 8. Vol. 1 (1965) p.47.

90. R.L.Cohen, P.G. Mullen, G.K. Wertheim: Rev. Sci. Instr. 34, 671 (1963); R.L. Cohen: Rev. Sci. Instr. 37, 957 (1966); G.K. Wertheim, R.L. Cohen: in Applications of the Mössbauer Effect in Chemistry and Solid State Physics, Technical Reports Series No. 50, IAEA, Viena (1966), p.48.

91. H. Sano and R.H. Herber: J. Inorg. Nucl. Chem. 30, 409 (1968).

92. S.C. Curran: Proportional Counter Spectroscopy, in Beta and Gamma ray Spectroscopy, K.Siegbahn (Ed.) (North Holland, Amsterdam, 1955), p.165.

93. M. Michalski, J. Piekoszewski and A. Sawicki: Nucl. Instr. Meth. 48, 349 (1967).

94. Ajay K. Singh Ph. D. Thesis Univ. of Roorkee, Roorkee (India) 1977.

95. J.J. Spijkerman, F.C. Ruegg, and J.R. Devoe., in Applications of the Mössbauer in Chemistry and Solid State Physics (Report of a Panel on Applications of the Mössbauer Effect in Chemistry and Solid State Physics, Vienna, 1965) IAEA Vienna, 1966) Tech. Reports Series No.50), p. 254.

96. J.G. Dash, R.D. Taylor, P.P. Craig, D.E. Nagle, D.R.E. Cuohran and W.E. Keller: Phys. Rev. Letters 5, 152 (1960).

97. R.D. Taylor: in Proceedings of the Second International Conf. on the Mössbauer Effect (D.M.J. Compton and R.H. Schoen (Eds.) (John Wiley and Sons, New York, 1962), p.203.

98. R.S. Preston: Phys. Rev. Letters 19, 75 (1967) and references therein.

99. P.P. Craig; in Ref.8 Vol.1 (1965) p. 135; R.C. Perisho, .,
    R. Segnan and W.A. Steyert: Phys. Rev. 138, A 1460 (1965).

100. W.A. Steyert and M.D. Daybell: in Ref. 8 Vol.4 (1968) p.1.

101. G.M. Kalvius and E. Kankeleit: in Mössbauer Spectroscopy and
     its Applications Proceedings of a Panel Vienna 24-28, May
     1971, p.9.

102. P.J. Schurer: Ph.D. Thesis, Rijksuniversiteit TE.
     Groningen 1972 p. 40.

103. B.K.Jain and K. Chandra: Indian Journal of Pure and Applied
     Physics 14, 858(1976).

104. U.R. Evans: in '' The Corrosion and Oxidation of Metals''
     (Scientific Applications) (Arnold Press, London, Edward,
     1960).

105. U.R. Evans: '' An Introduction to Metallic Corrosion''
     (London, Edward Arnold, Publishers Ltd., 1963).

106. J.C. Scully: '' Fundamentals of Corrosion'' (Pergamon Press
     Oxford London, 1966).

107. N.D. Tomashov: in '' Theory of Corrosion and Protection
     of Metals'' (Translated from Russian and Ed. by Bo:;is,H.
     Tylell. Isidore Geld and Herman S.Preiser (The Mcmillan
     Company, New York, 1966).

108. S. Miyake: Sci. Rep.: I.P.C.R. (Tokyo) 31, 161 (1937);
     Through I Nitta: X-ray Crystallography (Maruzen, Tokyo,
     1959) Vol.1 p. 650.

109. Y. Fujio: Japan   J. of Appl. Phys. 12, 1850 (1973).

110. A.M. Pritchard and C.M.Dobrin: Nature (London) 224,1295
     (1969).

111. G.W. Simmons, E.Kellerman and H. Leidheiser: Corrosion 29, 227 (1973).

112. R.L. Collins: in Ref.8. Vol.4 (1968) p. 129.

113. J.H. Terrell and J.J. Spijkerman: Appl. Phys. Letts. 13, 11, (1968).

114. K.R. Swanson and J.J. Spijkerman: J. Appl. Phys. 41, 3155 (1970).

115. Z. Bonchev, A. Jordanev and A. Minkova: Nucl.Instr. Meth. 70, 36 (1969).

116. W. Meisel and G. Kreysa: Z. Anorg. Allgchem. 395, 31 (1972).

117. W. Meisel: Werkst Korros 21, 249 (1970).

118. W. Meisel: Z. Chem. 11, 238 (1971).

119. H. Onodera, H. Yamamoto, H. Watanabe and H. Fbiko: Japan J. Appl. Phys. 11, 1380 (1972).

120. M.J. Tricker, J. M. Thomas and A.P. Winterbottom: Surface Sci. 45, 601 (1974).

121. T. Toriyama, M. Kigawa, M. Fujioka and K.K. Hisatake: Japan J. Appl. Phys. Suppl. 2 part 1, 733 (1974).

122. W.E.O.Grady, O.M. Bocknis : Surface Sci. (Netherlands). 38, 249 (1973).

123. D.A. Channing and M.J. Grahm: Corros. Sci. 12, 271 (1972).

124. D.A. Channing and M.J. Grahm: J. Elect. Chem. Soc. 117, 389 (1970).

125. D.A. Channing, S.M. Dicherson and M.J. Grahm: ibid, 13, 933 (1973).

126; I. Dezsi, A. Vertes and L. Kiss: Magykem 73, 421 (1967).

127. I. Dezsi, A. Vertes and L.Kiss: J. Radional Chem. 2, 183 (1969).

128. D.D. Joye and R.C. Axtmann: Annal. Chem. 40, 876 (1968).

129. G.M. Bancroft, J.E.O. Mayne and P. Ridgway: Brit.Corros. J. 6, 119 (1971).

130. K. Volenik, J. Cirak and M. Sebri'ni': British Corrosion Journal 10, 196 (1975).

131. N.A. Eissa and M.M. Abdel-Megid: Proc. of Conf. on Mössbauer Spectroscopy Vol.2 (Dresden 1971) p. 4440.

132. A.M. Vander Kraan : Phys. Stat. Solidi a (Germany) 18, 215 (1973).

133. B.K.Jain, Ajay K.Singh, K.Chandra and I.P. Saraswat: Japanese J. of Applied Physics 16 (Dec. 1977) To appear.

134. J.E.O. Mayne: J. Chem.Soc. 1953 p. 129; J. Iron Steel Inst. 176,140 (1954); J. Appl. Chem. 9, 673 (1959).

135. Mellors, Cohen and Beck: J. Electro. Chem. Soc. 105, 332 (1968).

136. R.M. Singru, K.S.Raju, V.G. Jadhao and C.N.R. Rao: Proc. Nucl. Phys. and Solid State Phys. Symposium (Department of Atomic Energy, Bombay, India) 3, 617 (1972).

137. Ch. Janot and P. Delecroix: J. de Physique C6, 35, 557 (1974).

138. Ch. Janot and H. Gibert: Bull. Soc. Fr. Min. Crist. 93, 213 (1970).

139. B. W Christ and P.M. Giles: Metallurgical uses of the Fe^{57} Mössbauer Effect in Metallic iron and Plain Carbon Steels. Ref.8 Vol.3 (1967). p.37

140. F. Gresovnik: Zelezarski 2B $\underline{3}$, 319 (1969).

141. O.Barb, M. Morariu, D.Tarina, I. Bibicu, S. Constantin escu and L. Dia Mandescu:Rumania Stud. and Cercet. Fiz Rumania $\underline{25}$, 17 (1973).

142. F.E. Fujita: In Topics in Applied Physics Vol.5. Mössbauer Spectroscopy, U. Gonser (Ed.) (Springer-Verlag Berlin Heidelberg New York, 1975) p. 201.

143. U. Gonser : An Introduction of Mössbauer Spectroscopy, L.May (Ed.) (Plenum Press, New York, 1971) p. 155.

144. N. Abe and L.H. Schwartz: Mater. Sci. Eng. $\underline{14}$, 239 (1974).

145. P.L. Gruzin, Yu. L. Rodionov and Yu. A. Li: Fiz. Met. Metalloved $\underline{38}$, 208 (1974)/ Phys. Met. Metalogr. (USSR).

146. J. Lauermannova: Koveve Mater $\underline{12}$, 566 (1974) (Czech).

147. I.N. Bogachev, S.D. Karakishev, V.S. Litvirov and V.V. Ovchinnikov: Izv Vyssh Uchebn Zaved, Fiz. $\underline{6}$, 83 (1974).

148. F.M. Galperin, I.L. Amelin, V.M. Erkin, A.N. Salugin, M V. Filin, A. Ya Khrapov and G.L. Marks: Phys. Stat.Sol. a $\underline{21}$, K85 (1974).

149. J. Lauermannova and T. Zemcik: Phys. Stat. Sol. a $\underline{21}$, K 49 (1974).

150. I.N. Bogachev, S.D. Karakishev, V.S. Litvinov and V.V. Ovchinnikov: Phys. Stat. Sol. a $\underline{24}$, 661 (1974).

151. E.S. Bokshtein, Yu B. Voitkovskii, E.G. Latash, A. Yu Nadzhafov and G.S. Nikol'skii: Metalloved Term Obrab Metal $\underline{6}$, 64 (1974); Met. Sci.Heat treatment (USSR) $\underline{16}$, 524 (1974).

152. B.K.Jain. Ajay K. Singh and K. Chandra: Phys. Stat. Sol.
     43, (1977), to appear.

153. Max. Hansen: Constitution of Binary Alloys (McGraw-Hill,
     New York, 1958).

154. E. Robert Reed-Hill: '' Physical Metallurgy Principles''
     (D.Van Nostrand Company, INC. Princeton, New Jersey,1964).

155. Annotated Metallurgical Specimens Supplied by Metallurgical
     Services Laboratories Ltd., Raliant Works, Brockhem Betch-
     Worth, Surray, England.

156. T. Shinjo, F. Itoh, H. Takaki and Y. Nakamura: J. Phys. Soc.
     Jap. 19, 1258 (1964).

157. M. Ron, H.Shechter, A.A. Hirsch and S. Niedzwiedz: Phys. Letters
     Letters 20, 481 (1966); M. Ron, H.Shechter, and S.Niedzwiedz:
     J.Appl. Phys. 39, 265 (1968).

158. H. Bernas, I.A. Champbell and R. Fruchart: J. Phys. and Chem.
     Solids 28, 17 (1967).

159. S. Gupta, K.B.Lal, T.M. Srinivasan and G.N.Rao: Phys. Stat.
     Sol. a 22, 707 (1974).

160. I. Vincze and I.A. Campbell: J. Phys.(F) 3, 647 (1973).

161. G. Grüner, I. Vincze and L. Cser: Solid State Comm. 10,
     347 (1972).

162. F.A. Cotton and G.Wilkinson: '' Advanced Inorganic Chemistry.
     (Interscience Publishers, 1962).

163. H. Fonces-Diacon: Comp. rend. 130, 1710 (1900).

164. L. Moser and E. Doctor: Z. anorg.Chem. 118, 285 (1921).

165. N. Alsen: Geol. Fören. i Stockholm Förh 47, 19 (1925).

166. G. Hägg and A.L. Kindström: Z. Physik Chem. B 22, 453 (1933).

167. S. Tengnér: Z. anorg. Chem. 239, 126 (1938).

168. G. Little : Liebigs Ann. 112, 211 (1859).

169. T. Herone and S.Chiba: J. Phys. Soc. Jap. 11, 666 (1956).

170. T. Herone and S. Maeda: J. Phys. Soc. Jap. 9, 497 (1954).

171. I. Maxim: Stud. Cer cetari Fiz. 9, 1429 (1958).

172. K. Ono, A. Ito and E. Hirahara: J. Phys. Soc. Jap. 17, 1615
     (1962).

173. H. Kasper and H.G. Drickamer: Proc. N.A.S. 1968 p. 773.

174. K.V. Reddy and S.C. Chetty: Phys. Stat. Sol. a 32, 585
     (1975).

175. A. Okazaki and K. Hirakawa : J. Phys. Soc. Jap. 11, 930 (1956).

176. K. Hirakawa: J. Phys. Soc. Jap. 12, 923 (1957).

177. A. Okazaki: J. Phys. Soc. Jap. 14, 112 (1958);
     J. Phys. Soc. Jap. 16, 1162 (1961).

178. M. Kawaminami and A. Okazaki: J. Phys. Soc. Jap. 22, 924
     (1967); J. Phys. Soc. Jap. 29, 649 (1970).

179. T. Kamikura, K. Kamigaki, T. Hirone and K. Sato: J. Phys.
     Soc. Jap. 22, 1235 (1967).

180. G.A. Fatseas: C.R. Acad. Sci. (Paris) 265, 1073 (1967).

181. Ok Hang Nam and Lee Sung Won: Phys. Rev. B 8, 4267 (1973).

182. C. Boumford and A.H. Morrish: Phys. Stat. Sol. a 22, 435
     (1974).

183. A.A. Temperley and H.W. Lefevre: J. Phys. Chem. Solids
     27, 85 (1966).

184. B.K.Jain, Ajay. K.Singh and K.Chandra; J. Phys.(F) Commun.

185. P. Troften and G.Kullerud;Caregie Inst. Wash. Year Book, 60, 1760 (1961).

186. A.F. Wells: '' Structural Inorganic Chemistry'' (Clarendon Press, Oxford, 1975).

187. Janusz Leciejewicz: Acta Crystallographica , 14, 1304 (1961).

188. A. Bystrom: Ark. Kerm Min. Geol. A 20, 1 (1945).

189. R.T. Sanderson: '' Inorganic Chemistry'' Van Nostrand Reinhold Co., New York (1967).

190. J.A. Pople and D.L. Beveridge: Approximate Molecular Orbital Theory, McGraw Hill Book Co., New York (1970).

191. Viswamittar and S.P.Puri: Phys. Rev. B 9, 4673 (1974); J. Chem. Phys. 61, 3720 (1974); Chem. Phys. Letters 23,510 (1973).

192. I. Bunget, M. Rusu, M. Andrees Cu and C. Nistor: An Univ. Bucarest, Ser Stunt Nat. 14, 9, (1965).

193. H.G. Nadler, J. Pebler and K. Dehnicke: Z. Anorg. Allg. Chem. 404, 230 (1974).

194. R.A. Stukan, V.A. Prusakov, Yu.N. Novikov, M.E. Vol'pin,. and V.I. Goldanskii, Zh. Strukt Khim 12, 622 (1971); J. Struct.Chem. (USSR) 12, 567 (1971).

195. E.F. Bertaut, P. Burlet and J. Chappert: Solid State Commun. 3, 335 (1965).

196. F. Berlaut: Bull. Soc. Sci. Brelagne 39(Horsser), 67 (1964) in French.

197. T. Hirone, S.Maeda, I. Tsubokawa and N. Tsuya: J. Phys. Soc. Jap. 11, 1083 (1956).

198. H. Schmid: Cobalt $\underline{7}$, 26 (1960).

199. R.M. Parke: in Metals Hand Book '' Constition of binary alloys, Taylor Lyman (Ed.) (The American Society for Metals, 7301. Euclid Ave. Cleveland 3, Ohio, 1948). P. 1216.

200. S. Ito, T. Ido, K. Sato and K. Adachi: Read at the meeting of Japan Institute of metals, March,1969: Read at the Meeting of the Physical Society of Japan, Oct.1969 .

201. K. Yamaguchi, Y. Yamaguchi, H. Yamamoto and H. Watanabe: Read at the Meeting of the Physical Society of Japan, April,1970 .

202. K. Yamaguchi, H. Watanabe, H. Yamamoto and Y.Yamaguchi: J. Phys. Soc. Jap. $\underline{31}$, 1042 (1971).

203. K. Yamaguchi, H. Yamamoto, Y. Yamaguchi and H. Watanabe: J. Phys. Soc. Jap. $\underline{33}$, 1292 (1972).

204. N.S. Kurnakow and N.S. Konstantinow, Z. amorg. Chem. $\underline{58}$, 1 (1908).

205. J. Steger and E. Kestiner: J. Solid. State.Chem. $\underline{5}$, 131 (1972).

206. F.A. Cotton: Chemical Applications of Group Theory (Inter-Science Publishers, New York, 1967).